THE APPLICATION OF FINITE ELEMENT THEORY TO

CURVED ELEMENTS

by

JAGDISH SINGH SIDHU

A THESIS SUBMITTED TO THE UNIVERSITY OF ASTON

IN BIRMINGHAM

FOR THE DEGREE OF DOCTOR OF PHILOSOPHY

AUGUST 1973

SUMMARY

A subroutine to solve a set of simultaneous symmetric equations is developed in this Thesis in which more than one load case can be dealt with at the same time. Advantage is taken of the backing store facilities to enhance the capacity of the subroutine to solve large problems.

Curved members are usually approximated with a number of straight members. The accuracy of the results improves with the increase in the number of sub-divisions. This, however, increases the degrees of freedom of the structure which in turn requires more core space and solution time. Using the finite element technique stiffness matrices are formulated for curved elements. The suitability of the polynomial displacement functions is investigated by obtaining results for some simple structures and comparing these with those obtained by the strain energy method.

One factor which influences the performance of the finite element method is the choice of the displacement functions. Even with coarse sub-division, good results are obtained by using the displacement functions which define the deformed shape of the element more closely. More accurate displacement functions are derived in this Thesis by considering the equilibrium of a curved element with unform cross-section. Using these derived functions, results are obtained for arches and bow girders. These results are then compared with those obtained by the strain energy method. The influence of further sub-division on the accuracy of the results obtained by using the displacement functions is also studied.

The stiffness matrices for curved elements with variable cross-sections are also developed. To obtain these, the displacement functions derived for the curved elements with uniform cross-sections are utilized. Results are obtained for some arches and a bow girder with variable cross-sections by using both the stiffness matrices and the experiments. The suitability of the stiffness matrices for the curved elements with variable cross-sections is established by comparing the two sets of results obtained.

Finally, attention is also paid to the irregularities which usually occur in civil engineering structures. Displacement transformation matrices are constructed which allow for some of these and particularly the effect of offsets and hinges. Two structures with these features are analysed. The first one is a tied arch bridge frame. This is analysed by approximating the arch with straight members as well as by representing the arch with curved members. The second structure is a bow girder with offsets and hinges. In addition to the theoretical analysis using curved elements, the results for the latter structure are also obtained by experiments. The two sets of results obtained for each structure are compared to check the validity of the theoretical work.

CONTENTS

C H A P T E R   1

HISTORICAL REVIEW AND SCOPE OF PRESENT WORK

1.1 Introduction

Arches have been built since the beginning of the 19th century. This is in spite of the fact that their design was beyond the knowledge of that time. Bresse was the first to present a theoretical method using equations similar to those obtained by considering the bending strain energy. In 1872, Castigliano published his strain energy theorems. These have been used to analyse arches as well as other types of redundant structures.

Modern structures are required to have longer spans and carry heavier loads. One of the ways to meet these demands is to use trussed-type structures. In the case of bridges, the arches may be connected to deck girders by vertical struts or hangers. Concrete arches can be strengthened further by constructing a slab monolithically with the arch rib. A good example of this is in reference 15. The strain energy method becomes unwieldy to analyse such complex structures.

Nowadays, multi-level exchanges are increasingly used in highway engineering. It is desirable that these structures should satisfy the following conditions:-

(a) for obvious reasons the roadway is curved in plan;

(b) the overall depth of construction should be a minimum to avoid longer approaches which require more excavation or filling;

(c) To permit clear vision, the number of columns should be reduced to minimum. Also

the site conditions may make it
necessary to offset the columns from
the centre line of the roadway.

Usually, the dimensions of these structures are such that
they can be analysed as bow girders. Again it is easy to
analyse simple bow girders by using the strain energy method
but the problem becomes more difficult as the structure be-
comes complex.

More efficient methods in structural analysis use matrix
algebra. The operations involved in the analysis are inde-
pendant of the size and the complexity of the structure. There-
fore, a computer can be used to carry out the complete analysis.

The structure is first idealised by dividing it into a
number of discrete elements. These elements are connected to
each other at their nodes only. For each type of element into
which the structure has been divided, the load-displacement
relationship should either be known, assumed or could be
determined. A set of matrix operations is then performed on
the idealised structure. It is assumed that the strain ener-
gies of the idealised and the actual structure are equal.

The exact load-displacement relationship for straight
prismatic members is known and some structures may be composed
of such members entirely. The strain energy of these struc-
tures is nearly equal to that of their idealised models. Hence,
more accurate results may be obtained for such problems. For
some types of structural elements, the exact load-displacement
relationship is not known and may be difficult to obtain by
solving the governing differential equations. In these cases,
the finite element method can be used to derive an approximate

stiffness matrix for such elements (2, 4). Then the strain energies of the actual structure and its idealised model are different and consequently the results are only approximate. However, the accuracy of these problems can be improved by using a finer sub-division. This requires more computer core space as well as solution time. The advantages of finding the exact load-displacement relationship for structural elements are, therefore, obvious.

1.2 The Finite Element Method

(i) The Displacement Functions

The displacement functions should describe the deflected shape of the element as nearly as possible. Exact displacement functions can, for certain elements, be obtained by solving the governing differential equations. For most cases, however, it is difficult to derive these. In these cases, the displacement functions are assumed, often in the form of a polynomial. For one dimensional elements, the polynomial displacement functions are assumed to be of the form:-

$$y = a_i \, x^{i-1} \qquad\qquad (1.1)$$

where a_i are the arbitrary constants equal in number to the known boundary conditions;

X is the distance to a point in the element which is under consideration. This distance is usually measured from the first end of the member.

and y is the deflection of the point.

By substituting the boundary conditions into equations (1.1) a set of simultaneous equations is obtained which can be

expressed in matrix form as:-

$$\{\delta\} = [C] \{a\} \qquad (1.2)$$

where $\{\delta\}$ is a column vector which lists all the
nodal displacements of the element;

$\{a\}$ is another column vector whose elements
are the arbitrary constants of the dis-
placement functions;

and $[C]$ is a square matrix which relates the
nodal displacements to the arbitrary
constants.

The set of equations (1.2) may be solved explicitly to
express the arbitrary constants in terms of the nodal displace-
ments giving in matrix form:-

$$\{a\} = [C]^{-1} \{\delta\} \qquad (1.3)$$

where $[C]^{-1}$ is the inverse of matrix $[C]$ and the
vectors $\{a\}$ and $\{\delta\}$ have already been
defined.

The elements of matrix $[C]$ and its inverse $[C]^{-1}$ are con-
stants which depend on the properties of the structural elements
only.

(ii) The strain-displacement relationships

The equations relating the strains to the corresponding
displacements can be found in reference (1, 2). Substituting
the displacement functions into these equations yields the
following relationship in matrix form:-

$$\{\varepsilon\} = [A] \{a\} \qquad (1.4)$$

where $\{\varepsilon\}$ is the column vector of strains considered;

and [A] is a rectangular matrix which relates
the strains $\{\varepsilon\}$ to the arbitrary con-
stants $\{a\}$.

Combining equations (1.2) and (1.4) gives:-

$$\{\varepsilon\} = [A] [C]^{-1} \{\delta\} \qquad (1.5)$$

or $\qquad \{\varepsilon\} = [B] \{\delta\} \qquad (1.6)$

where $\qquad [B] = [A] [C]^{-1} \qquad (1.7)$

Equation (1.6) relates the strains $\{\varepsilon\}$ to the nodal
displacements $\{\delta\}$ through matrix [B] .

(iii) The stress-strain relationships

The stresses in an elastic body are related to the strains
by Hooke's law. The equations can be written in matrix not-
ation as:-

$$\{\sigma\} = [D] \{\varepsilon\} \qquad (1.8)$$

where $\{\sigma\}$ is the stress vector corresponding to
the strains, $\{\varepsilon\}$;
and [D] is a square symmetric matrix known as the
elasticity matrix whose elements may be
the extensional and flexural properties,
the shear and the torsional rigidity of
the element.

Substituting equation (1.6) into (1.7) leads to:-

$$\{\sigma\} = [D] [B] \{\delta\} \qquad (1.9)$$

Equation (1.9) relates the stresses, $\{\sigma\}$, to the corres-
ponding nodal displacements $\{\delta\}$.

(iv) The stiffness terms

The stiffness matrix can be obtained by applying either the virtual work or the unit displacement theorem. The results will be identical. Using the virtual work theorem, all the nodes are given arbitrary virtual displacements. The strain energy stored in the element is then calculated from:-

$$U = \int \{\varepsilon^*\}^T \{\sigma\} \, dVol \qquad (1.10)$$

where $\{\varepsilon^*\}$ is the strain vector corresponding to the virtual nodal displacements. The supperscript T denotes the transpose of a matrix or a vector.

From equation (1.6) the strain vector in its transposed form is:-

$$\{\varepsilon^*\}^T = \{\delta^*\}^T [B]^T \qquad (1.11)$$

where $\{\delta^*\}$ is the vector of virtual displacements.

Combining equations (1.9) to (1.11) the strain energy stored in the element is obtained, viz:

$$U = \int \{\delta^*\}^T [B]^T [D] [B] \{\delta\} \, dVol \qquad (1.12)$$

The work done by the nodal forces in moving through the virtual displacements is:-

$$W = \{\delta^*\}^T \{P\} \qquad (1.13)$$

where $\{P\}$ is the vector of the nodal forces in the element.

By equating the work done to the strain energy stored in the element, and remembering that the virtual displacements are

scalar quantities, it is found that:-

$$\{P\} = \int [B]^T [D] [B] \{\delta\} \, dVol \tag{1.14}$$

i.e. $\quad\quad \{P\} = [K] \{\delta\}$ (1.15)

where $\quad\quad [K] = \int [B]^T [D] [B] \, dVol$ (1.16)

Equation (1.16) gives the required stiffness matrix, $[K]$, of the element, while equation (1.15) is the equilibrium equation of the element relating the nodal forces and displacements.

1.3 Historical Review

Towards the end of the 19th century, relatively accurate methods of structural analysis became available. Amongst these are Castigliano's strain energy methods, Mohor's slope deflection equations and the principle of virtual work. Application of any one of these methods leads to a set of simultaneous equations whose number equals the number of unknowns. The solution of these equations yields the unknown displacements or the forces. Even for structures of modest size, this results in a large number of simultaneous equations. Since it is difficult to solve a large set of equations, considerable research was devoted to devise methods to circumvent the solving of these equations explicitly. This research led to the development of model analysis as well as various iterative methods such as moment distribution and finite differences.

(i) The Matrix Methods

During the 20th century, aircraft structures rapidly grew in size and complexity. An accurate analysis of these structures is more desirable than in other fields. Therefore,

research in the aircraft industry was concentrated in two
directions; firstly, to find ways of solving simultaneous
equations accurately and quickly and secondly, to devise better
methods for obtaining these equations. This was helped by the
development of computers and matrix methods of structural
analysis.

It was found that matrix algebra is most suitable to use
with computers. There are basically two distinct methods known
as the displacement method and the force method. These are
well known and can be found in texts dealing with this subject
(2, 3, 5). In the displacement method, the forces in the
members are expressed in terms of the nodal displacements.
This step makes use of the stress-strain relationships, the
strain-displacement relationships and the compatibility con-
ditions. The application of the equilibrium conditions then
yields a set of simultaneous equations whose solution gives the
unknown nodal displacements. Finally, the forces in the members
are obtained by substituting the nodal displacements into the
load-displacement equations for the members. The fact that
the structure is statically determinate or indeterminate does
not influence the analysis. This is one reason for its pop-
ularity among engineers. Furthermore, this method can be
easily automised for a computer.

In the force method, the member end displacements are
expressed in terms of the unknown forces and the compatibility
conditions are used to obtain the set of simultaneous equa-
tions. The solution of these gives the required forces. Here
the redundant forces may be chosen arbitrarily, consequently
the whole process of structural analysis cannot be easily

automised. However, this method was favoured by engineers in the beginning as it usually leads to a smaller number of sim- ultaneous equations. In this Thesis, the displacement method is used.

Argyris (9) was one of the first to employ matrix methods to analyse structures. Livesley produced computer programmes to analyse framed type structures in which the instability functions were included to allow for the effect of axial loads. It was shown that for tall, slender structures, the influence of these axial loads can be considerable (3, 5).

In the case of several prismatic members connected to a joint, it is not always possible to make their centroidal axes meet at a point. In steel structures, members are sometimes deliberately offset to reduce the size of the gusset plates. Similarly an intermediate column supporting a bow girder may be offset to counter some of the twisting moment in the girder. To obtain representative results for structures with these features, the mathematical model should allow for these offsets (14).

There are two ways of allowing for irregularities such as offsets and hinges. One is to modify the stiffness matrix for the member (12, 41, 43). The other is to allow for these effects through the displacement transformation matrix. The latter method is neater and was introduced by Jennings and Majid (11). The offsets contribute to the lateral displace- ments at the ends of the member. These contributions are proportional to the offsets and the end rotations of the member in the local co-ordinates. Therefore, the member end displacements were obtained by using an intermediate step.

This method is also used in this Thesis.

(ii) The Finite Element Method

By using the unit displacement theorem Argyris (9) obtained a stiffness matrix for a rectangular plate element subjected to in-plane stresses. A node of the element was given a unit in-plane displacement in a particular direction while all the other displacements were maintained at their zero values. The forces and the reactions required to produce this condition formed one column of the stiffness matrix. Similarly each of the other nodal displacements contributed a column to the stiffness matrix.

The stiffness matrix for a triangular plate element suffering in-plane displacements was developed by Turner et al (16). The notion of displacement functions was introduced for the first time. Constant strains were assumed throughout the element and then the strain-displacement equations were integrated to obtain the displacement functions. It was pointed out that the number of arbitrary and integration constants should be equal to the number of nodal displacements. A stiffness matrix for a quadrilateral element was also derived. This was carried out by dividing the quadrilateral element into four triangles meeting at a node within the element and then simply adding the stiffnesses of these elements. Since the loads at the fifth node within the element were zero, the corresponding displacements were eliminated. To represent a variable stress field across the elements, the use of extra nodes was suggested. For the case of triangular elements, for instance, these can be at the mid-points of the sides.

The stresses in the aircraft skin are predominantly
membrane and the bending action is negligible. Making use of
this fact Argyris formulated the stiffness matrix for a
rectangular plate by considering the in-plane stresses only.
Melosh (17) produced a stiffness matrix for a thin rectangular
plate element in bending. A polynomial displacement function,
for the out of plane displacements, was chosen in a manner
similar to that proposed by Turner et al. The strain energy
of the element in bending was calculated. The application of
Castigliano's theorem (part 1) then yielded the required stiff-
ness matrix. Melosh obtained a stiffness matrix for a triang-
ular plate element in bending by eliminating the fourth corner
of a rectangle, but this yielded unsatisfactory results.

The principle of unit displacement and the strain energy
method had been used to derive the stiffness matrices for
various structural elements. To these was added the concept
of virtual work. Zienkiewicz and Cheung (18) used this prin-
ciple to develop a stiffness matrix for a rectangular iso-
tropic or orthotropic plate in bending. A polynomial displace-
ment function of twelve terms, one for each nodal displacement,
was assumed.

The uniformly distributed loads are, usually, equally
divided among the nodes and applied as concentrated forces.
This is a reasonable approach, particularly when the size of
the elements is small. However, a better approximation is
achieved by equating the work done by the equivalent nodal
forces to the work done by the uniformly distributed loads.
This yields bending couples as well as shear forces at the
nodes thus improving the results (18, 36).

The polynomial displacement functions used in the derivation of stiffness matrices for triangular and rectangular elements do not define the normal slope along the edges of the elements uniquely. Therefore, discontinuities develop along the common boundaries of the elements as the structure deforms. This is one of the factors which contributes to the inaccuracy of the results. Harvey and Kelsey (56) rectified this defect by enforcing slope compatibility. The normal slope at the mid-point of a side was specified to be equal to half the sum of normal slopes at the nodes bounding that side.

The strain energy due to shear is usually not included when deriving the stiffness matrices. Melosh (48) and Utku (49) obtained more accurate stiffness matrices by taking the transverse shears into consideration. The rate of convergence of results can be further improved by taking more terms of the displacement functions as suggested by Pian (60) and used by Stricklin and Haisler (54).

Shells were first approximated as an assembly of flat plate elements (4, 48). This assumed that there is no coupling effect between the in-plane and out of plane displacements. Within the small deflection theory, this assumption is only true for straight members, but it is not so for curved elements even when the deflections are small. For a very fine mesh size,flat elements give equally good results as obtained by using more refined curved elements (24).

Grafton and Strome (22) introduced a new type of element, a frustum, to analyse axi-symmetric shells of revolution. Here the nodal points were replaced by nodal circles, thereby reducing the number of possible nodal displacements to three.

For deep shells, the use of frustum type elements gave bending moments in regions where only membrane forces were expected. The magnitude of these, however, decreased as the number of elements representing the shell was increased (23).

Percy et al (42) improved the cone element of Grafton and Strome by using a better approximation for the strain energy. The displacements and the loads were expressed in Fourier Series. A greater number of terms was taken in the displacement functions as suggested by Pian (60). Finally, a more accurate numerical integration was carried out whereas Grafton and Strome had used the 'trapizoidal rule'.

The surface of the shells in references (22, 23 and 42) was assumed to be linear. A fine mesh is required when using any one of these elements to obtain good results. For the element developed by Jones and Strome (40), the surface of the shell was assumed to vary quadratically, thereby approximating it more closely. The polynomial displacement functions were modified to include some trigonometeric terms which allowed for the rigid body displacements. To improve the results even further, the equivalent loads were obtained by using the principle of virtual work. This element gave better results than the cone elements, particularly when the curvature varied more rapidly.

The polynomial displacement functions have also been used to develop the stiffness matrices of shell elements (35, 46). Bogner et al (46) developed a 48 x 48 stiffness matrix for a cylindrical shell element by using polynomial displacement functions both for in-plane and out of plane displacements. Cantin and Clough (24) pointed out the inability of such

functions to allow for the rigid body displacements without straining the element. As in the case of curved element for axi-symmetric shells (40), they incorporated some trignometeric terms into the displacement functions to cater for the rigid body movements of the element which improved the results.

The stiffness matrix for a triangular shell element of uniform curvatures was obtained by Utku (49). He considered the total potential energy and then used Ritz' procedure to transform the integration into a summation over a finite difference mesh. Dhatt (55) derived a better stiffness matrix than that given in reference (49). The curved geometry of the element was approximated by a shallow quadratic surface. Conforming polynomial displacement functions were assumed by taking more terms than the number of degrees of freedom. The final stiffness matrix was reduced by minimising the potential energy as well as by using the normal slopes at the mid-points of the sides which were taken to be equal to half the sum of the normal slopes at the nodes bounding that side. Excellent results have been reported.

The similarity of shells to plates on elastic foundations was made use of by Sabir and Ashwell (25). Polynomial displacement functions were used to obtain stiffness matrices for a shallow shell element that consisted of a bending stiffness matrix, a matrix for the elastic foundation and a stiffness matrix associated with fictitious loads due to in-plane strains. These three matrices were then combined to obtain satisfactory results with a fine mesh.

The problem of a thin circular ring under radial load was studied by Zagustin and Young (26). By considering the

equilibrium of an element of such a ring, a differential equation for bending was obtained. The form of this equation is similar to the well known differential equation for deflection of curved bars. The differential equation for bending was used to investigate the stability of arches under radial loads.

The curved shell element of Cantin and Clough (24) was reduced to an arch element by Murray (61) and applied to an arch along with other curved elements. The reduced shell element yielded the best results. He also investigated the influence of Timoshenko's and Flügge's theory of strain-displacement relationship and found that the rate of convergence was the same for both.

A circular ring can be loaded perpendicular to the plane of initial curvature. Considering the equilibrium of an element of such a ring Witecki (27) obtained the equation for bending moment. In the derivation of this equation, it was assumed that for shallow bow girders, the influence of the twisting moments on the bending moments was negligible. The twisting moments, however, were given as a function of the bending moments and the applied torque, the latter being due to the eccentricity of the load. The results showed that the bending moments in shallow bow girders differed slightly from those in straight beams of length equal to the curved length.

The unit load theorem was used by Basi et al (28) to derive a flexibility matrix for a bow girder. The whole structure was first reduced to a cantilever by removing sufficient restraints. A unit load was then applied for each restraint released which yielded a column of the flexibility matrix.

The redundant reactions were calculated by imposing the compatibility conditions. The results showed the influence of the curve on the bending moments. Witecki's assumption about the effect of the twisting moments on the bending moments being small was shown to be reasonable.

The stiffness matrices formulated for a sector (53, 63) can be reduced to those for an element of a bow girder by eliminating the variable for the radial direction. Alternatively the strain energy method may be used to derive the required stiffness matrices (7, 50). However, the latter method becomes cumbersome when dealing with elements of variable cross-section.

(iii) Numerical Integration in the Finite Element Method

Explicit evaluation of the stiffness matrices has been favoured in the past. This involves a large volume of algebra and integrations which increases with the complexity of the element and the displacement functions employed. Consequently, the use of the finite element method has been restricted to simple elements only and even for some of these numerical integration had to be partially used (22, 40, 42, 55). Employing simple elements, it is necessary to use a finer subdivision in the region of rapidly varying stress fields which sometimes leads to an ill-conditioned overall stiffness matrix. The alternative is to use larger and more complicated elements made available by numerical integration.

In the formulation of the stiffness matrices, a number of simultaneous equations are obtained which are solved explicitly to express the arbitrary constants in terms of the nodal displacements of the elements. The simultaneous equations vary from element to element. Consequently, the stiffness

matrix is developed afresh for each type of element. The solution of equations is equivalent to the matrix inversion. Irons (29, 57) has recommended the use of a computer to perform this matrix inversion numerically. Similarly, the numerical integration can be used, instead of the explicit integration usually employed, to evaluate the stiffness terms.

Irons has asserted that by their reluctance to use numerical integration, research workers are restricting the development of the finite element method. The extra computer time required for calculating the stiffness matrices numerically is compensated by the savings made in solving fewer simultaneous equations which result from the use of a coarser grid.

During the past few years, Zienkiewicz et al (62) have developed the isoparametric element with which curved boundaries can be easily considered. New methods of obtaining the displacement functions have been put forward which obviate the need for matrix inversions. Intermediate as well as the usual corner nodes are used to define uniquely the curved boundary and the displacement function for the element. Naturally, the expressions involved in the formulation of the stiffness matrix become so complex that the use of numerical integration becomes essential. It has been found that isoparametric elements have a distinct advantage over conventional elements in the analysis of three dimensional problems.

Several methods of numerical integration, varying in degree of accuracy, are available (30). Grafton and Strome (22) used the simple 'trapizoidal rule' to evaluate the stiffness matrix for the conical element, while other authors

(40, 42, 55) employed more accurate numerical integrations. For two and three dimensional elements Irons (29, 57) and Zienkiewicz (4, 62) have used Gauss' quadrature formulae which are twice as efficient as the more simple Simpson's rule. The latter method is used in this Thesis because of its simplicity.

(iv) The Criteria for Choosing a Displacement Function

It has been found from previous research that a good displacement function should satisfy the following conditions:-

(a) the displacement function should describe the actual deformed shape of the element as nearly as possible;

(b) the displacements and the slopes within the elements and along the boundary should be continuous and compatible with the adjacent elements;

(c) the number of terms taken in the displacement functions should be equal to, or greater than, the number of nodal displacements;

(d) the displacement functions should allow for the rigid body displacements without straining the element; and

(e) the displacement of a point should not alter when the element is sub-divided.

The displacement functions which satisfy condition (a) yield good results even with coarse sub-division. Consider, for example, the pin-ended strut shown in figure 1.1. The strut is in equilibrium under the action of the axial loads P.

Choosing the origin of X and Y axis at the mid-point, the deflected shape is better approximated by the following displacement function:-

.*FIG. 1.1*

$$y = A \cos \frac{Bx}{L} \tag{1.17}$$

where A and B are arbitrary constants.

A polynomial displacement function, though uses more terms, gives poor results than equation (1.17).

Condition (c) makes sure that the inversion of matrix [c] , equation (1.2), exists. When more terms than the number of nodal degrees of freedom are taken, the principle of minimum potential energy is used to obtain the extra equations. It has been claimed that inclusion of more terms improves the results (20, 21, 38, 39, 60).

In the rigid body movement, no work is done by the nodal forces. However, if the element is strained during rigid body displacement, strain energy is stored in the element. This violates the equality of the work done and the strain energy stored. Cantin and Clough (24) maintain that the displacement functions should allow for the rigid boyd displacements explicitly, while Haisler and Stricklin (47) have claimed that there is no need for this.

The criteria for choosing displacement functions discussed above is due to Melosh (19). Khanna and Hooley (44, 45) studied various stiffness matrices and found that matrices giving higher strain energy densities yield better results.

(v) The Solution of Equations

The matrix analysis of structures leads to a set of simultaneous equations. Gauss' methods of solving such equations are well known. These are the direct elimination and the iterative methods. Several variations of these two basic methods have been developed, all of which can be found in texts on numerical methods (30).

The above methods are general and, therefore, can be used to solve any set of equations. The stiffness matrix of a structure is always symmetrical. This follows from Maxwell's reciprocal theorem. Choleski's method of solving the equations makes use of this property. The details of this method are given in reference (30). The matrix of the left hand coefficients is reduced to an upper and a lower triangle. The upper triangle is the transpose of the lower triangle, furthermore, the product of the two is equal to the original matrix. This can be expressed as:-

$$[L] \, [L]^T = [A] \tag{1.18}$$

An intermediate vector $\{y\}$ is used in the solution, which is found from the following equation:-

$$[L] \, \{y\} = \{b\} \tag{1.19}$$

where $\{b\}$ is the vector of the right-hand side coefficients.

Finally, the solution vector $\{x\}$ is obtained from the following relationship:-

$$[L]^T \, \{x\} = \{y\} \tag{1.20}$$

Gauss' and Choleski's methods of solving a set of simul-

taneous equations have been known for a long time. The difficulties in using these in hand calculations are obvious. Methods were, therefore, developed to bypass the solution of the equations altogether. These are the moment distribution method, the relaxation methods, model analysis and others. The advent of computers revived the interest in solving the equations explicitly. Several authors (31, 34, 58, 59, 64) have contributed to this science.

The earlier programmes used sub-routines in which all the coefficients of the left-hand side array were stored. The limited core available in the earlier computers restricted the size of the structures that could be analysed. To solve large problems, the stiffness matrix had to be partitioned into sub-matrices (31, 64). Furthermore, zero elements occuring inside the sub-matrices only were stored. This method is akin to analysis by substructures (37).

The stiffness matrices of structures have some special features. These are:-

(a) the proportion of non-zero elements is small. This decreases with the increase in the size of the structure;

(b) as already mentioned, the stiffness matrix is always symmetric;

(c) by numbering the nodes in a certain way, the non-zero elements can be brought within a band parallel to the leading diagonal. The width of this band is proportional to the largest difference between any two nodes connected by a member; and

(d) zero elements outside the band remain

zero when using the direct elimination

method without row or column interchange.

Because of the symmetry of the stiffness matrices, only half the symmetric elements need be stored. The band method of storage (32), of which the tri-diagonal method (59) is a special case, take advantage of the above-mentioned properties. In the case of direct elimination method, a particular row is used to reduce only a few of the subsequent rows. Hence, only a few equations need be in the working core at a time, the rest being in the backing store. The only drawback of this method is the time spent in transferring the rows to and from the backing store.

For large structures, the band is usually thin. The solution time for such problems is proportional to the square of the band-width. Therefore, any reduction in the band-width results in the saving of not only the storage space but also in solution time. Jennings (33) devised a method of locally variable band-width. To increase the capacity of this method even further, backing store has been used (34). In certain computers, with the facility of buffer core, it is possible to transfer at once a block of elements of fixed size. It is preferable to make few large transfers than several small ones. A variation of this method is presented in the next chapter.

1.4 The Scope of Present Work

The curved members can be approximated by a number of straight members. The results of such an approximation improve with the refinement of the sub-division. This, however,

increases the number of degrees of freedom in the structure which in turn increases the required storage and the solution time of the computer. Therefore, the advantages of obtaining the stiffness matrices for curved elements are obvious.

There are several methods of obtaining the load-displacement relationship of structural elements. For members of uniform cross-section, the strain energy method can be used. The easiest way is to use the unit load theorem (7, 50). This gives the flexibility matrix which can be inverted to obtain the required stiffness matrix. Another method is to use the finite element technique which is adopted in this Thesis.

Two types of displacement functions are investigated, a polynomial type and another derived ones. The polynomial functions are chosen according to the recommendations of section 1.3 (iv). The governing differential equations are formulated by considering the equilibrium of a curved element of uniform cross-section. These equations are then solved to obtain the derived displacement functions.

The above displacement functions are also used to obtain the stiffness matrices for curved elements of variable cross-section. Various structures are analysed by using the stiffness matrices, the results are compared with those obtained by:-

    (a) the strain energy method for simple arches

         and bow girders of uniform cross-sections;

    (b) approximating the arches and the bow girders

         by a number of straight prismatic members; and

    (c) experiments where the strain energy method

         becomes too involved.

The in-plane stiffness matrices are developed in Chapter 3. Three types of curvature - displacement relationships are considered. These are:-

(a) the curvature, $\chi = \dfrac{d^2w}{dx^2}$;

(b) the curvature, $\chi = " + \dfrac{w}{R^2}$; and

(c) the curvature, $\chi = " + \dfrac{1}{R}\dfrac{du}{dx}$.

where   w   is the radial displacement;

       u   is the tangential displacement;

       x   is the distance to the point under consideration measured along the length of the members from end 1;

and   R   is the radius of the curve.

The curvature - displacement expressions (b) and (c) are due to Flügge and Timoshenko respectively. It is noticed that in both of these, the second term on the right allows for the influence of the initial curvature. Furthermore, as the radius, R, is increased to infinity both expressions reduce to that given by (a) which is for straight beams. In the case of polynomial functions, all three relationships are used. On the other hand, the derived displacement functions utilize the first two expressions only.

The in-plane curvature-displacement relationships for curved members are well known. However, the curvature-displacement relationship for the out of plane case is not known. This is derived in Chapter 5. The out of plane stiffness matrices are then obtained using the cubic and the derived displacement functions, both of which use the same curvature-displacement relationship.

Civil engineering structures are often irregular and offsets of members from their joints are unavoidable in these structures. In areas prone to appreciable unequal settlement, mechanical pins are used to prevent structural damage. To obtain representative results, the influence of these features should be taken into account. In Chapter 7 displacement transformation matrices, both for the in-plane and out of plane cases, are constructed which allow for the effect of offsets as well as the hinges. Results for two structures with offsets and hinges are given. One is an arch bridge in which the arch is part of a plane frame. The other is a bow girder. The theoretical results for the latter are compared with those obtained experimentally.

C H A P T E R   2

THE SOLUTION OF A SET OF SIMULTANEOUS EQUATIONS

2.1 Introduction

The sub-routine developed to solve a set of symmetric simultaneous equations is described in this chapter. Because of its efficiency in the use of store, a locally variable band-width method of storage is used for the coefficients of the variables. Both the left and the right-hand sides are divided into blocks for storage in the backing store. This increases the size of the problem that can be solved with a given core space in the computer.

Choleski's method of factorisation is best suited to solve such a set of equations, but it gives inaccurate results for equations with weak diagonal elements which can occur in instability problems. The direct elimination method does not suffer from such draw-backs. Furthermore, if used without row or column interchange, more than one right-hand side can be dealt with. A variation of the latter method is adopted here.

2.2 Method of Storage

The coefficients of the left-hand side matrix are stored in a one-dimensional array. This is called the main sequence. The elements are stored row by row, starting from the first non-zero element up to and including the diagonal elements. The zero elements outside the boundary of the locally variable band remain zero during the solution process, hence they are not stored.

The coefficients of the right-hand sides are also stored row by row in a one-dimensional array. The solution vectors,

whose elements are always non-zero, overwrite the left-hand
side vectors. The right-hand sides are, therefore, stored
in full.

To use the backing store facilities more efficiently, both
sides are divided into blocks. The number of elements in any
block is equal to, or less than, a specified number. For
computers with the facility of buffer zone, the size of the
blocks should be equal to the size of the buffer zone. However,
when using a computer without a buffer zone, the user fixes
the block size. This is done according to the core store
available. Every block must contain an integral number of rows.
A block may consist of only one equation. This condition
imposes a restriction ~~of~~ *on* the maximum number of elements to be
stored for any one row. Therefore, when numbering the nodes,
care should be taken to ensure that the number of elements, to
be stored, for any row does not exceed the number of elements
permitted in a block. If necessary, extra nodes should be
introduced to reduce the bandwidth locally (32). Finally, a
block of the right-hand side contains the same number of rows
as the corresponding block of the left-hand side.

An address sequence array, IS, is used to locate the
elements stored in the main sequence. The elements of the IS
array give the position of the diagonal elements. Utilizing
this information, the position of an element a_{ij} , for example,
is computed from the following formula:-

$$m = IS(i) - i + j \qquad\qquad (2.1)$$

where   IS(i) gives the position of the diagonal
           element of row i.

The element a_{ij} occupies the mth position in the main
sequence.

2.3 Compact Elimination Method

In the direct elimination method, all the elements below the leading diagonal are reduced to zero while those on the leading diagonal are reduced to unity. The elements in the first column are eliminated by subtracting suitable multiples of the first row from the subsequent ones. Then suitable multiples of the second, modified row are subtracted from the subsequent rows to reduce the elements of the second column to zero. This process is continued until all the elements below the leading diagonal have been reduced to zero. Finally, each element on the leading diagonal is made equal to unity by dividing the equation by the diagonal element itself.

Thus an element a_{ij} occuring in the upper triangle may be modified several times as its counterpart a_{ji} is eliminated. In the compact elimination method, an element is completely modified in one step. It is easy to show that this compact elimination is carried out as follows:-

For the off diagonal elements:-

$$a_{ij} = c_{ij} \; a_{ij} \tag{2.2}$$

where
$$c_{ij} = a_{ij} - \sum_{k=r}^{j-1} c_{ik} \; a_{jk} \tag{2.3}$$

and for the diagonal elements:

$$a_{ii} = 1/c_{ii} \tag{2.4}$$

where
$$c_{ii} = a_{ii} - \sum_{k=r}^{i-1} c_{ik} \; a_{ik} \tag{2.5}$$

In equations (2.2) and (2.5) r is equal to the column number of first non-zero element of row i or j; whichever is the greater of the column numbers.

From equations (2.2) to (2.5) it is obvious that the coefficients c_{ij} are needed to modify the subsequent elements of row i. These coefficients must be stored until they are no longer needed. The store space required for c_{ij}'s is termed the temporary store. For row by row elimination, the size of the temporary store required is equal to the maximum number of elements stored for any row. However, in the sub-routine developed here, the elimination is carried out column by column. The size of the temporary store required in this case is equal to the block size.

Parallel operations are performed on the right-hand sides as well. All the steps in the modification of an element of the right-hand side can be expressed in compact form as:-

$$b_{ij} = a_{ii}[\; b_{ij} - \sum_{k=r}^{i-1} c_{ik}\, b_{kj}\;] \tag{2.6}$$

where r is the column number of first non-zero element of row i.

Two subscripts for the element, b_{ij}, indicate that more than one right-hand side can be dealt with.

After both sides have been completely reduced, the last equation, n, gives the values of the unknowns x_{nj}. Substituting these values of x_{nj} into equation n-1 yields the values of the corresponding unknowns. This process of back substitution is repeated until all the elements of the solution matrix have been calculated. All the steps involved in the back substitution can also be expressed in compact form. Doing this, the following expression is obtained:-

$$x_{ij} = b_{ij} - \sum_{k=i+1}^{m} a_{ki}\, x_{kj} \tag{2.7}$$

where m is the largest row number of an element

        stored for column k of the left-hand side

        matrix.

2.4 Elimination by Blocks

The core space available may not be sufficient to solve
a large set of simultaneous equations. The use of backing store
then becomes necessary. The transferring of the information to
and from the backing store is a slow process compared to the
speed of the fast store. It is better to make few large tran-
sfers than several small ones.

The coefficients on both sides are divided into blocks as
explained in section 2.2. If the division is done by hand and
the information fed into the computer as data, no problem
arises. However, the size and the shape of the stiffness matrix
changes with the structure and the method of numbering the nodes
of the structure adopted. Furthermore, the stiffness matrices
are, preferably, constructed by the computer. This reduces
the data to be fed into the computer. It is preferable to use
the computer to divide the stiffness matrix and the load array
into blocks. To do this, the computer needs the address se-
quence array which has been defined and explained in section
2.2.

In addition to the address sequence array, two more arrays
are needed in the solution by blocks. The use of the latter
arrays will become clear later in this section. These arrays
are:-

(i) IR - array : this array holds the last row number

                in each block; and

(ii) IB - array :   this array gives the first block
                    required by each block in the
                    reduction process.

The three arrays mentioned above are constructed auto-
matically from the information supplied to the computer. How
this is done is explained in section 2.5.

To reduce row i, row j may be needed. It is possible that
rows i and j are held in different blocks. Hence sufficient
working core is required to hold two blocks at the same time.
The block in which row i occurs is called the active block.
The block which holds row j is called the passive block. At
some stage of the reduction process an active block, P, is read
from the backing store. It is possible to bring the first block
into the working core to act as the passive block. Then the
successive blocks act as the passive blocks, one at a time.
But the first few blocks may not be needed to reduce the active
block, P. This depends on the position of the elements of the
active block in the left-hand side matrix. To save computer
time, such unnecessary block transfers should be avoided al-
together.

The IB array, defined earlier, is used for this purpose.
It gives the first passive block, Q, required by an active
block, P. A test is made to determine whether block Q is
already in the working core. If it is not, then it is read
from the backing store into the working core. With these
blocks in the working core, the active block, P, is reduced as
much as possible. Block Q + 1 is then brought from the backing
store to reduce the active block further. Then block Q + 2
becomes the passive block and so on. Eventually a stage is

reached when all the equations required to complete the reduction of block P are held within the active block itself. The active block is then reduced completely and transferred to the backing store. The contents of the temporary store are also written into the backing store. Block P + 1 is then read into the working core to become the active block. The whole process is then repeated. In this manner, all the blocks are reduced and written into the backing store.

Parallel operations can be performed on the right-hand sides. Alternatively, as is done in this sub-routine, the right-hand sides can be reduced after the left-hand side has been reduced completely. The process is similar to that used in the reduction of the left-hand side.

From the information held in array IR, the row numbers of the first and last row held in a block are determined. This specifies which rows, of the active block, are to be reduced. The row numbers of the passive block decide the extent to which the active block can be reduced with a given passive block. Thus the start and the finish of various reduction cycles, for a particular active and a passive block, is determined by using the IR array.

When both sides have been completely reduced, the process of back substitution is started using the last blocks of both sides first. The right-hand side block is transformed into the solution block by back substitution. This solution block is then transferred to the backing store where it occupies the same space as previously occupied by the corresponding block of the right-hand sides. The preceding blocks, to the last ones, of both sides are then read from the backing store.

Further back substitution and solution is carried out. After a block of the right-hand sides has been transformed into a solution block, it is written into the backing store. This process is repeated until the right-hand sides have been completely transformed into the solution matrix and written into the backing store.

Thus the process of back substitution is in some ways the reverse of the elimination.

2.5 Automatic Construction of Address Sequence and Other Arrays

The construction of address sequence and other arrays, required to solve a set of simultaneous equations by blocks, is best illustrated by an example. For simplicity, only a plane frame is considered. The principle, however, is the same for three dimensional structures. A rigid jointed plane roof truss is shown in fig. 2.1. All the free nodes are numbered consecutively. The supports do not contribute to the stiffness matrix. Alternatively, to render the stiffness matrix non-singular columns and rows corresponding to the supports are removed from it. The stiffness matrix is then as shown in fig. 2.2. As the matrix is symmetric, the elements above the leading diagonal have been left out. The shaded squares indicate the possible non-zero elements. The elements within the boundary are stored as the main sequence.

(i). The Address Sequence Array

Consider a joint, j, of the structure. The lowest joint number, i, to which joint j is connected by a member is determined from the data supplied to the computer. The number of elements stored for the first row for joint j is then cal-

culated from the following expression:-

$$m = n \cdot (j - i) + 1 \qquad (2.8)$$

where   n is equal to the degrees of freedom of

the joints of the structure.

For each subsequent rows, for the joint j, the number of elements increases by one. This can be seen from fig. 2.2.

Starting with the first joint of the structure, the number of elements to be stored for each row is computed. A simple addition of the number of elements for m rows gives the location of the diagonal element of mth. row in the main sequence. The number obtained by adding the number of elements of m rows is also the mth element of the address sequence.

(ii) IR Array

Given the block size, the computer divides the stiffness matrix into blocks by scanning the address sequence array. The blocks are required to contain an integral number of rows. From fig. 2.2, it is seen that the last element stored for each row is a diagonal element. Consider block P. Let the last row for block P - 1 be q and the last row for block P be p. Then the difference between the pth and qth element of the address sequence array is equal to or just less than the block size. The difference between the p + 1th and the qth element is greater than the block size. The row numbers q and p form two of the consecutive elements of the IR array.

(iii) IB Array

The IR array gives the row numbers held in a block. The column number of the first non-zero element of each row can be determined from the address sequence array. The column numbers, c's, of each row in a block, P, are examined. The lowest, q,

of the c's is determined. Then the first passive block, Q, required to reduce block, P, holds row q. Thus the Pth element of the IB array is put equal to Q. Similarly, consideration of all the blocks completes the construction of the IB array.

2.6 The Flow Diagram

A detailed flow diagram for the sub-routine to solve a set of simultaneous equations is given in figs. 2.3 and 2.4. More than one right-hand sides can be solved. The computer programme appears in Appendix A as sub-routine CDM. The flow diagram is self-explanatory.

The size of the blocks is treated as variable. The left-hand side is divided into blocks and stored in the backing store block by block. The right-hand sides are stored in the backing store as a continuous.array. The alterations are simple and few to modify the programme so that blocks of fixed size are transferred. At present, the arrays are transferred to and from the backing store in parts.

2.7 Error in Solution

The substitution of a solution vector into the original left-hand side yields a vector. Comparing this vector with the corresponding original vector of the right-hand sides gives an estimate of the error involved in the solution sub-routine. The sub-routine, however, has been checked by solving some problems whose solution was already known.

2.8 Conclusions

1. The locally variable bandwidth method used for the

storage of the left-hand side matrix requires minimum storage space (33).

2. More than one right-hand side can be dealt with.

3. The use of backing store facilities enables large problems to be solved.

4. The direct elimination method used is known to give reasonable results, even for ill-conditioned equations (32).

5. The column by column elimination adopted for the left-hand side requires more searching operations. Therefore, it is better to use row by row reduction. Alternatively, the left-hand side should be stored column by column as suggested by Barron and Swinnerton-Dyer (58).

6. Both sides of the equations should be reduced simultaneously. This reduces the number of block transfers and obviates the need to store the contents of the temporary store. However, if a set of simultaneous equations with the same LHS but different RHS is to be solved, it is better to store the contents of the temporary store for future use. Alternatively, the whole problem will have to be solved afresh.
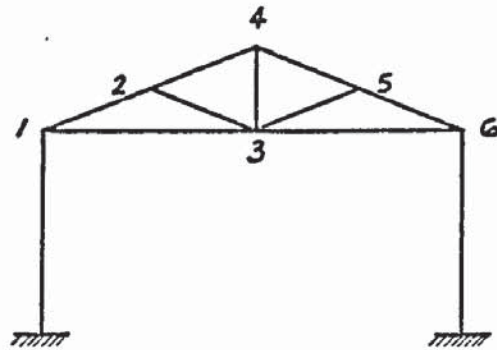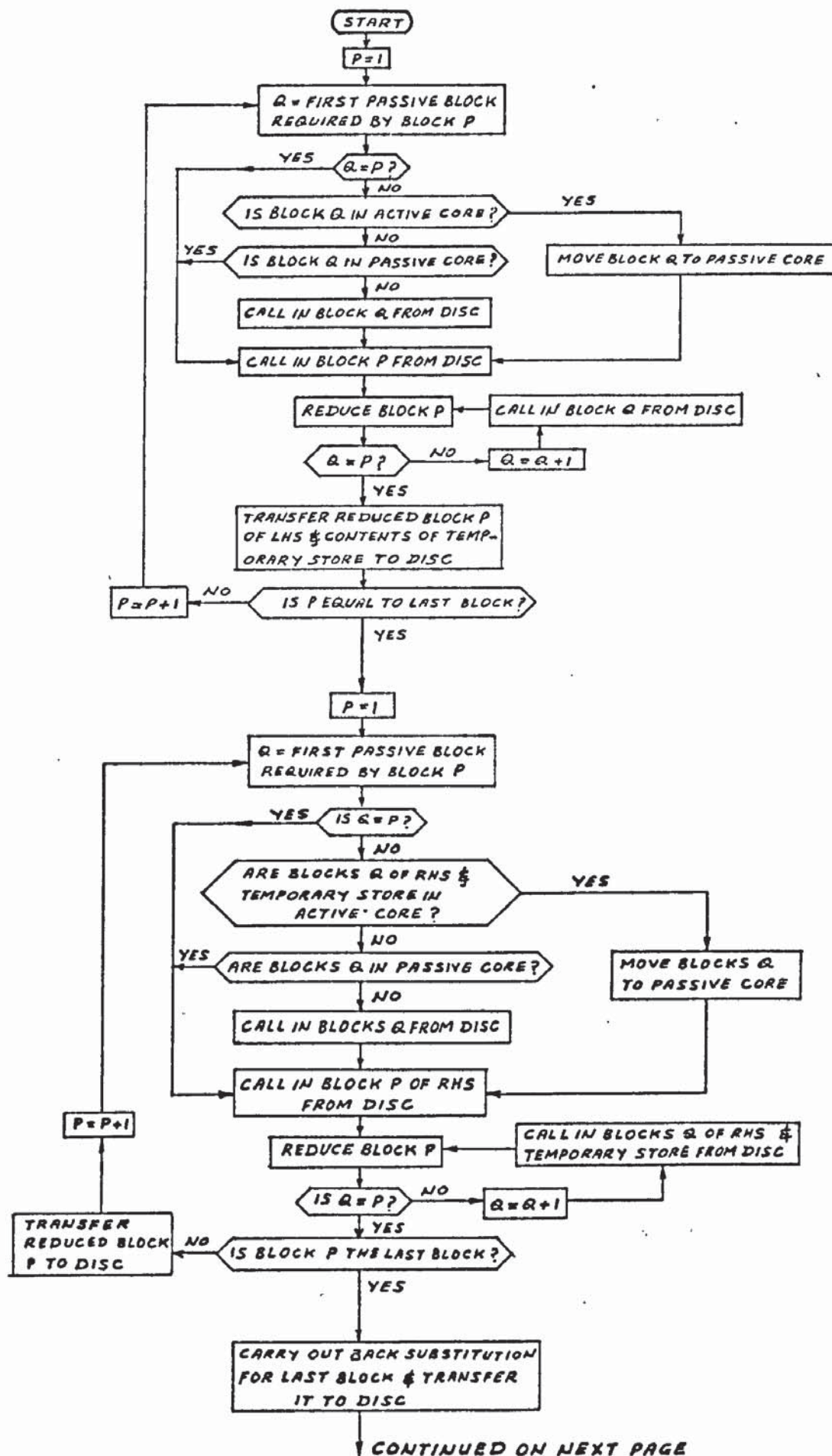
RIGID-JOINTED PLANE FRAME
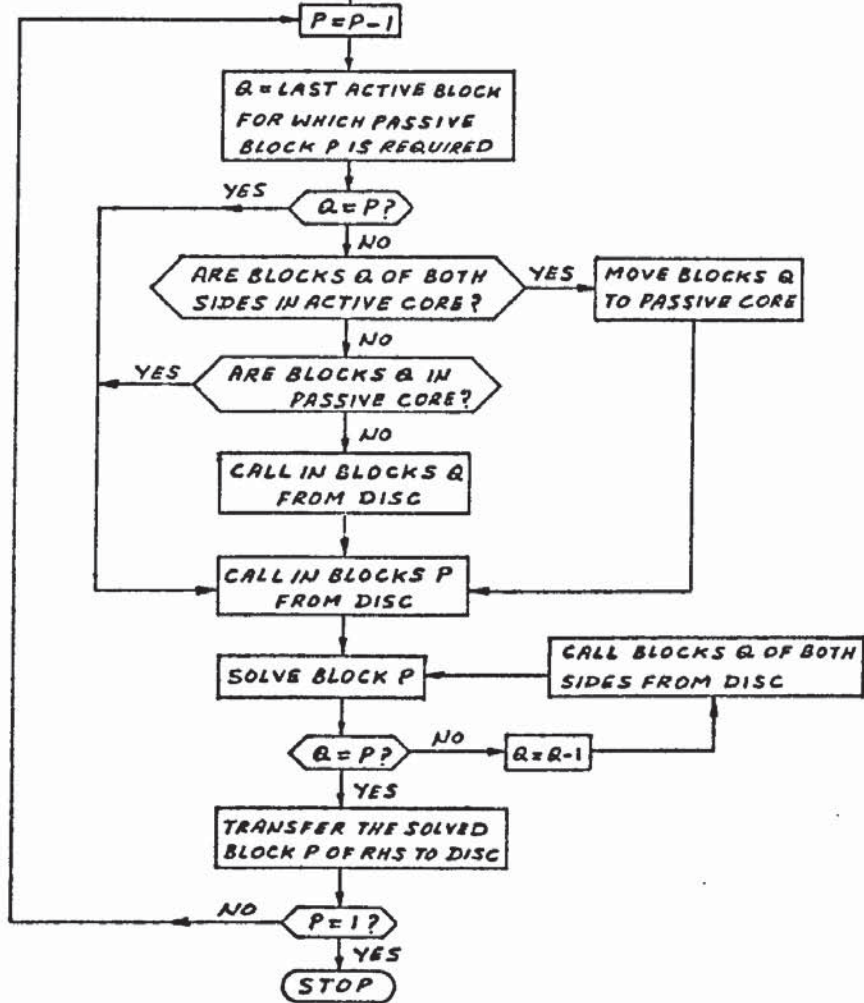
FIG. 2.1
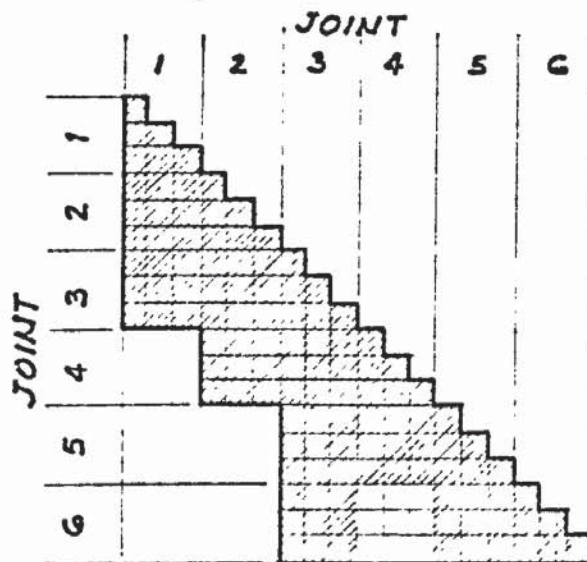
SHAPE OF OVERALL STIFFNESS MATRIX

FIG. 2.2

FLOW DIAGRAM FOR REDUCTION OF BOTH SIDES
OF EQUATIONS

FIG. 2.3

CONTINUED FROM PREVIOUS PAGE

FLOW DIAGRAM FOR BACK SUBSTITUTION

FIG. 2.4

THE FLOW DIAGRAM SHOWN IN FIGS. 2.3 AND 2.4 IS FOR
SUBROUTINE CDM TO SOLVE A SET OF SIMULTANEOUS
EQUATIONS

C H A P T E R   3

CURVED MEMBERS LOADED IN-PLANE

3.1 Introduction

In this chapter, the stiffness matrices for curved elements are developed by using the finite element techniques. Assumed as well as exact displacement functions are used. The latter are obtained by solving the governing differential equations which are obtained by considering an element of a curved member of uniform cross-section. Finally, the same displacement functions are also used to obtain the stiffness matrices for curved elements with variable cross-sections.

3.2 Sign Convention

To interpret the results meaningfully, some datum is required for reference. A set of orthogonal axes, called the global axes, is chosen for this purpose. It is possible to obtain the stiffness matrix for a member in the global co-ordinates directly (16). However, it is more convenient to derive the load-displacement relationships in co-ordinates local to the member. Like the global axes, the local axes are also orthogonal and are so orientated that one local axis coincides with the longitudinal axis of the member. The stiffness matrix, in local co-ordinates, is dependant on the properties of the member only. It is easy to transform the stiffness matrix from local to global co-ordinates. A transformation matrix is used for this purpose, the elements of which are functions of the position of the member in the structure and its inclination to the global axes.

A set of global axes is shown in fig. 3.1. The forces applied at the joints of the structure are positive when acting along the positive directions of the axes. The positive directions for the applied moments at the joints are as shown in the figure. The resulting joint displacements are positive when they follow the positive directions for the corresponding forces or moments. The axes, forces and the displacements as shown obey the right-hand screw rule.

Fig. 3.2 shows a set of local axes for a curved member. P-axis is chosen along the tangent and the Q-axis lies along the radial direction, directed towards the centre. The position and direction of the R-axis is then fixed by the right-hand screw rule. The positive directions for member forces and displacements are obtained by following the right-hand screw rule.

3.3 The Stiffness Matrix by Assumed Displacement Functions

(i) The Displacement Functions

Using the criteria in section 1.3(iv), the following displacement functions of polynomial form are assumed:-

For the radial displacements:-

$$w = a_1 + a_2 x + a_3 x^2 + a_4 x^3 \tag{3.1}$$

and for the tangential displacements:-

$$u = a_5 + a_6 x \tag{3.2}$$

where $a_1 - a_6$ are the arbitrary constants;

and x is the distance from end 1 to the point in

the member under consideration measured

along the curve.

The displacement functions chosen, equations (3.1) and (3.2), indicate that the radial and the tangential displacements are independant of each other. This assumption is reasonable for straight prismatic members within the small deflection theory. The displacement functions, equations (3.1) and (3.2), are sometimes called the beam functions.

There are three in-plane displacements for each end of the member, a displacement along the tangent, a radial displacement towards the centre, and a rotation about the R-axis. These six nodal displacements define the six arbitrary constants, $a_1 - a_6$, used in the displacement functions uniquely.

The equation for slope is obtained by differentiating equation (3.1) with respect to x; thus:-

$$\frac{dw}{dx} = a_2 + 2a_3 x + 3a_4 x^2 \tag{3.3}$$

Substituting the end conditions into equations (3.1) to (3.3) gives:-

For end 1 ; x = 0 :

The radial displacement   ; $w_1 = a_1$ (3.4)

The tangential displacement; $u_1 = a_5$ (3.5)

and the slope at end 1   ; $\theta_1 = a_2$ (3.6)

For end 2, x = L; the curved length of the element:

From eqn. (3.1), the radial displacement is given by:-

$$w_2 = a_1 + a_2 L + a_3 L^2 + a_4 L^3 \tag{3.7}$$

from eqn. (3.2), the tangential displacement is:-

$$u_2 = a_5 + a_6 L \tag{3.8}$$

and finally from eqn. (3.3), the slope at end 2 is:-

$$\theta_2 = a_2 + 2a_3 L + 3a_4 L^2 \tag{3.9}$$

Solving the simultaneous equations, (3.4) to (3.9), the six arbitrary constants are expressed in terms of the six nodal displacements. Writing these relationships in matrix form yields:-

$$
\begin{bmatrix} a_1 \\ a_2 \\ a_3 \\ a_4 \\ a_5 \\ a_6 \end{bmatrix} = \begin{bmatrix} 1 & 0 & 0 & 0 & 0 & 0 \\ 0 & 1 & 0 & 0 & 0 & 0 \\ -\dfrac{3}{L^2} & -\dfrac{2}{L} & \dfrac{3}{L^2} & -\dfrac{1}{L} & 0 & 0 \\ \dfrac{2}{L^3} & \dfrac{1}{L^2} & -\dfrac{2}{L^3} & \dfrac{1}{L^2} & 0 & 0 \\ 0 & 0 & 0 & 0 & 1 & 0 \\ 0 & 0 & 0 & 0 & -\dfrac{1}{L} & \dfrac{1}{L} \end{bmatrix} \begin{bmatrix} w_1 \\ \theta_1 \\ w_2 \\ \theta_2 \\ u_1 \\ u_2 \end{bmatrix}
$$

(3.10)

or in compact form this is:-

$$\{a\} = [C]^{-1} \{\delta\}$$

(3.11)

Equation (3.11) is seen to be the same as equation (1.3). The vectors, $\{a\}$ and $\{\delta\}$, and the matrix, $[C]^{-1}$, are defined in section 1.2.

(ii) The Strain - Displacement Relationships

For curved members within the small deflection theory, there are two components of strain. The first part is identical to that for straight members. The second contribution represents the influence of the initial curvature, R, of the member. The latter can be obtained by considering the radial displacement of a curved member. The total strains are obtained by adding the two components.

Fig. 3.3 shows a curved member of radius R. The curved length AB subtends an angle θ at the centre. The member suffers

radial displacements only as shown in the figure.

(a) The Axial Strain in the Member

The initial curved length AB of the member is given by:-

$$l = R \cdot \Theta \tag{3.12}$$

After straining due to radial displacements, the length of the member becomes:-

$$l' = (R - w) \cdot \Theta \tag{3.13}$$

From equations (3.12) and (3.13) the axial strain in the member , due to w, can be obtained; viz:

$$\varepsilon = \frac{l-l'}{l} \tag{3.14}$$

Substituting equations (3.12) and (3.13) into eqn. (3.14), yields:-

$$\varepsilon = -\frac{w}{R} \tag{3.15}$$

Superimposing the axial strain due to the radial displacement given by equation (3.15) onto that obtained for straight member leads to the following relationship:-

$$\varepsilon_x = \frac{du}{dx} - \frac{w}{R} \tag{3.16}$$

(b) The Bending Cruvature

From fig. 3.3, it is obvious that after deformation the radius, R, of the member reduces to R - w. This produces a bending curvature in the member which is:-

$$\chi' = \frac{1}{R-w} - \frac{1}{R} \tag{3.17}$$

Upon simplification, equation (3.17) becomes:-

$$\chi' = \frac{w}{R(R-w)} \tag{3.18}$$

The displacement, w, is very small compared to the radius, R, of the member. The following approximation can, therefore, be made:-

$$R - w \simeq R \tag{3.19}$$

Substituting equation (3.19) into equation (3.18) gives the bending curvature due to w as:-

$$\chi' = \frac{w}{R^2} \tag{3.20}$$

Once again, superimposing the strains due to the radial displacement, w, given by eqn. (3.20) onto that obtained for straight members leads to the following expression:-

$$\chi = \frac{d^2w}{dx^2} + \frac{w}{R^2} \tag{3.21}$$

In equations (3.16) and (3.21) the radial displacement, w, is assumed to be positive when towards the centre. This is the reason for choosing the local axis, Q, as directed towards the centre as shown in fig. 3.2 and discussed in section 3.2. It is noticed from equations (3.16) and (3.21) that the influence of the initial curvature, R, of the element is represented by the second term on the right-hand side. For straight members, the radius, R, becomes infinity. When this is substituted in equations (3.16) and (3.21) the second terms on the right vanish and the equations revert back to those which are obtained for straight members.

Differentiating equation (3.2) with respect to x gives:-

$$\frac{du}{dx} = {}^a\varepsilon \tag{3.22}$$

Similarly, differentiating equation (3.3) with respect to x yields:-

$$\frac{d^2w}{dx^2} = 2a_3 + 6a_4x \tag{3.23}$$

Substituting equations (3.1) and (3.22) into eqn. (3.16) and equations (3.1) and (3.23) into eqn. (3.21) leads to the following matrix relationship for the axial strain and the bending curvature:-

$$\begin{bmatrix} \varepsilon_x \\ \\ \chi \end{bmatrix} = \begin{bmatrix} -\frac{1}{R} & -\frac{x}{R} & -\frac{x^2}{R} & -\frac{x^3}{R} & 0 & 1 \\ \\ \frac{1}{R^2} & \frac{x}{R^2} & \frac{2+x^2}{R^2} & \frac{6x+x^3}{R^2} & 0 & Q \end{bmatrix} \begin{bmatrix} a_1 \\ a_2 \\ a_3 \\ a_4 \\ a_5 \\ a_6 \end{bmatrix} \tag{3.24}$$

In more condensed form, equation (3.24) is written as:-

$$\{\varepsilon\} = [A] \{a\} \tag{3.25}$$

Equation (3.25) is the same as eqn. (1.4). The vectors, $\{\varepsilon\}$ and $\{a\}$, and the matrix, $[A]$, have already been defined. In matrix $[A]$ the terms containing R account for the influence of the initial curvature. Increasing R to infinity reduces matrix $[A]$ to that obtained for straight members.

For long thin members, the strain energy due to shear is negligible compared to the strain energy due to bending and axial forces. Therefore, only axial strains and bending curvatures have been considered.

Following the steps outlined in equations (1.5) to (1.7), the strains can be expressed in terms of the nodal displacements. This strain-nodal displacement relationship is expressed by equation (1.6).

(iii) The Stress-Strain Relationships

The curved members dealt with in this Thesis are one-dimensional. For elastic material which obeys Hooke's law, the forces are related to the strains as follows:-

The axial force, $\quad\quad\quad \sigma = EA \ \varepsilon_x \quad\quad\quad\quad$ (3.26)

and the bending moment, $\ M = E I \ \chi \quad\quad\quad\quad$ (3.27)

where E is the modulus of elasticity of the material;

A is the cross-sectional area of the member;

and I is the second moment of area of the member for in-plane bending.

Writing equations (3.26) and (3.27) in matrix form:-

$$
\begin{bmatrix} \sigma \\ M \end{bmatrix} = \begin{bmatrix} EA & 0 \\ 0 & EI \end{bmatrix} \begin{bmatrix} \varepsilon_x \\ \chi \end{bmatrix} \quad\quad (3.28)
$$

or to write equation (3.28) more concisely:-

$$
\{\sigma\} = [D] \ \{\varepsilon\} \quad\quad\quad\quad (3.29)
$$

Equation (3.29) is seen to be the same as equation (1.8). The vectors, $\{\sigma\}$ and $\{\varepsilon\}$, and the matrix, $[D]$, are already defined.

The strain energy due to shear can be included. This adds another row to the strain matrices, $[A]$ and $[B]$, and the elasticity matrix, $[D]$. The latter then becomes a 3 x 3 matrix; the third element being the shear rigidity of the member.

(iv) The Stiffness Terms

The stiffness matrix is obtained by carrying out the triple matrix multiplication in equation (1.16) and integrating the results. This exercise leads to the following recurssive

formula for the stiffness elements:-

$$k_{mn} = \int_{o}^{L} (EAB_{1m} B_{1n} + EI B_{2m} B_{2n}) \, dx \qquad (3.30)$$

where B_{rs} are the elements of the strain matrix $[B]$.

The integration in equation (3.30) is with respect to length and not over the volume as was the case in equation (1.16). This is due to the resultant forces in equation (3.30) instead of the stresses that are implied in equation (1.16).

Carrying out the integrations, equation (3.30) yields the elements of the stiffness matrix for a member. These stiffness elements for a curved member of uniform cross-section are:-

$$k_{11} = EA \left(\frac{13}{35} \frac{L}{R^2}\right) + EI \left(\frac{12}{L^3} + \frac{13}{35} \frac{L}{R^4} - \frac{12}{5} \frac{1}{R^2 L}\right)$$

$$k_{12} = EA \left(\frac{11}{210} \frac{L^2}{R^2}\right) + EI \left(\frac{6}{L^2} + \frac{11}{210} \frac{L^2}{R^4} - \frac{6}{5} \frac{1}{R^2}\right)$$

$$k_{13} = EA \left(\frac{9}{70} \frac{L}{R^2}\right) + EI \left(\frac{-12}{L^3} + \frac{9}{70} \frac{L}{R^4} + \frac{12}{5} \frac{1}{R^2 L}\right)$$

$$k_{14} = -EA \left(\frac{13}{420} \frac{L^2}{R^2}\right) + EI \left(\frac{6}{L^2} - \frac{13}{420} \frac{L^2}{R^4} - \frac{1}{5} \frac{1}{R^2}\right)$$

$$k_{15} = EA \left(\frac{1}{2R}\right)$$

$$\qquad (3.31)$$

$$K_{16} = -k_{15}$$

$$k_{22} = EA \left(\frac{1}{105} \frac{L^3}{R^2}\right) + EI \left(\frac{4}{L} + \frac{1}{105} \frac{L^3}{R^4} - \frac{4}{15} \frac{L}{R^2}\right)$$

$$k_{23} = - k_{14}$$

$$k_{24} = - EA \left(\frac{1}{140} \frac{L^3}{R^2}\right) + EI \left(\frac{2}{L} - \frac{1}{140} \frac{L^3}{R^4} + \frac{1}{15} \frac{L}{R^2}\right)$$

$$k_{25} = EA \left(\frac{L}{12R}\right)$$

$$K_{26} = - k_{25}$$

(3.31) Continued

$$k_{33} = k_{11}$$

$$k_{34} = -k_{12}$$

$$k_{35} = k_{15}$$

$$k_{36} = -k_{15}$$

$$k_{44} = k_{22}$$

$$k_{45} = -k_{25}$$

$$k_{46} = k_{25}$$

$$k_{55} = \frac{EA}{L}$$

$$k_{56} = -k_{55}$$

$$k_{66} = k_{55}$$

(3.31)

Once again, substituting infinity for R in equations (3.31), the stiffness terms are seen to reduce to those for straight prismatic members. This indicates that the displacement functions given by equations (3.1) and (3.2), are exact for straight members.

Writing the load-displacement equations, it can be shown that the axial forces are dependant on tangential displacements only. Similarly, the shear forces and the bending moments are functions of the radial displacements and rotations only. This is due to the assumed displacement functions being independant of each other.

The bending cruvature-displacement relationship expressed by equation (3.21) is due to Flügge. Another expression commonly employed for curved beams is due to Timoshenko. The

latter is obtained from equations (3.16) and (3.21) as follows:-

From equation (3.16) the following relationship is obtained:-

$$\frac{w}{R^2} = \frac{1}{R} \frac{du}{dx} - \frac{\varepsilon_x}{R} \qquad (3.32)$$

Substituting equation (3.22) into equation (3.21) and neglecting the effect of the axial strain, ε_x, on the curvature yields:-

$$\chi = \frac{d^2w}{dx^2} + \frac{1}{R} \frac{du}{dx} \qquad (3.33)$$

However, for shallow beams, the influence of the initial curvature can be ignored. Equations (3.21) and (3.33) then become identical to the expression obtained for straight members. That is:-

$$\chi = \frac{d^2w}{dx^2} \qquad (3.34)$$

Stiffness matrices were also obtained using equations (3.33) and (3.34) instead of equation (3.21). The stiffness terms for these are not produced here. Results were obtained using all three matrices for various arches to investigate the influence of the three curvature-displacement approximations, equations (3.21), (3.33) and (3.34). Table 3.1 shows typical results for an arch. The radius, R, of the arch is equal to 15 units and the span is equal to 20 units of length. The cross-section of the arch is uniform and is equal to 1.0 x 1.0 unit. The arch is fixed at both ends and carries a unit load at the mid-point. The results tabulated overleaf are for the deflections under the load.

TABLE 3.1

NM	2	4	6	8	10
$\dfrac{d^2w}{dx^2} + \dfrac{w}{R^2}$	0.3464	0.7175	0.8611	0.9147	0.9426
$\dfrac{d^2w}{dx^2} + \dfrac{1}{R}\dfrac{du}{dx}$	0.3451	0.7125	0.8574	0.9124	0.9411
$\dfrac{d^2w}{dx^2}$	"	0.7073	0.8449	0.8964	0.9224
Straight Members	0.5155	0.9669	0.9903	0.9955	0.9974

The assumed displacement functions are approximate. To obtain the rate of convergence of the results the arch was, therefore, divided into various numbers of segments. The number of members is shown in the row marked NM. The deflections obtained by using various methods were divided by the deflection obtained by strain energy. These ratios are tabulated. The last row in the table shows the results obtained by approximating the arch by a number of straight members. The stiffness terms obtained by using the cubic functions allow for the influence of the initial curvature, R, of the member. The cubic functions, therefore, are expected to yield better results than those obtained by approximating the arch with straight members. However, it is surprising to notice that the latter has yielded better results than the cubic functions. Similar observations have been made about the polynomial displacement functions for curved shell elements (24, 61).

It is further observed from Table 3.1, and other results

not produced here, that various expressions for the bending curvature have negligible effect on the results.

This confirms similar observations made by Murray (61). Perhaps the improvement in the results, due to the refinement of the expression for bending curvature, is masked by the approximations involved in the assumed displacement functions. The results obtained by using the stiffness matrix given in equation (3.31) are presented in the next chapter and are marked C.F.

3.4 Derivation of the Exact Displacement Functions.

Fig. 3.4 shows an element of uniform cross-section cut from a thin circular ring of radius R. The curved length of the element is dx and subtends an angle $d\theta$ at the centre 0. Also shown in the figure are the resultant forces transferred from the adjoining elements. These forces are:-

(a) an axial force, P, at end 1 which increases along the length, dx , of the element to P + dP at end 2;

(b) a shear force, S, at end 1 which increases to S + dS at end 2; and finally.

(c) a bending moment, M, at end 1 which increases to M + dM at the second end of the element.

Consider the equilibrium of the element along the bi-secting line OC:-

$$(2P + dP) \sin \frac{d\theta}{2} + (S + dS) \cos \frac{d\theta}{2} = 0 \qquad (3.35)$$

For small angles the following assumptions can be made:-

$$\sin \frac{d\theta}{2} \simeq \frac{d\theta}{2} \qquad (3.36)$$

and $\cos \dfrac{d\theta}{2} \simeq 1.0$ (3.37)

Substituting equations (3.36) and 3.37) into equation (3.35), and ignoring the second order quantities equation (3.35) reduces to:-

$$P \cdot d\theta + dS = 0 \qquad (3.38)$$

Summing the forces along a line passing through the ends of the element gives:-

$$(P + dP) \cos \frac{d\theta}{2} - (S + dS) \sin \frac{d\theta}{2} - P \cos \frac{d\theta}{2} - $$
$$S \sin \frac{d\theta}{2} = 0 \qquad (3.39)$$

Again invoking the relationship for small angles, equations (3.36) and (3.37), and ignoring the second order terms yields:-

$$dP - S \, d\theta = 0 \qquad (3.40)$$

Finally, summing the moments about an axis passing through the second end of the element leads to the third equation of static equilibrium. This equation is:-

$$M + dM - M - S.R \sin d\theta + P.R (1 - \cos d\theta) = 0 \qquad (3.41)$$

Once again making use of the approximations for small angles and neglecting the terms of second order, equation (3.41) is reduced to:-

$$dM - SR \, d\theta = 0 \qquad (3.42)$$

The angle, $d\theta$, subtended at the centre is related to the curved length, dx, of the element as follows:-

$$d\theta = \frac{dx}{R} \qquad (3.43)$$

Substitution of equation (3.43) into the equations of static equilibrium of the element leads to the following differential equations for forces:-

From eqn. (3.38): $P = -R \dfrac{dS}{dx}$ (3.44)

"   "   (3.40): $S = R \dfrac{dP}{dx}$ (3.45)

and finally from eqn. (3.42): $S = \dfrac{dM}{dx}$ (3.46)

Elininating P and S among equations (3.44) to (3.46) yields the basic differential equation for the bending moment in curved beams. This equation is:-

$$\frac{d^3 M}{dx^3} + \frac{1}{R^2} \frac{dM}{dx} = 0$$ (3.47)

Equation (3.47) is similar to equation (6a) of reference (26).

Using the bending curvature-displacement relationship for straight beams, the bending moment is given by:-

$$M = -EI \frac{d^2 w}{dx^2}$$ (3.48)

The term $\dfrac{d^2 w}{dx^2}$ is the curvature in terms of the radial displacements, w, as given in equation (3.34). Differentiating equation (3.48) appropriately and substituting the results into equation (3.47) leads to the required governing differential equation for the radial displacements, w. This equation, after simplification, becomes:-

$$\frac{d^5 w}{dx^5} + \frac{1}{R^2} \frac{d^3 w}{dx^3} = 0$$ (3.49)

The solution of this differential equation is:-

$$w = a_1 + a_2 x + a_3 x^2 + a_4 \sin \frac{x}{R} + a_5 \cos \frac{x}{R}$$ (3.50)

where $a_1 - a_5$ are the arbitrary constants;

and x is the curved distance from end 1 measured along the member.

Eliminating S between equations (3.44) and (3.46) relates the axial force, P, to the bending moment, M, as follows:-

$$P = -R \frac{d^2M}{dx^2}$$ (3.51)

Differentiating equation (3.48) with respect to x twice and substituting the results into equation (3.51) yields:-

$$P = EIR \frac{d^4w}{dx^4}$$ (3.52)

The axial force, P, is related to the axial strain, ε_x, by Hooke's law as:-

$$P = EA \left(\frac{du}{dx} - \frac{w}{R}\right)$$ (3.53)

The quantity in parenthesis in equation (3.53) is the axial strain in curved members and is the same as given in equation (3.16). The right-hand sides of equations (3.52) and (3.53) are equal to each other. From this equality the following relationship is obtained between the axial and the radial displacements:-

$$\frac{du}{dx} = \frac{I}{A} R \frac{d^4w}{dx^4} + \frac{w}{R}$$ (3.54)

Differentiate eqn. (3.50) with respect to x four times and substitute the results thus obtained, together with eqn. (3.50) itself into eqn. (3.54). This yeilds the required differential equation for the tangential displacements whose solution is:-

$$u = a_1 \frac{x}{R} + a_2 \frac{x^2}{2R} + a_3 \frac{x^3}{3R} - a_4 \left(1 + \frac{I}{AR^2}\right) \cos \frac{x}{R}$$
$$+ a_5 \left(1 + \frac{I}{AR^2}\right) \sin \frac{x}{R} + a_6$$ (3.55)

where $a_1 - a_5$ are the same arbitrary constants as in eqn. (3.50)

and a_6 is an additional constant of integration.

Equations (3.50) and (3.55) are the displacement functions for the radial and the tangential displacements respectively. The displacement functions have been obtained using the curvature-displacement relationships for straight members. Therefore, these functions are expected to yield reasonably accurate results for shallow curved members for which the influence of the initial curvature is small. These are called the approximate functions and the results obtained by using these are marked A.F.

More accurate displacement functions can be obtained by using the curvature-displacement relationship given in equation (3.21). All the steps involved in the derivation of these functions are the same as used to obtain equations (3.50) and (3.55). The following displacement functions are obtained:-

For the radial displacements:-

$$w = a_1 + a_2 \sin \frac{x}{R} + a_3 \cos \frac{x}{R} + a_4 \, x \sin \frac{x}{R} +$$

$$a_5 \, x \cos \frac{x}{R}$$

(3.56)

and for the tangential displacements:-

$$u = a_1 \frac{x}{R} - a_2 \cos \frac{x}{R} + a_3 \sin \frac{x}{R} + a_4 \left[\left(R - \frac{2I}{AR} \right) \sin \frac{x}{R} - \right.$$

$$\left. x \cos \frac{x}{R} \right] + a_5 \left[\left(R - \frac{2I}{AR} \right) \cos \frac{x}{R} + x \sin \frac{x}{R} \right] + a_6$$

(3.57)

where $a_1 - a_6$ are the arbitrary constants.

The displacement functions, equation (3.56) and (3.57), are called the exact functions and the results obtained by using these are marked E.F. The influence of the initial curvature, R, can be seen by comparing the two sets of displacement functions.

It is observed that the form of the approximate functions, equations (3.50) and (3.55), is similar to the displacement functions obtained by reducing the Cantin and Clough (24) shell element to an arch element (61).

3.5 The Exact Stiffness Matrix

Various steps involved in the formulation of the exact stiffness matrix for the curved elements are the same as outlined in section 1.2 and used in section 3.3. The algebraic expressions, however, become more complex than was the case with the cubic displacement functions. Therefore, all the details are given in Appendix B.

(i) The Displacement Functions

Only the exact displacement functions, equations (3.56) and (3.57), are used here. Although the results for the approximate functions, equations (3.50) and (3.55), are also presented in the next chapter, the details for the development of the stiffness matrix using these functions have been left out.

The equation for the slope at any point along the curve of the element is obtained by differentiating equation (3.56) with respect to x. Substituting the boundary conditions into the equations for the displacements and the slope yields a set of simultaneous equations which express the nodal displacements in terms of the arbitrary constants. These equations are then solved to express the arbitrary constants in terms of the nodal displacements. The final result is similar to that represented by equations (3.10) and (3.11) for the cubic functions.

(ii) The Strain-Displacement Relationships

The strain-displacement relationships employed in the

derivation of the displacement functions are also used here. These are given in equations (3.16) and (3.21). Differentiate the displacement functions, equations (3.56) and (3.57), as required and substitute the results into the equations for axial strain, equation (3.16), and the bending curvature, equation (3.21). The strains are then expressed in terms of the arbitrary constants. Writing these relationships leads to the following equations, in matrix form:-

$$
\begin{bmatrix} \varepsilon_x \\ \chi \end{bmatrix} = \begin{bmatrix} 0 & 0 & 0 & \psi_1 & \psi_2 & 0 \\ \dfrac{1}{R^2} & 0 & 0 & \psi_3 & \psi_4 & 0 \end{bmatrix} \begin{bmatrix} a_1 \\ a_2 \\ a_3 \\ a_4 \\ a_5 \\ a_6 \end{bmatrix} \qquad (3.58)
$$

where $\psi_1 = -\dfrac{2I}{AR^2} \cos \dfrac{x}{R}$; $\psi_2 = \dfrac{2I}{AR^2} \sin \dfrac{x}{R}$;

$$(3.59)$$

$\psi_3 = \dfrac{2}{R} \cos \dfrac{x}{R}$; and $\psi_4 = -\dfrac{2}{R} \sin \dfrac{x}{R}$

Consideration of equations (3.58) and (3.59) show that as the radius, R, becomes infinity, the strains vanish. The exact displacement functions, therefore, cannot be used for straight members by making R equal to infinity. Similar observations were also made for the approximate functions.

(iii) The Stress-Strain Relationships

The stress-strain relationships are the same as used in section 3.3 for the cubic functions and are given in equations (3.26) to (3.29).

(iv) The Stiffness Terms

The formula for the stiffness terms is the same as for the cubic functions, equation (3.30). However, the various expressions in the strain matrix are now more complicated and the integrations involve trignometric functions. Final results are given in Appendix B.

3.6 Curved Members with variable Cross-Section

(i) Variation of Cross-Section

The cross-section of a member can vary in several ways. The simplest way to represent the variation is to use a polynomial expansion for the area and the second moment of area of the cross-section. Any type of variation can be allowed for by including sufficient number of terms of the polynomial. The coefficients of the polynomial may vary from member to member. These coefficients, therefore, will have to be calculated for each member with variable cross-section and fed into the computer as data. The alternative is to make the variation of the cross-section less ambitious.

It is assumed that the dimensions of the cross-section vary linearly from end one to end two of the member. The first three terms of the polynomial give the cross-sectional area at any point along the length of the member accurately. Similarly the second moment of area is defined uniquely by the first five terms of the polynomial. The coefficients of the two polynomial equations are easily expressed in terms of the dimensions of the cross-sections at the ends of the member. Furthermore, these expressions for the coefficients are applicable to all members with variable cross-sections.

(ii) The Cubic Displacement Functions

The polynomial displacement functions, equations (3.1) and (3.2), can be used to develop the stiffness matrix for a curved element with variable cross-section. The equations (3.1) to (3.25) remain unaltered as these are independent of the cross-sectional properties of the element. The polynomials for the area, A, and the second moment of area, I, should be substituted into eqn. (3.30) before the integrations are performed to obtain the stiffness terms.

(iii) The Exact Displacement Functions (as used for uniform members)

In section 3.4, the displacement functions were derived by assuming that the cross-section of the curved element was uniform. For elements with variable cross-section the area, A, and the moment of inertia, I, of the cross-section should be treated as variables. This makes the derivation of the displacement functions more difficult. For this reason, the displacement functions obtained for elements with uniform cross-section are used to develop the stiffness matrix for a curved element with variable cross-section.
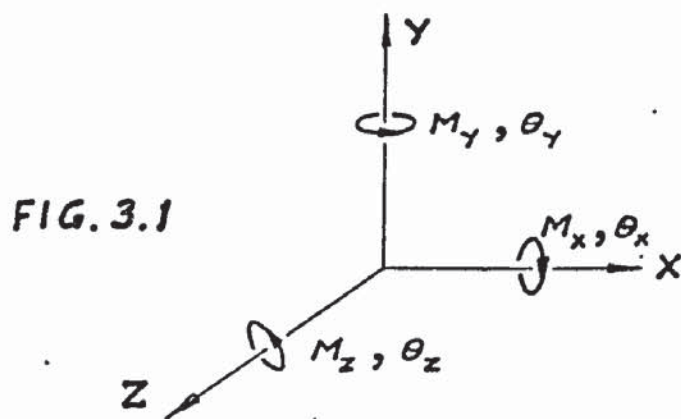
In the displacement functions, the properties of the cross-section, A and I, can be treated as variables. However, since the displacement functions are for members of uniform cross-section, it is more logical to use the values of A and I for average cross-section. This means that the strains in the curved member with the variable cross-section are the same as in the member with uniform cross-section. The strain energy, however, is obtained by integrating over the volume of the member with the variable cross-section.

It is more convenient to use numerical integration to obtain the stiffness terms. It is easy to calculate the dimensions of the cross-section at the point under consideration and use these to obtain the area, A, and the second moment of area, I.
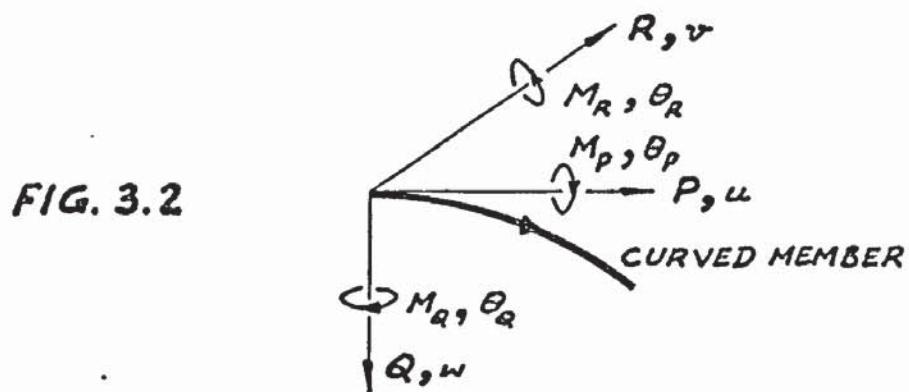
The details of the stiffness matrices for curved elements with variable cross-section are not produced in this Thesis.
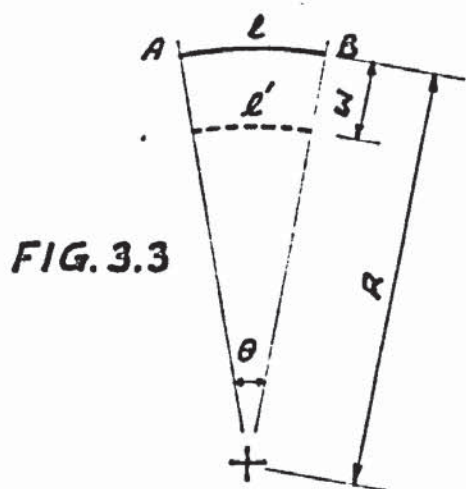
3.7 Uniformly Distributed Loads.

In the matrix analysis of structures the loads are assumed to act only at the nodes of the structure. Equivalent static loads are applied at the nodes for the members carrying uniformly distributed loads. There are two methods of calculating the equivalent nodal forces more accurately. One method is to use the principle of virtual work in which the work done by the equivalent nodal forces is equated to the work done by the uniformly distributed loads. The other method is to use the strain energy method to calculate the fixed end reactions for a curved member carrying uniformly distributed loads. The latter method is used in this Thesis.

FIG. 3.1

M_Y, θ_Y

M_X, θ_X X

M_Z, θ_Z

Z

Y

SIGN CONVENTION FOR GLOBAL AXES

FIG. 3.2

R, v

M_R, θ_R

M_P, θ_P

P, u

CURVED MEMBER

M_Q, θ_Q

Q, w

SIGN CONVENTION FOR LOCAL AXES

FIG. 3.3

A ℓ B

ℓ' 3

R

θ

STRAINS DUE TO RADIAL
DISPLACEMENTS

FIG. 3.4

S c

M $M+dM$

P $P+dM$

$S+dS$

$d\theta$

O
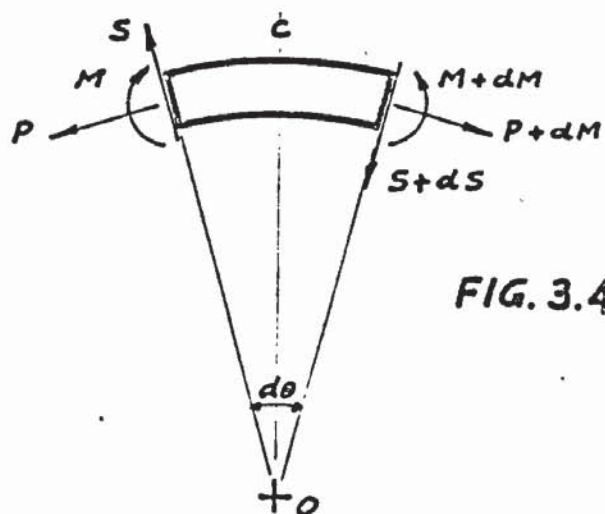
FREE-BODY DIAGRAM OF AN ARCH
ELEMENT

C H A P T E R   4

ANALYTICAL AND EXPERIMENTAL RESULTS FOR ARCHES
LOADED IN THEIR OWN PLANE

4.1 Introduction

The stiffness matrices for curved elements, subjected to
in-plane forces, were obtained in Chapter 3. In this chapter
these matrices are used to obtain results for several arches
under various types of loads. The strain energy method is also
employed to obtain results for arches with uniform cross-
sections and results for arches with variable cross-sections
are also obtained by experiments. Some of the arches are approx-
imated by a number of straight members. Finally, the results
obtained by the various methods are compared with those given
by the strain energy method or with those obtained by ex-
periments.

4.2 Arches of Uniform Cross-Sections

The fixed ended circular arch shown in fig. 4.1 is of
radius R and has a uniform cross-section. The following
dimensions and properties are assumed for the arch:-

The radius, R   =   254.0 mm,

the cross-section =   25.4 x 25.4 mm,

and the modulus of elasticity, E, of the material of the arch
is 207.0 KN./mm^2. The length ACB of the arch subtends an angle
α at the centre O as shown in the figure. Points D and E
divide the arch into three equal parts.

Arches with angle α varying from 30° to 180° are investi-
gated. The results for these arches have been obtained by
using various methods of analysis. The curves on all the

graphs are marked to indicate the method employed. The meaning of some of the abbreviations used, A.F., E.F., and C.F. has already been explained in the preceding chapter. In addition to these, two more abbreviations are used. These two are defined below:-

    (a)   S.E.   indicates the results obtained by using the strain energy method; and

    (b)   S.M.   indicates the results obtained by approximating the arches with a number of straight prismatic members.

(i) Concentrated Load at the Centre

A concentrated load of 1.0 kgf. was applied at the midpoint C of the arch shown in fig. 4.1. To analyse the arch by using the derived displacement functions, E.F. and A.F., the arch was divided into two equal parts. For the analysis using straight prismatic members, the arch was approximated by 4 to 16 members. However, only the results obtained by simulating the arch with 8 members are presented here. The arch was divided into 2 to 16 equal parts for analysis by using the cubic displacement functions. On the graphs the number in parenthesis indicates the number of sub-divisions used to obtain those particular results.

From the results presented here and from those omitted it is observed that the exact displacement functions, E.F., yield results identical to those obtained by using the strain energy method. It is further observed that the results obtained by using the derived displacement functions, E.F. and A.F., do not improve upon further sub-division. The comments made in this paragraph also apply to other load cases. This suggests

that the derived displacement functions are correct.

The deflections under the load are shown in fig. 4.2. It is seen that the straight member approximation yields results which are within 4% of those given by the strain energy method. The curve for the approximate functions, A.F., shows that the influence of the initial curvature, R, is negligible for arches with angle α less than 60°. For a semi-circular arch, this influence causes an error of about 10%. The results obtained by using the cubic functions are rather poor, the deflections being about 50% for a semi-circular arch even when it is split into 8 parts. Throughout, all the percentages are with respect to results obtained by using the strain energy method.

It is known (24) that the cubic functions cannot allow for the rigid body movement of curved elements without straining the element. The resulting stiffness matrix obtained by using the cubic functions is over-stiff. Consequently, the displacements are under-estimated. However, upon further subdivision, some rigid ~~boyd~~ body mode is seen to be recovered and this improves the results.

The slopes of the curves for the displacements shown in fig. 4.2 are seen to vary with angle α . Two factors contribute to the displacements, the axial strain and the bending strain. The strain energies due to the axial thrust and the bending moments vary with angle α at different rates. In arches with α less than 20° membrane action predominates. On the other hand, the bending action becomes predominant in arches with α greater than 70°. This results in the curve for the displacements being in three parts. The first and last part

correspond to the membrane and the bending action, respectively, being predominant. The middle part represents the transitional state.

The results for bending moments at the mid-point, C, are shown in fig. 4.3. The approximate functions, A.F., and the straight member approximation, S.M., yield results which compare well with those obtained by using the strain energy method. The cubic functions give reasonably good results for shallow arches with angle α less than 30°. For deeper arches, the curve marked C.F.(2) is seen to diverge from the curve, S.E., representing the strain energy method. Upon further subdivision, the results near the shallow range improve, while those near the deeper range deteriorate. This shows that the convergence of results obtained by using the cubic functions is not always monotonic.

Fig. 4.4 shows the results obtained for bending moments at the fixed support. It is seen that the various curves are very near to each other for angle α up to about 80°. Beyond that, the curves diverge from each other faster than is the case in fig. 4.3. Observations made in the preceding paragraph about bending moments under the load equally apply to the results for bending moments at the support.

The magnitude of the bending moment at the support increases with angle α up to about 40° and decreases beyond. At angle α equal to 70° the bending moment is seen to change sign. This is as expected. Consider two extreme cases; a very short arch and an almost complete ring. Both are carrying a point load at the centre. With angle α very small, the arch behaves like a straight beam. Obviously the bending

moment at the left-hand support is anti-clockwise. As angle
α increases, so does the span which causes greater bending
moments at the support. Now consider the free body diagram
of the left half of the almost complete ring. This gives the
support moments as acting clockwise, i.e. opposite to those in
the short arches. This trend is shown by the results in fig. 4.4.

Consider the static equilibrium of half of the arch. The
bending moment at the crown can be written in terms of the
shear force and thrust at the mid-point and the support moment
as follows:-

$$M_C = SR \sin \frac{\alpha}{2} - HR \left(1 - \cos \frac{\alpha}{2}\right) - M_A \qquad (4.1)$$

where   S   is the shear in the arch at the crown,

and   H   is the thrust in the arch at the crown.

An examination of equation (4.1) reveals that the thrust,
H, has very little effect on the bending moment, M_C, when
angle α is small. The magnitude of the support moment, M_A, is
in any case very small as can be seen from fig. 4.4. Therefore,
for small values of angle α the bending moment is approximately
equal to the first term in equation (4.1). With the increase
in angle α the magnitude of the thrust, H, increases as well as
its lever arm. For α between 40° and 80° the increase in the
bending moment due to the first term appears to be offset by
the decrease due to the other two terms in equation (4.1). This
is shown by the nearly flat parts of curves in figure 4.3. As
expected, after reaching a maximum value at about 70° the
thrust, H, starts decreasing. At about the same instance,
the sign of the support moment changes as can be seen from fig.
4.4. The result is a net increase in the bending moment at the

crown as α becomes greater than 80°.

It is noticed from fig. 4.2 that the deflections obtained by using cubic functions improve upon further sub-division. On the other hand, the bending moments do not always improve as can be seen from figs. 4.3 and 4.4. When displacement functions are used instead of the stress functions, better results are usually obtained for displacements than for forces. The inability of the cubic functions to allow for the rigid body movement has already been pointed out. This seems to affect the forces more than it does the displacements. Shallow arches of the same radius undergo small deflections, hence the rigid body displacements in these structures are also small. This is one of the reasons for obtaining good results for the lower range of angle α. The second reason is the small magnitude of the quantities involved, the scales of the graphs do not show the small differences.

(ii) Eccentric Point Load

A point load of 1.0 kgf. acts at the third point, D, of the arch shown in fig. 4.1. The arch is divided into three equal parts for the analysis by using the derived displacement functions. The results presented for the straight member approximation of the arches are for 9 sub-divisions. The number of sub-divisions employed to obtain the results by using the cubic functions are shown in parenthesis alongside the appropriate curves.

The horizontal and the vertical displacements of point D, X_D and Y_D respectively, are tabulated in Table 4.1. For each arch, the first row of the results shows the displacements obtained by using the strain energy method and the exact

displacement functions. Those obtained by other methods have been divided by the corresponding displacements obtained by using the strain energy method. The ratios thus obtained appear in the rows marked A.F., C.F. and S.M.

It is seen from the table that approximating the arches to a number of straight members yields excellent results; the displacements being within 2% for a semi-circular arch. The influence of the initial curvature, R, can be seen from the results for the approximate functions. It is noticed that this influence becomes appreciable for arches with angle α greater than 60° and reaches approximately 23% for a semi-circular arch. This appears to be a large error compared to the 10% recorded for the arch loaded at the centre. A comparison of the displacements in the two cases shows that the displacements in the eccentric load case are very small compared to those for the symmetric point load case. Rounding off errors affect small values more than larger ones. The cubic functions yield poor results; being less than 50% for an arch with angle α equal to 180°. The reasons given in the preceding section are also valid in the present case. In addition to those, the small magnitude of the results also contributes to the discrepancies.

The bending moments under the load are plotted in fig. 4.5. The straight member approximation yields results which are very close to those given by the strain energy method. The results obtained by using the approximate functions deviate less for the bending moments than was the case for the displacements. For a semi-circular arch, the error is less than 4%. The results yielded by the cubic functions remain poor. However, it is noticed from the figure that a finer sub-

division improves results over the whole range of angle α . The reasons for the poor performance of the cubic functions have already been given.

(iii) Skew-Symmetric Point Loads

A load of 1.0 kgf. was applied at each third point of the arch shown in fig. 4.1. The load at E being opposite to that acting at D. The arches were divided in the same manner as in the previous section.

The results for the displacements are tabulated in Table 4.1. It is observed that these are similar to the results obtained for the eccentric load case. The results for the bending moments at the support and at point D are plotted in figs. 4.6 and 4.7 respectively. The graphs in fig. 4.7 are similar to those in fig. 4.5. Therefore, various observations made for the latter also apply for the present load case. It is noticed from fig. 4.6 that the bending moments at the support obtained by using various methods differ from each other by a vide margin. Results obtained by straight member approximation agree very well with those obtained by using the strain energy method. The error introduced by the curvature, R, is about 27% for a semi-circular arch as can be seen from the curve marked A.F. The cubic functions yield support moments which are good for shallow arches with α about 50°. Beyond that the curve, C.F.(2) sharply deviates. Further subdivision is seen to improve the results. However, the results for deeper arches remain poor.

Results for other quantities not given in this Thesis were closer to the corresponding results obtained by using the strain energy method than those presented here.

(iv) Uniformly Distributed Loads

The arch shown in fig. 4.1 was also loaded with a uni-
formly distributed load. Only the strain energy method and the
exact displacement functions were used to analyse the arches.
The arches were divided into from 2 to 16 members of equal
length to obtain results by using the exact displacement
functions. However, the results given are for 2 sub-divisions
only.

(a) Symmetric U.D.L.

A load of 1.0 kgf/mm of the horizontal span
acts over the whole span of the arches. The
results obtained are tabulated in Table 4.2. It
is noticed that all the results yielded by the
exact functions agree very well with those obtained
by using the strain energy method.

(b) Skew Symmetric U.D.L.

The u.d.l. of 1.0 kgf/mm over half of the span
acts in the opposite direction to that acting over
the other half. The results for this load case
are tabulated in Table 5.3. Again, excellent
agreement is noticed between the two sets of
results obtained. There is some difference be-
tween the displacements for shallow arches. This
is due to the very small magnitude of the dis-
placements concerned.

The results presented in Tables 4.2 and 4.3
are for the thrust, shear force and bending
moment. The subscripts refer to the point in
the arch shown in fig. 4.1. The columns marked

by δ_c are for the displacements of the mid-
point, C.

(v) Arches with Both Ends Pinned

Arches with both ends pinned were also analysed by using
the methods employed for the analysis of fixed arches. The
exact displacement functions gave results identical to those
obtained by using the strain energy method. Results obtained
by approximating the arches with a number of straight pris-
matic members were seen to converge towards the correct values
upon further sub-division. Once again, the approximate func-
tions demonstrated that the influence of the initial curvature,
R, was negligible for shallow arches and increased as the
arches became deeper. The point at which this influence became
appreciable varied for the various displacements and forces as
well as the load cases. It was further observed that the re-
sults obtained by using the derived displacement functions did
not improve upon refining the sub-division. Finally, the cubic
functions gave generally poor results.

4.3. Arches with Variable Cross-Sections

In the previous chapter, a stiffness matrix was developed
for curved elements with variable cross-sections by utilizing
the exact displacement functions obtained for a curved element
with uniform cross-section. This stiffness matrix was used

to analyse some arches with variable cross-sections. Models were made of the same arches and tested to obtain results which are compared with those obtained theoretically.

The stiffness matrices were formulated by assuming that the modulus of elasticity, E, of the material of a member is constant. Structures composed of elastic materials only can, therefore, be analysed by using these matrices. Arches for experiments could have been made more easily from materials such as perspex, wood or reinforced concrete. Unfortunately, these materials exhibit non-linear characteristics which could have invalidated the comparison between experimental and theoretical results. It was, therefore, decided to use mild steel which is almost exactly linear in the elastic range.

(i) Fabrication of the Arches

The dimensions and details of the arches are given in Drawing Nos. 1 and 2. Further details can be seen from Plates 1 to 5.

Theoretically, an arch when loaded in its plane should have zero displacements out of the plane, but due to some un-controlable factors, this sort of movement can occur in actual structures. The main factor is probably the misalignments in arches or in setting up the experiments. To guard against the possibility of the arches buckling out of the plane, a width equal to several times the thickness was chosen.

The machine to roll the arches cold to the required radius was not available. The alternative was to apply heat treatment to the bent bars so that upon cooling they will retain their curved shapes. This was adopted.

The oven available could not accommodate the whole arch.

The arches were, therefore, made in halves. Two moulds were prepared, one for arches of radius equal to 1270.0 mm and the other for arches of 635.0 mm radius. The details of the smaller mould can be seen in Plate 6. Suitable lengths of mild steel plate with dimensions of 76.2 mm x 15.3 mm were cut and machined down to the required size. The prepared bar was bent to the required radius and clamped in position on the mould. This whole assembly was put into the oven. The temperature in the oven was raised slowly to prevent any temperature gradients being set up in the mould which could deform it. After reaching the maximum value, the temperature was maintained at that level for three hours to allow the whole of the material to achieve the same temperature. The oven was then allowed to cool slowly.

After the heat treatment, the thin ends of two halves with the same radius were butt welded to form an arch. The other ends were welded to the pins or the hollow sections as required. The pins for the loading brackets were only tack welded to the arches to avoid local stiffening.

One half of each arch was divided into 8 equal parts. At each eighth point, a 6.35 mm electrical resistance strain gauge was fixed to each face of the arch. Where the eighth point coincided with the loading point, the pair of strain gauges at that point was moved to one side to avoid the loading pin.

The other half of each arch was divided into 4 equal parts. At each quarter point, a pair of deflection dial gauges was placed to measure the horizontal and the vertical displacements. The pins of the deflection dial gauges rested against the horizontal or the vertical face of the perspex packings which

can be seen in Plates 1 to 3. Without any such packings, a horizontal deflection dial gauge, for instance, with its pin resting against an inclined surface will register a horizontal displacement even when the surfact moves vertically only. Perspex packing was used because it is easier to fabricate into the required shape. Furthermore, it does not add to the stiffness of the structures as used here.

For obvious reasons, the strain gauges and the deflection dial gauges were placed over the same length of the curved cantilevers.

Drawing No. 1 also shows details and dimensions of the loading brackets made from mild steel. The load was applied via a mild steel rod hanger threaded through the middle hole of the bracket. The loading brackets and hangers can be seen in Plates 1 to 4. A bracket transfers the load to the loading pins as two equal knife edges. By centring the bracket, the arches are loaded in their own plane. An out of plane eccentricity of the load applies a torque to the arch about its longitudinal axes. This in turn produces the undesirable out of plane displacements mentioned earlier.

A frictionless pin is desirable for the pinned support. A small error in the end rotation is magnified in displacements along the length of the arch in proportion to the distance of the point under consideration from the support. Any misalignment in the structure causes the pin to bear heavily against the bearings, thus increasing the resistance to rotation of the pin. One way to avoid this is to provide some play between the pin and its bearings. However, such a play can cause displacements due to the lateral movement of the pin

during loading. It was, therefore, decided to use the arrange-
ment shown in Drawing No. 2 and Plate 5. The ball bearings
used not only reduce the friction, but also allow out of plane
rotation of the ends to accommodate any misalignment of the
arches. The pin can move parallel to its axis by 3.0 mm. This
helps in the setting up of the experiment without straining
the arches. The ball bearings are mounted from inside the
host plates as can be seen from the drawing. There is, there-
fore, no danger of the arch slipping off the bearings during
testing. Finally, the end plates are bolted to the base plate
as shown in the drawing and Plate 5. The same end brackets
can, therefore, be used for all pin ended arches.

(ii) Test Specimens

Two test specimens were prepared from the same material
and given the same treatment as the arches. The dimensions of
the test specimen are shown in Drawing No. 3. The width and
the thickness shown for each specimen is the average of three
measurements taken near the middle of the specimen. On each
test specimen, two 6.35 mm electrical resistance strain gauges
were fixed to measure the longitudinal strains and two strain
gauges to measure the transverse strains. One strain gauge
of each pair was fixed to one face of the test specimen.

The load was applied to each test specimen with a Denison
machine in 8 increments of 250.0 kgf. After reaching the full
load, it was decreased in the reverse order. For each stage
of the load, the strain gauge readings were recorded. From
these the average of the readings for the loading and un-
loading cycle at each load stage was calculated. The average
strain gauge readings thus obtained for each strain gauge were

plotted against the load. The best straight line was drawn through each set of points and the strains corresponding to a load of 2000.0 kgf. were computed from the graphs. The average of the strains for a pair of strain gauges was obtained for each test specimen.

The dimensions of a test specimen yielded its cross-sectional area. The longitudinal stress was obtained by dividing the maximum test load by the cross-sectional area of the specimen. With the stress and the strain known, it is easy to calculate the modulus of elasticity, E. Poisson's ratio, ν , is simply equal to the ratio of the transverse strain to the longitudinal strain. The latter property of the material is required to analyse bow girders in Chapter 6. The average of the properties of the material for the two test specimens were assumed to be the required values. These final values obtained are:-

the modulus of elasticity, E = 188.0 KN/mm^2;

and the Poisson's ratio, ν = 0.28

(iii) Tests on Arches

A general view of the pin ended arch with the radius equal to 1270.0 mm is shown in Plate 1. The deflection dial gauges are seen to be supported from a dexian frame. The three loading brackets with the hangers in position are clearly visible in the picture. Plate 2 shows the smaller pin ended arch in position for testing. Some of the deflection dial gauges were removed for clarity. For the same reason, only the middle loading bracket with the hanger is shown. The pins of the deflection dial gauges are seen to be resting against the

horizontal and vertical surfaces provided by the perspex packings.

The arch with the radius equal to 1270.0 mm was loaded in 6 increments of 4.0 kgf. and a final one of 1.0 kgf. After reaching 25.0 kgf. the load was decreased in the reverse order. For each stage of the load, the strain and deflection dial gauge readings were recorded.

The same procedure was followed for all the tests, only the loads were different. The arches with the radius of 635.0 mm were loaded in 5 increments of 8.0 kgf. The cantilever with the larger radius was loaded in 5 increments of 2.0 kgf. The load was applied in 5 increments of. 4.0 kgf. to the cantilever with the smaller radius.

As for the test specimens, the average values for the strain and deflection dial gauge readings were calculated. These were plotted against the loads and the best line was drawn through each set of points. From the graphs, the strains and the deflections corresponding to the maximum load in each case were computed.

Using the known cross-sectional properties and the modulus of elasticity obtained in section 4.3(ii), the strains at each section were converted into the axial force and the bending moment. Some of the results obtained for the arches are presented in the next section.

(iv) Results for the Arches

A load of 25.0 kgf. was applied at the centre of the longer arch. The results obtained for the deflections under the load are plotted in fig. 4.8. For analysis by computer, the arch was divided into 2 to 20 segments of equal length. The results

shown in the figure have been obtained as follows:-

(a) by using the stiffness matrix developed
in section 3.6 (iii) for the curved element
with variable cross-section;

(b) by using the exact stiffness matrix ob-
tained for the curved element with uniform
cross-section; and finally

(c) by approximating the arch with a number of
straight prismatic members.

The cross-section for a member in case (b) and (c) was
assumed to be equal to the cross-section at the mid-point of the
corresponding element in case (a). The theoretical results
were divided by the deflection obtained by experiment. The
ratios thus obtained are plotted in fig. 4.8. It is noticed
from the graphs that method (a) yields better results than
either (b) or (c). The latter two methods over-estimate the
stiffness of the structure. However, upon refining the sub-
division, the results are seen to be improving. Further sub-
division gives more marked improvement in the results by method
(a) in the range of coarse sub-division. After reaching the
90% mark, the curve is seen to level off. The 10% difference
between the theoretical and experimental deflections can be
due to several reasons. Among these is the modulus of elas-
ticity, E, for the actual structure being less than that
obtained from the control tests. Small defects in the fabri-
cation of the arch can make the structure more flexible or
rigid.

The bending moment diagrams and the deflected shapes of
some of the arches are plotted in figs. 4.9 to 4.12. Results

for other load cases are tabulated in Tables 4.5 to 4.7. The
computer results have been obtained by using the stiffness
matrix for the curved elements with variable cross-section.
The arches were divided into 16 equal parts for the bending
moments and into 8 equal parts for the deflections. The
results for the cantilever are for 8 and 4 sub-divisions re-
spectively. It is seen that the theoretical and experimental
results agree remarkably well.

The fixity provided by the hollow sections was suspect.
A vertical bar was, therefore, welded to the arch near to one
support. A deflection dial gauge was fixed to measure the
horizontal displacement of a point on the vertical bar 250.0 mm
above the centre line of the arch. This arrangement can be
seen from Plate 4. From the deflection dial gauge readings
the rotations of the ends of the arch were calculated.

Fig. 4.10a shows the bending moment diagram for the fixed
arch. The computer results have been adjusted to allow for
end rotations. Excellent agreement is observed between the
theoretical and the experimental results.

The deflected shape of the arch is shown in fig. 4.10b.
It is seen that the theoretical deflection at the centre is
about 80% of that obtained by experiment. Since no adjustment
was made for end rotations, some of the error is due to this
cause.

The bending moment diagram for the same arch under eccen-
tric point load is shown in fig. 4.11a. The results have not
been adjusted to allow for end rotations. The influence of
these rotations is clearly discernible from the graph.

The bending moments in a cantilever are not affected by the fixed end yielding under load. The disagreement between the two sets of results shown in fig. 4.12a could only be due to the reasons discussed in the next section.

The end rotation of the cantilever, however, causes rigid body displacements of all points in the structure. This movement is a function of the end rotation and the distance of the point from the support. Since the end rotations of the cantilevers were not measured, no adjustment has been made for such movements. In spite of this, the two sets of results for displacements shown in fig. 4.12b are seen to be close to each other.

4.4 Conclusions

From the results presented in this chapter, the following conclusions are drawn:-

(i) Arches with Uniform Cross-sections

    (a) The exact displacement functions describe the deformed shape of curved bars accurately. The strain energy obtained for the structure by using these functions is the same as obtained by using the strain energy method. Consequently, the exact functions yield results identical to those obtained by using the strain energy method.

    (b) In the derivation of the approximate functions, the influence of the curve of the member was ignored in the expression for bending curvature. The results show that for shallow arches no accuracy is lost by neglecting the influence of initial curvature. The boundary where this influence becomes appreciable

shifts from quantity to quantity. Arches with angle
α up to about 60° can be considered shallow for all
purposes.

(c) The exact displacement functions represent the deflec-
ted shape of the curved member accurately. No improve-
ment, therefore, can be expected in the results upon
further sub-division. This is confirmed by the results
obtained. It was observed that the results obtained by
using the approximate functions do not improve either.
The reason for this is that the same expression for bend-
ing curvature was used both in the derivation of the
functions and the stiffness matrix. As a result, the
strain energy of the structure obtained by using these
functions is not affected by the number of sub-divisions
used. The approximate functions will yield better re-
sults upon refining the mesh if a more accurate expres-
sion for bending curvature is used to formulate the
stiffness matrix.

(d) The inadequacy of the polinomial displacement func-
tions to approximate the deformed shape of curved
members has been substantiated. The displacements were
seen to improve upon further sub-division. The results
for forces, however, sometimes deteriorated as the
mesh was refined. This is because displacement func-
tions have been used and not stress functions. The
cubic functions were expected to yield better results
than straight member approximation as an allowance was
made for the influence of the curve of the member in
the derivation of the stiffness matrix. The results,
however, showed that the straight member approximation

always gave far better results than the cubic functions. It can, therefore, be assumed that the rigid body mode was not recovered in the case of cubic functions with the mesh size employed. This may be recovered and the results improved upon further sub-division.

(e) It was noticed that approximating semi-circular arches with less than ten straight prismatic members yielded results which were very close to those obtained by using the strain energy method. Therefore, it is better to use straight members to simulate an arch where a large number of sub-divisions is to be used. Using the exact functions derived in this Thesis, however, only the minimum number of sub-divisions are required to obtain accurate results. Thus saving the core space and solution time of the computer.

(ii) Arches with Variable Cross-sections

The stiffness matrix obtained for curved elements with variable cross-section yields good results. The difference between the theoretical and the experimental results could be due to the following reasons:-
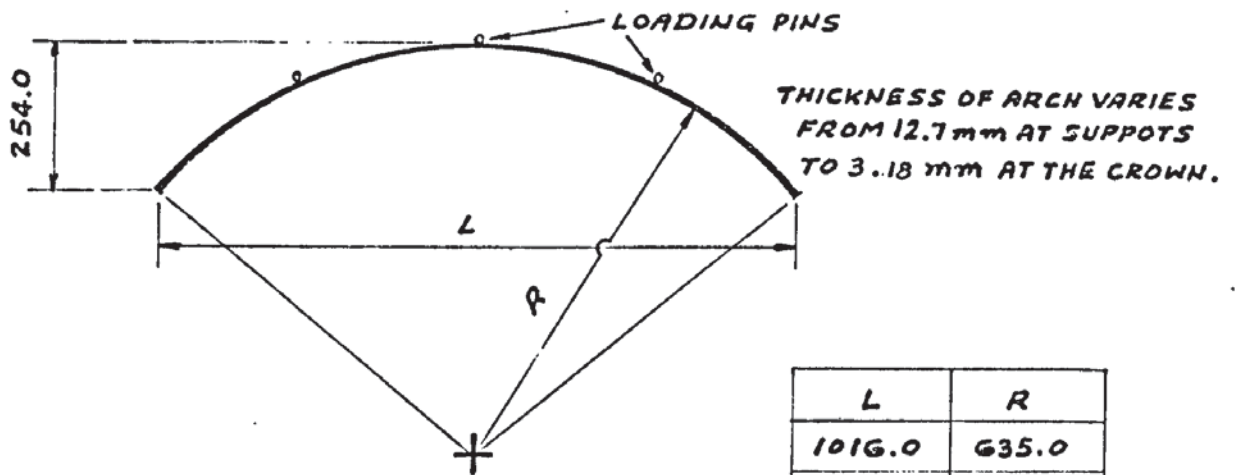
(a) The displacement functions used to develop the stiffness matrix were obtained for a curved member with uniform cross-section. The assumption that the strains in the curved member with variable cross-section are the same as in a member with uniform cross-section is only approximate. Consequently, the stiffness matrix is also approximate. This approximation, however, becomes more accurate as the variation of the cross-section of the member decreases upon further sub-

division. The improvement in the results obtained confirms this.

(b) The modulus of elasticity, E, for the arches was obtained from the test specimens. In spite of the care taken to give the test specimens the same treatment as given to the arches, some deviation is unavoidable. It is, therefore, possible that the Young's modulus for the arches was different from that obtained from the test specimens. Indeed it was observed that the two specimens yielded results slightly different from each other.

(c) Similarly, the two halves of an arch can be different from each other. This accounts for the small horizontal displacements of the mid-point in symmetric load cases. For the same reason, skew symmetric load cases yielded some vertical displacements of the mid-point. The asymmetry of the arches must have contributed to the difference between the theoretical and the experimental results. No such check was made other than the observations made above. This was not possible as the strain and deflection dial gauges were placed over one half of the arches only.

(d) The inaccuracies in the strain gauges used. Table 4.6c shows the axial force in the pin ended arch under a 40.0 kgf. load at the centre. The computer results show that the axial compression does not vary much from the support to the mid-point. On the other hand, the axial force obtained by experiment not only varies from point to point along the length of the member, but is seen to be tensile at some sections. This is
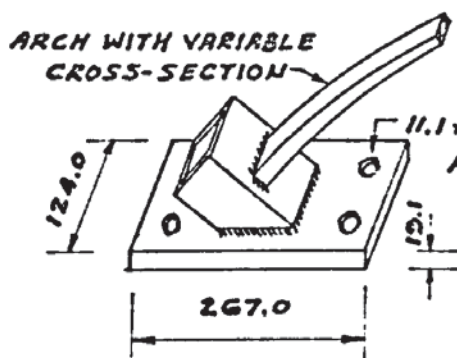
due to the errors in the strains measured.

(e) For the eccentric and skew symmetric load cases the complete results were obtained by superimposing the results of two tests. This was necessitated by the strain and deflection dial gauges being placed over one half of the arch only.

(f) The loading pins cause some concentration of stresses. It is possible that this affected the readings of the strain gauges in the vicinity of the loading points.
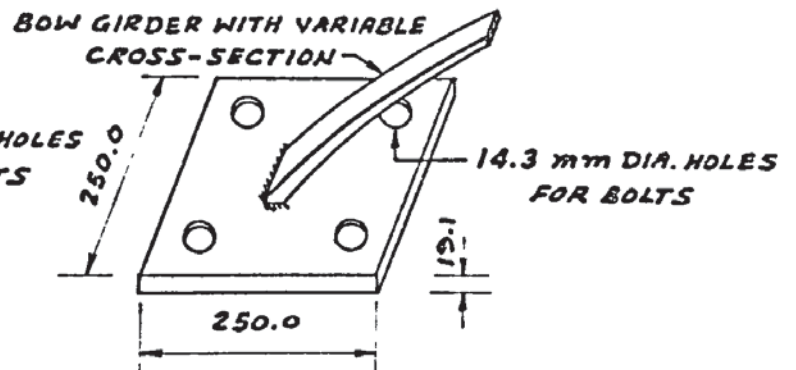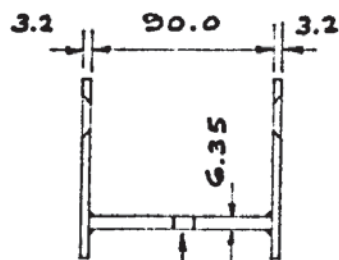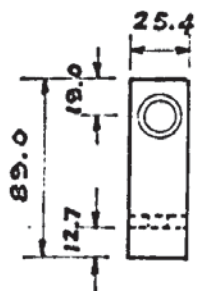
LOADING PINS

THICKNESS OF ARCH VARIES
FROM 12.7 mm AT SUPPORTS
TO 3.18 mm AT THE CROWN.

254.0

L

R

L	R
1016.0	635.0
1524.0	1270.0

ELEVATION OF ARCHES SHOWN DIAGRAMATICALLY

NOTE : ALL DIMESIONS ARE IN mm .

ARCH WITH VARIABLE
CROSS-SECTION

11.1 mm DIA. HOLES
FOR BOLTS

124.0

12.1

267.0

DETAILS OF THE FIXED END
OF ARCH

BOW GIRDER WITH VARIABLE
CROSS-SECTION

250.0

14.3 mm DIA. HOLES
FOR BOLTS

12.1

250.0

DETAILS OF FIXED END
OF BOW GIRDER

25.4

19.0

89.0

12.7

3.2   90.0   3.2

6.35

8.5 mm DIA. FOR HANGER

DETAILS OF LOADING BRACKET FOR ARCHES

DRAWING NO. 1

VARIES FROM 12.7 TO 3.18 mm

76.2

38.0

102.0

19.0

25.0   75.0   25.0

12.7   102.0   12.7

ELEVATION A-A
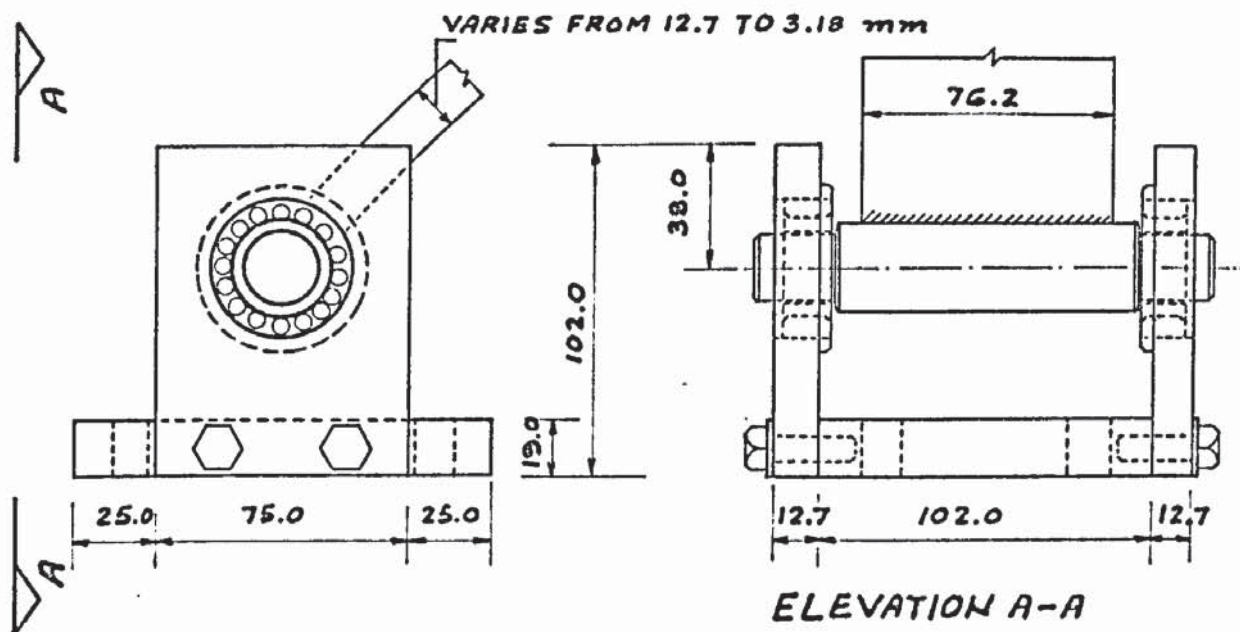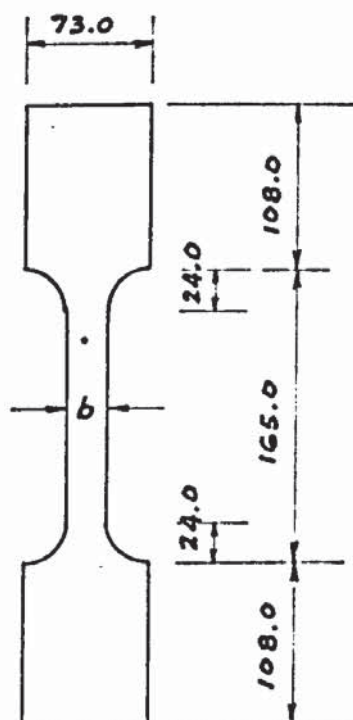
DETAILS OF BRACKET TO PROVIDE PINNED SUPPORT
TO ARCHES

DRAWING NO. 2

NOTE: ALL DIMENSIONS ARE IN MILLIMETERS

73.0

108.0

24.0

b

165.0

24.0

108.0

SPECIMEN	b	t
1	25.33	6.16
2	25.34	6.22

DETAILS OF TEST SPECIMENS

DRAWING NO. 3
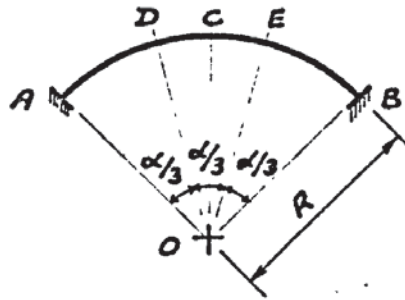
CIRCULAR ARCH OF UNIFORM CROSS-SECTION

FIG. 4.1
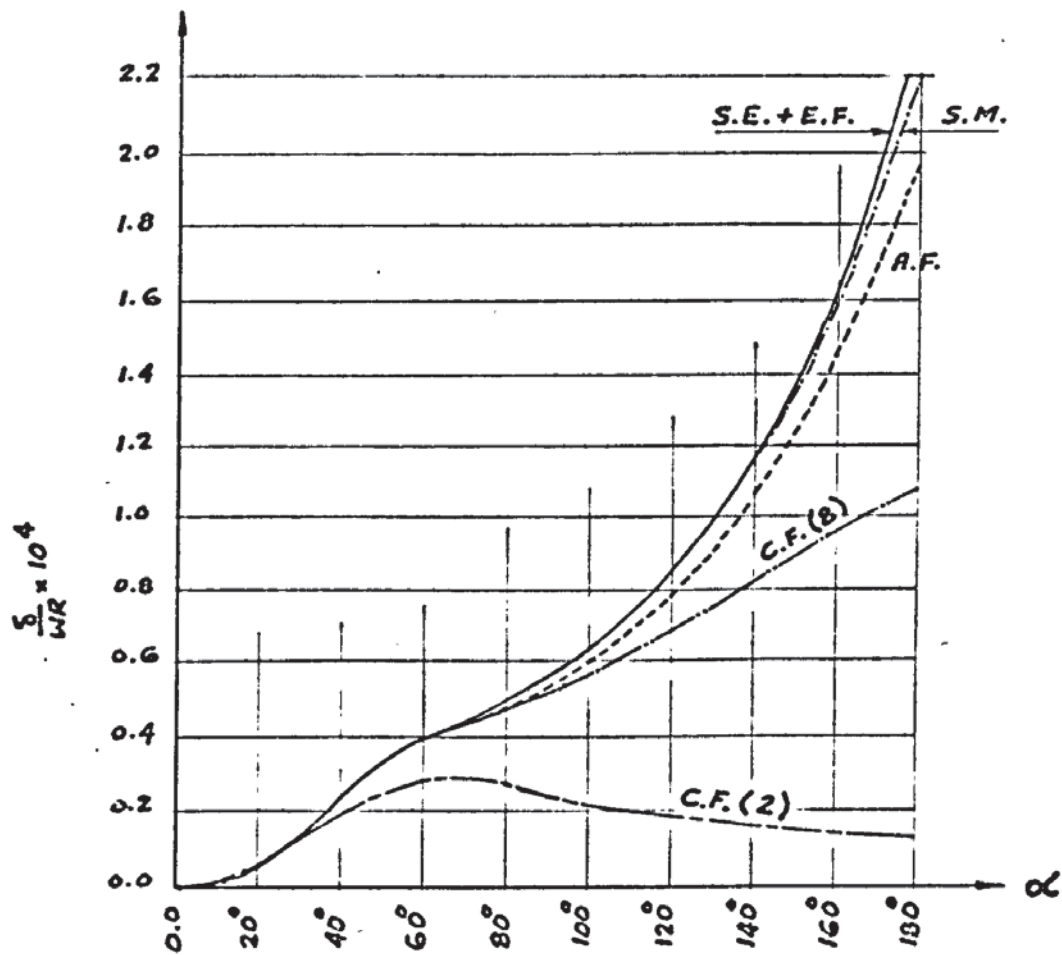
DEFLECTIONS AT MID-POINT OF THE ARCHES
UNDER A SYMMETRIC UNIT LOAD

FIG. 4.2
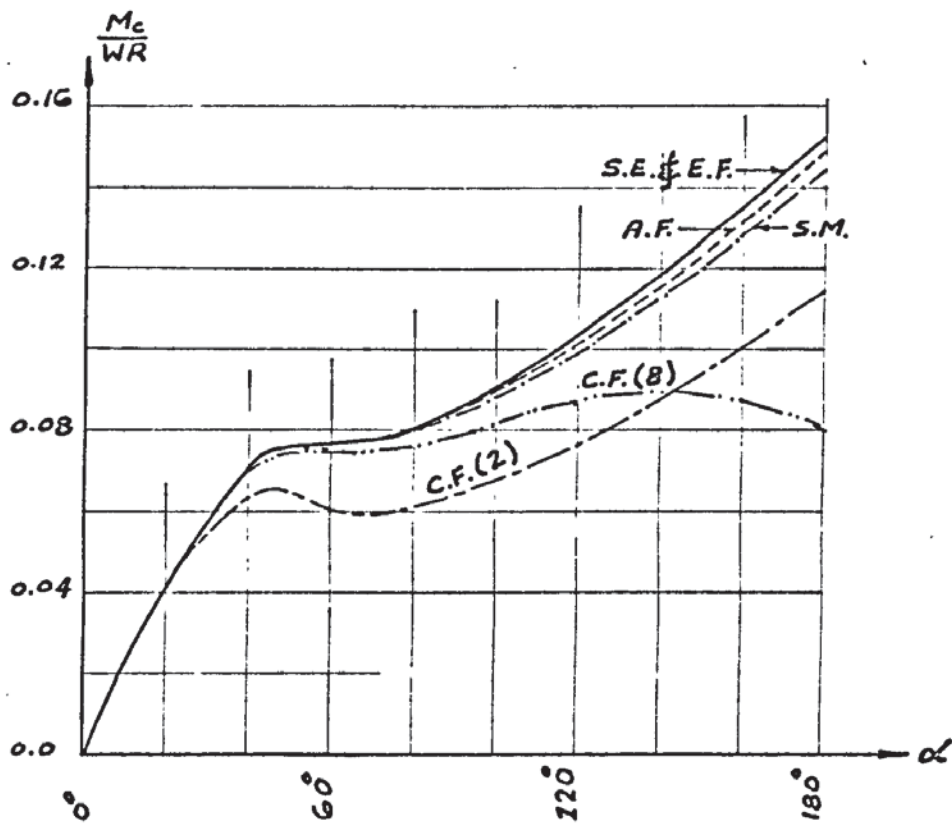
BENDING MOMENTS AT MID-POINTS OF ARCHES
UNDER A SYMMETRIC UNIT LOAD

FIG. 4.3
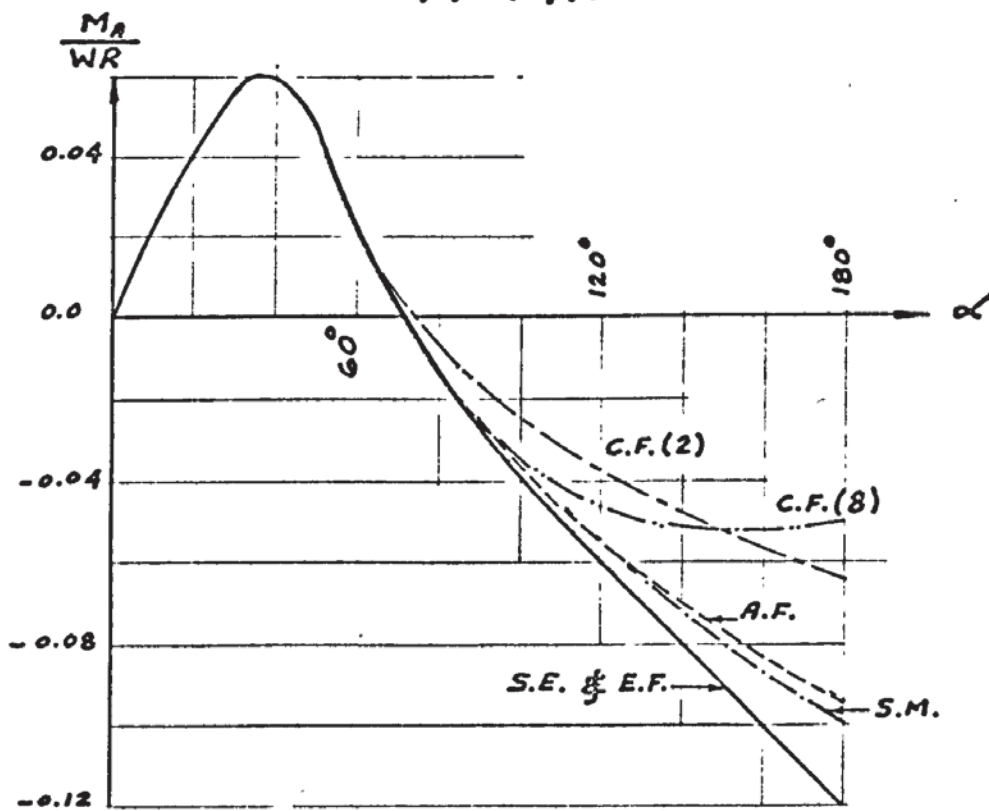
BENDING MOMENTS AT SUPPORTS OF ARCHES
UNDER A SYMMETRIC UNIT LOAD

FIG. 4.4
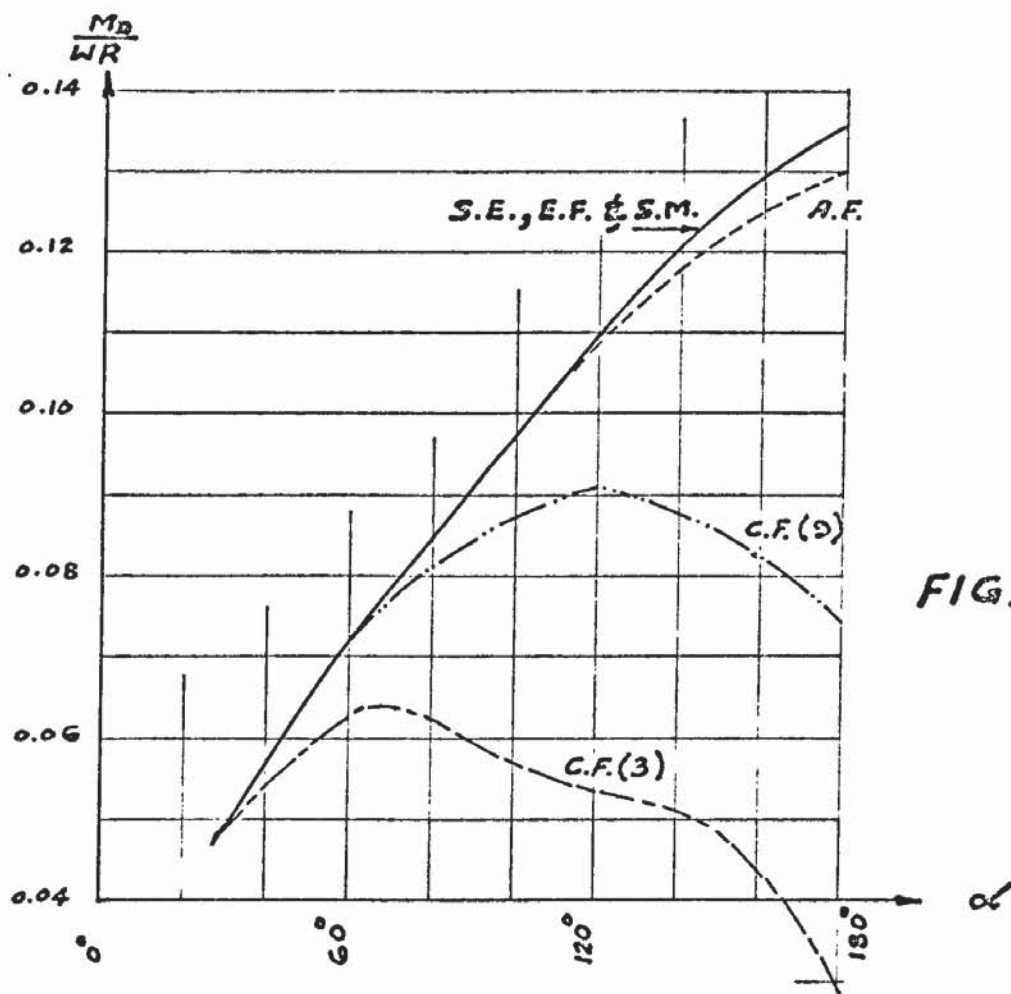
FIG. 4.5

BENDING MOMENTS AT QUARTER POINT
DUE TO ECCENTRIC POINT LOAD
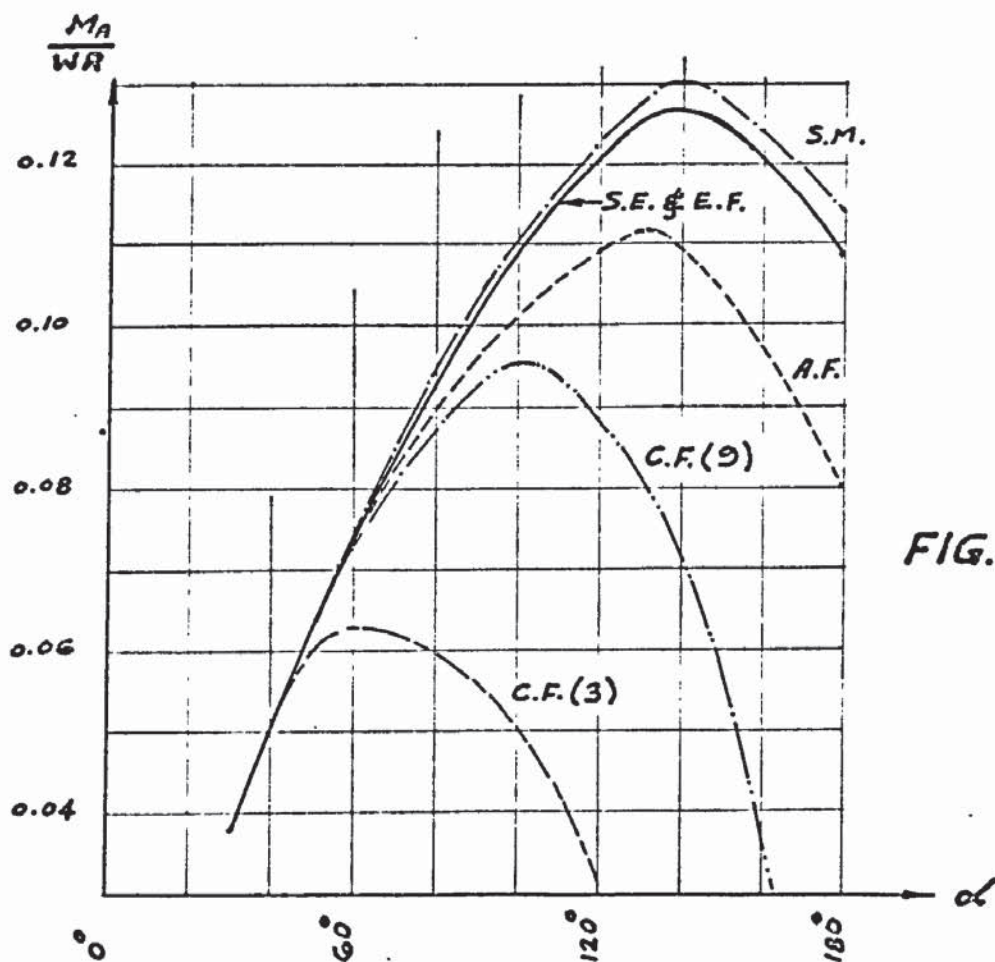
FIG. 4.6

BENDING MOMENTS AT SUPPORT
DUE TO ECCENTRIC POINT LOAD
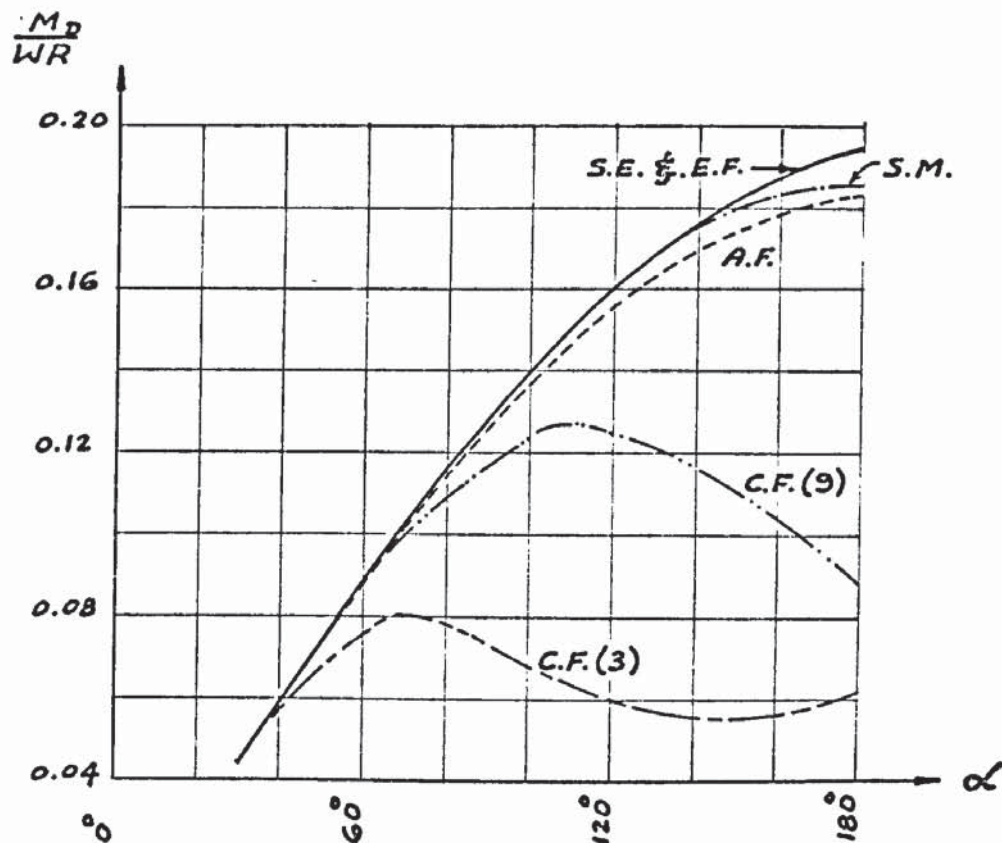
BENDING MOMENTS AT QUARTER POINT
DUE TO SKEW SYMMETRIC POINT LOADS

FIG. 4.7

γ IS EQUAL TO RATIO OF DEFLECTIONS WITH
RESPECT TO EXPERIMENTAL RESULTS

CURVED MEMBERS WITH VARIABLE CROSS-SECTION

CURVED MEMBERS OF UNIFORM CROSS-SECTION

STRAIGHT PRISMATIC MEMBERS

FIG. 4.8

N = NO. OF SUB-DIVISIONS
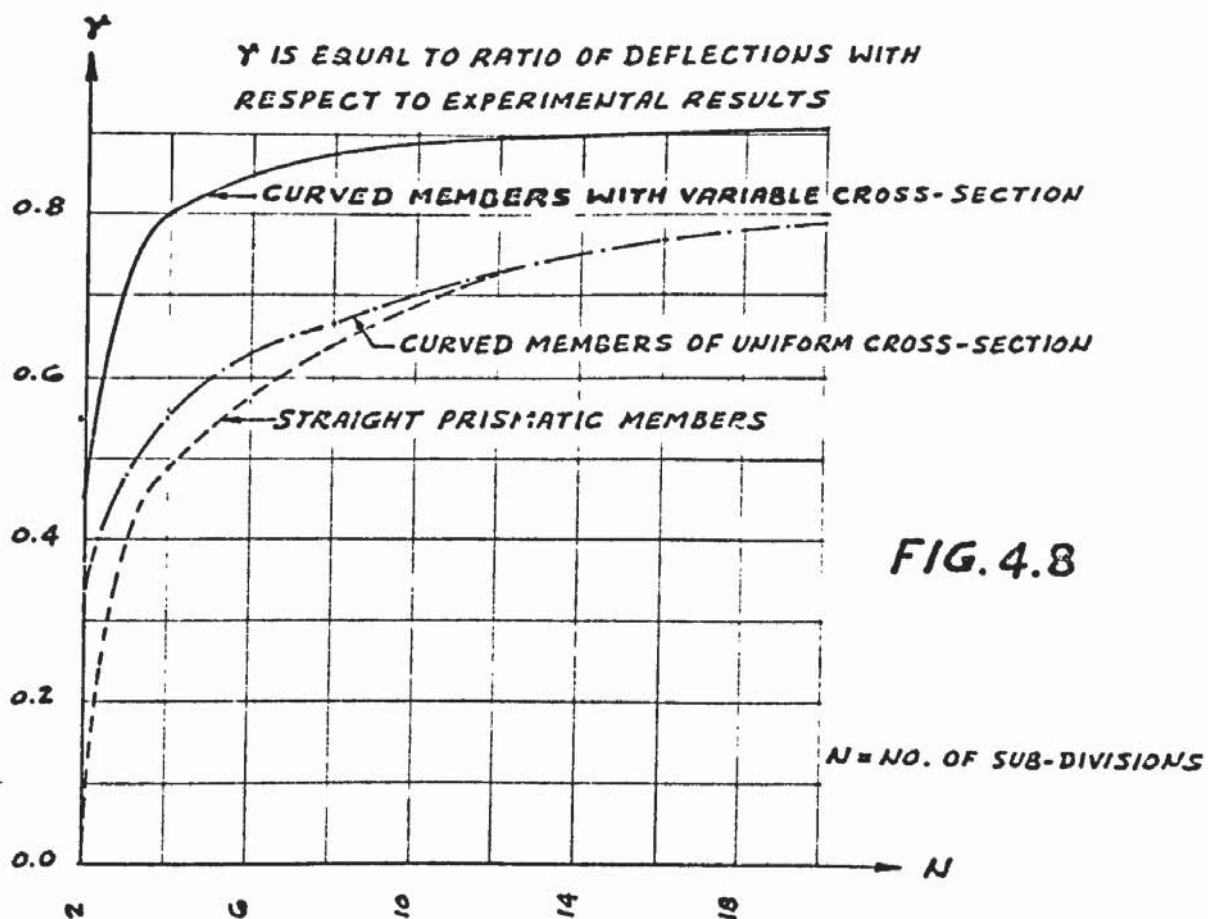
COMPARISON OF THEORETICAL AND EXPERIMENTAL
DEFLECTIONS OF MID-POINT OF LONGER ARCH

COMPUTER
EXPERIMENT
37.0 KN-mm

BENDING MOMENT DIAGRAM

FIG. 4.9 a

COMPUTER
EXPERIMENT
ORIGINAL POSITION
3.57 mm
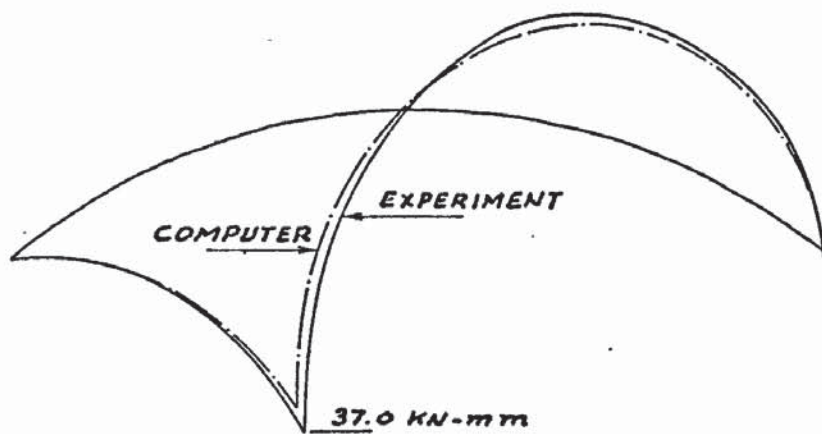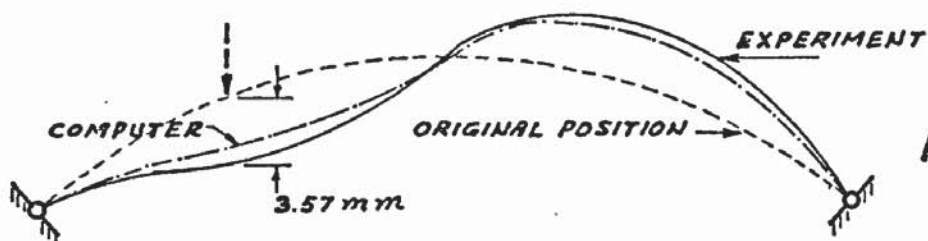
DEFLECTED SHAPE OF LONGER ARCH UNDER
ECCENTRIC POINT LOAD

FIG. 4.9 b

BENDING MOMENT DIAGRAM
SYMMETRICAL ABOUT ₵.

EXPERIMENT
COMPUTER
21.6 KN-mm
27.3 KN-mm

BENDING MOMENT DIAGRAM

FIG. 4.10 a

DEFLECTED SHAPE SYMMETRIC ABOUT ₵.
COMPUTER
1.02 mm
ORIGINAL POSITION
EXPERIMENT
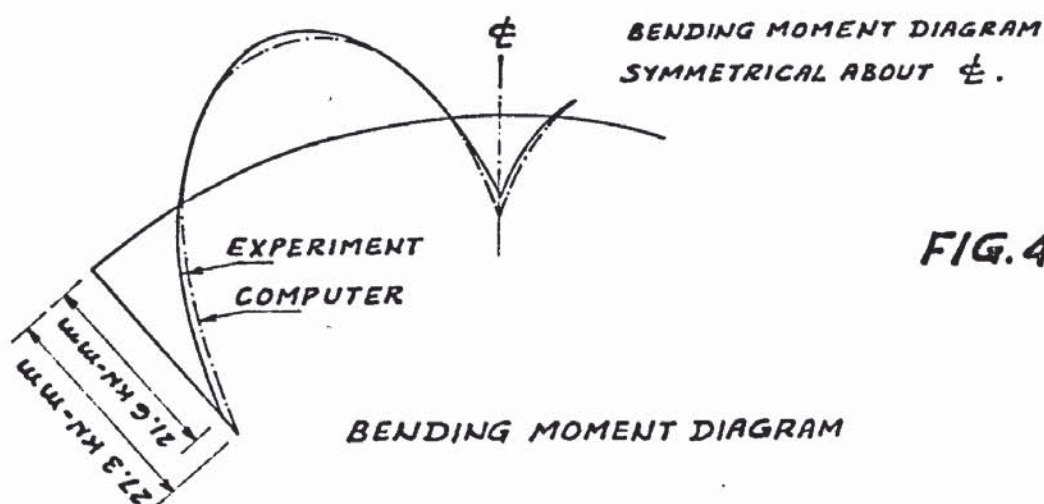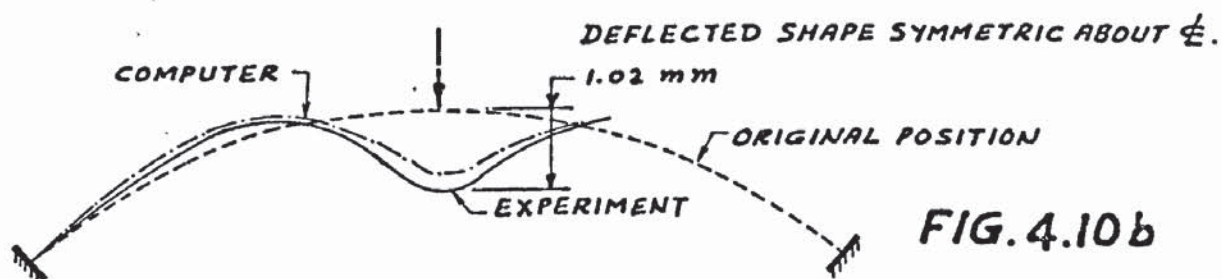
DEFLECTED SHAPE OF FIXED ARCH UNDER
SYMMETRIC POINT LOAD

FIG. 4.10 b

BENDING MOMENT DIAGRAM

FIG. 4.11 a

Labels in figure: COMPUTER, EXPERIMENT, 35.9 KN-mm, 28.5 KN-mm, 17.5 KN-mm, 21.5 KN-mm, 19.0 KN-mm, 20.8 KN-mm

DEFLECTED SHAPE OF FIXED ARCH UNDER ECCENTRIC POINT LOAD

FIG. 4.11 b

Labels in figure: 0.225 mm, COMPUTER, EXPERIMENT, 0.3 mm, ORIGINAL POSITION

BENDING MOMENT DIAGRAM

FIG. 4.12 a

Labels in figure: EXPERIMENT, COMPUTER, 99.7 KN-mm, 85.0 "

DEFLECTED SHAPE OF SMALLER CURVED CANTILEVER

FIG. 4.12 b

Labels in figure: ORIGINAL POSITION, COMPUTER, 5.05 mm, 12.25, EXPERIMENT

TABLE 4.1

DISPLACEMENTS OF FIXED ARCHES

	Method	Point Load at D X_D/WR	Point Load at D Y_D/WR	Skew Symmetric Loads X_D/WR	Skew Symmetric Loads Y_D/WR
30°	S.E. + E.F.	1.96×10^{-9}	4.23×10^{-8}	1.55×10^{-9}	1.43×10^{-8}
	A.F.	0.99	0.99	0.99	0.99
	C.F.(3)	0.98	0.99	0.98	0.99
	C.F.(9)	1.0	1.0	1.0	1.0
	S.M.	1.0	1.0	1.02	1.0
60°	as for 30°	2.67×10^{-8}	1.63×10^{-7}	3.66×10^{-8}	1.08×10^{-7}
		0.97	0.99	0.97	0.97
		0.84	0.88	0.82	0.83
		0.98	0.99	0.98	0.98
		1.0	1.0	1.0	1.0
90°	as for 30°	1.05×10^{-7}	2.75×10^{-7}	1.87×10^{-7}	3.32×10^{-7}
		0.94	0.96	0.94	0.94
		0.50	0.61	0.46	0.49
		0.92	0.94	0.91	0.92
		1.0	1.0	0.99	1.0
120°	as for 30°	2.92×10^{-7}	4.51×10^{-7}	5.59×10^{-7}	6.83×10^{-7}
		0.90	0.92	0.89	0.90
		0.27	0.33	0.20	0.23
		0.75	0.80	0.74	0.76
		0.99	0.99	0.99	0.99
150°	as for 30°	6.23×10^{-7}	6.77×10^{-7}	1.23×10^{-6}	1.09×10^{-6}
		0.84	0.87	0.84	0.85
		0.06	0.19	0.08	0.11
		0.53	0.62	0.52	0.55
		0.99	0.98	0.98	0.99
180°	as for 30°	1.07×10^{-6}	8.98×10^{-7}	2.16×10^{-6}	1.41×10^{-6}
		0.77	0.83	0.77	0.79
		x	0.16	0.03	0.06
		0.33	0.45	0.32	0.37
		0.98	0.97	0.98	0.98

TABLE 4.2

FORCES, MOMENTS AND DEFLECTIONS IN FIXED ARCHES UNDER SYMMETRIC U.D.L.
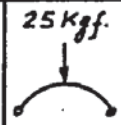
	Method	T_S	S_S	$B.M_S$	T_C	$B.M_C$	δ_c
30°	S.E.	1.548	-2.265	2.016	-0.909	1.023	7.039×10^{-7}
	E.F.	"	"	2.025	"	1.014	7.028 "
60°	S.E.	7.795	-1.273	2.740	-6.114	1.570	4.248×10^{-6}
	E.F.	7.794	-1.274	2.788	-6.112	1.524	4.243 "
90°	S.E.	10.573	0.573	0.688	-7.881	1.228	6.127×10^{-6}
	E.F.	10.572	0.572	0.735	"	1.183	6.119 "
120°	S.E.	11.282	2.220	-1.893	-7.563	1.578	8.594 "
	E.F.	11.281	"	-1.859	"	1.543	8.582 "
150°	S.E.	11.055	3.938	-5.506	-6.665	2.757	1.564×10^{-5}
	E.F.	"	"	-5.475	"	2.726	1.562 "
180°	S.E.	10.0	5.558	-10.384	-5.558	4.803	3.275 "
	E.F.	10.025	5.533	-10.260	-5.557	4.729	3.229 "

TABLE 4.3

FORCES, MOMENTS AND DEFLECTIONS IN FIXED ARCHES UNDER SKEW SYMMETRIC U.D.L.

	Method	T_S	S_S	$B.M._S$	S_C	δ_H @ C
30°	S.E.	0.418	−1.560	−0.829	−0.974	6.516×10^{-9}
	E.F.	0.362	−1.569	−0.835	−0.979	1.029×10^{-8}
60°	S.E.	1.553	−2.689	−3.027	−1.895	3.917×10^{-7}
	E.F.	1.362	−2.753	−3.089	−1.935	4.260 "
90°	S.E.	3.081	−3.081	−5.805	−2.715	2.953×10^{-6}
	E.F.	2.798	−3.228	−6.020	−2.810	3.115 "
120°	S.E.	4.560	−2.633	−8.100	−3.325	1.113×10^{-5}
	E.F.	4.274	−2.849	−8.545	−3.534	1.173 "
150°	S.E.	5.554	−1.488	−8.892	−3.909	2.830 "
	E.F.	5.262	−1.803	−9.769	−4.109	3.044 "
180°	S.E.	5.752	0.0	7.523	−4.248	5.419 "
	E.F.	5.435	−0.55	3.165	−4.559	6.065 "

TABLE 4.4 a

BENDING MOMENTS IN THE EXPERIMENTAL ARCH

Load Case	Point / Method	1	2	3	4	5	6	7	8
25 Kgf.	Exper.	6.5	12.9	15.8	16.7	14.8	9.1	-1.28	-8.0
	Comp.	8.32	13.9	16.6	16.5	13.6	7.9	-0.57	-11.76

Note:- Moments are positive when outer fibres in tension. The units are KN – mm

TABLE 4.4 b

DISPLACEMENTS OF THE EXPERIMENTAL ARCH

Load Case	Displ. / Method	X_2	Y_2	X_4	Y_4	X_6	Y_6	X_8	Y_8
25 Kgf.	Exper.	-0.395	0.52	-0.38	0.70	0.02	-0.38	0.015	-2.45
	Comp.	-0.32	0.50	"	0.62	-0.16	-0.36	0.0	-2.15

Note:- The units of displacements are mm

TABLE 4.5 a

BENDING MOMENTS IN THE EXPERIMENTAL ARCH
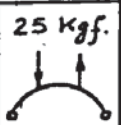
Load Case	Point / Method	1	2	3	4	5	6	7	8
25 Kgf.	Exper.	-11.0	-35.6	-39.8	-53.0	-46.0	-31.0	-12.7	2.14
	Comp.	-10.87	-22.31	-34.24	-46.58	-35.2	-23.6	-11.84	0.0

TABLE 4.5 b

DISPLACEMENTS OF THE EXPERIMENTAL ARCH

Load Case	Displ. / Method	X_2	Y_2	X_4	Y_4	X_6	Y_6	X_8	Y_8
25 Kgf.	Exper.	2.47	-3.54	3.55	-6.39	3.01	-6.0	1.53	0.0
	Comp.	1.82	-2.88	2.85	-5.23	2.81	-4.86	2.48	0.0

TABLE 4.6 a

BENDING MOMENTS IN THE EXPERIMENTAL ARCH

Load Case	Point / Method	1	2	3	4	5	6	7	8
40 Kgf.	Exper.	11.8	16.5	18.5	16.5	12.3	7.38	−0.65	−7.74
	Comp.	9.72	16.24	19.47	19.38	15.95	9.24	−0.67	−13.63

TABLE 4.6 b

DISPLACEMENTS OF THE EXPERIMENTAL ARCH

Load Case	Displ. / Method	X_2	Y_2	X_4	Y_4	X_6	Y_6	X_8	Y_8
40 Kgf.	Exper.	−0.28	0.185	−0.17	0.26	−0.03	−0.26	−0.04	−1.23
	Comp.	−0.27	0.254	−0.33	0.32	−0.14	−0.25	0.0	−1.32

TABLE 4.6 c

AXIAL FORCES IN THE EXPERIMENTAL ARCH

Load Case	Point / Method	1	2	3	4	5	6	7	8
40 Kgf.	Exper.	−0.03	0.0	0.39	−0.56	1.03	0.8	0.01	0.6
	Comp.	0.38	0.39	"	0.39	0.38	0.36	0.34	0.36

Note:- Axial force is positive when compressive.

TABLE 4.7 a

BENDING MOMENTS IN THE EXPERIMENTAL ARCH
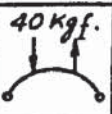
Load Case	Point / Method	1	2	3	4	5	6	7	8
40 Kgf.	Exper.	−11.8	−22.6	−34.8	−38.7	−28.4	−20.9	−10.9	−1.98
	Comp.	−10.41	−22.18	−35.15	−49.14	−37.44	−25.25	−12.71	0.0

TABLE 4.7 b

DISPLACEMENTS OF THE EXPERIMENTAL ARCH

Load Case	Displ. / Method	X_2	Y_2	X_4	Y_4	X_6	Y_6	X_8	Y_8
40 Kgf.	Exper.	1.55	−1.04	1.93	−2.23	1.86	−2.03	1.0	−0.1
	Comp.	1.44	−1.36	2.29	−2.63	2.31	−2.56	2.06	0.0

C H A P T E R   5

CURVED MEMBERS LOADED OUT-OF-PLANE

5.1 Introduction

The curved members loaded out of plane are considered in this chapter. The load-displacement relationships for these are obtained by using the polynomial as well as the derived displacement functions. The latter are obtained by considering the out of plane equilibrium of a curved element with uniform cross-section. The strain-displacement relationships for the curved members suffering out of plane displacements are not given in text books and are, therefore, developed here. These relationships are utilized in formulating the stiffness matrices by using both the polynomial and the derived displacement functions. Finally, as for the in-plane case, the above-mentioned displacement functions are employed to obtain the stiffness matrices for the curved elements with variable cross-sections.

5.2 The Strain-Displacement Relationships

A curved element of radius R, measured from the centre O to the centroidal axis AB, is shown in fig. 5.1. The arc AB subtends an angle θ at the centre. Also shown in the figure are the cartisian axes X and Y with their origin at A.

The curved member twists when displaced out of the plane. Therefore, a point, E, in the member displaces by a different amount than another point, D. Thus the out of plane displacement, w, is a function of the arc length AB and the radial distance r . This relationship can be written as:-

$$w = f(p, r) \tag{5.1}$$

where   p   is the arc   length AB measured from A;

and   r   is the radial distance from the centroidal

axis to the point, E, in the member under

consideration.

From fig. 5.1 the following relationships are obvious:-

$$(R - r)^2 = x^2 + (R - y)^2 \tag{5.2}$$

$$\cos \theta = \cos \frac{p}{R} = \frac{R - y}{R - r} \tag{5.3}$$

and $\sin \theta = \sin \frac{p}{R} = \frac{x}{R - r}$ \tag{5.4}

To obtain the variation of the out of plane displacement,
w, the variations of both p and r are required. Differntiating
eqn. (5.2) with respect to x and comparing the results with
eqn. (5.4) gives:-

$$\frac{\partial r}{\partial x} = - \sin \frac{p}{R} \tag{5.5}$$

Similarly, it is easy to show that the variation of r
with respect to y is given by the following equation:-

$$\frac{\partial r}{\partial y} = \cos \frac{p}{R} \tag{5.6}$$

The length of the arc, p , is a function of angle θ .
From the geometry of fig. 5.1, angle θ and, therefore, p can
be expressed in terms of x and y as follows:-

$$p = R.\tan^{-1} \frac{x}{R - y} \tag{5.7}$$

Differentiating eqn. (5.7) with respect to x and y and
making use of the eqns. (5.2) to (5.4) the variations of p are
obtained. These are:-

$$\frac{\partial p}{\partial x} = \frac{R}{R - r} \cos \frac{p}{R} \tag{5.8}$$

and $\qquad \dfrac{\partial p}{\partial y} = \dfrac{R}{R-r} \sin \dfrac{p}{R}$ $\qquad$ (5.9)

Applying the rule of partial differentiation to eqn. (5.1) yields the following relationships:-

$$\frac{\partial w}{\partial x} = \frac{\partial w}{\partial p}\frac{\partial p}{\partial x} + \frac{\partial w}{\partial r}\frac{\partial r}{\partial x} \qquad (5.10)$$

and

$$\frac{\partial w}{\partial y} = \frac{\partial w}{\partial p}\frac{\partial p}{\partial y} + \frac{\partial w}{\partial r}\frac{\partial r}{\partial y} \qquad (5.11)$$

Substituting eqns. (5.5) and (5.8) into eqn. (5.10) gives:-

$$\frac{\partial w}{\partial x} = \frac{\partial w}{\partial p}\frac{R}{R-r}\cos\frac{p}{R} - \frac{\partial w}{\partial r}\sin\frac{p}{R} = m \qquad (5.12)$$

To obtain the required curvature-displacement relationship eqn. (5.12) is to be differentiated further with respect to x and y. An intermediate variable, m, has been introduced to make the differentiation easier. It is obvious that like w the intermediate variable, m, is also a function of p and r. Writing this relationship in the form of eqn. (5.1) gives:-

$$m = f(p, r) \qquad (5.13)$$

where p and r are already defined for eqn. (5.1).

Applying the rule of partial differentiation to eqn. (5.13) yields:-

$$\frac{\partial^2 w}{\partial x^2} = \frac{\partial m}{\partial p}\frac{\partial p}{\partial x} + \frac{\partial m}{\partial r}\frac{\partial r}{\partial x} = \frac{\partial m}{\partial x} \qquad (5.14)$$

when p = o:

From eqn. (5.8) : $\qquad \dfrac{\partial p}{\partial x} = \dfrac{R}{R-r}$ $\qquad$ (5.15)

and $\quad$ " $\quad$ " $\quad$ (5.5) : $\qquad \dfrac{\partial r}{\partial x} = 0$ $\qquad$ (5.16)

Substituting eqns. (5.15) and (5.16) into eqn. (5.14) reduces the latter to the following equation.

$$\frac{\partial^2 w}{\partial x^2} = \frac{R}{R-r} \quad \frac{\partial m}{\partial p} \qquad (5.17)$$

Differentiating eqn. (5.12) with respect to p and substituting the results into eqn. (5.17) yields:

$$\frac{\partial^2 w}{\partial x^2} = \frac{R}{R-r} \left[\frac{\partial^2 w}{\partial p^2} \quad \frac{R}{R-r} \quad \cos \frac{p}{R} - \frac{\partial w}{\partial p} \quad \frac{1}{R-r} \quad \sin \frac{p}{R} \right.$$
$$\left. - \frac{\partial^2 w}{\partial p \, \partial r} \sin \frac{p}{R} - \frac{\partial w}{\partial r} \quad \frac{1}{R} \cos \frac{p}{R} \right] \qquad (5.18)$$

Substituting the values of sin and cos when p = o, equation (5.18) is simplified to become:-

$$\frac{\partial^2 w}{\partial x^2} = \left(\frac{R}{R-r} \right)^2 \quad \frac{\partial^2 w}{\partial p^2} - \frac{1}{R-r} \quad \frac{\partial w}{\partial r} \qquad (5.19)$$

For thin circular members with the radius much larger compared to the dimensions of the cross-section, the following approximations can be made:-

$$R - r \simeq R \qquad\qquad (5.20)$$

and

$$\frac{\partial w}{\partial r} = \gamma \qquad\qquad (5.21)$$

where γ is the angle of twist of the curved member.

Combining eqns. (5.19) to (5.21) yields the required expression for the out of plane bending curvature which is:-

$$\chi = \frac{\partial^2 w}{\partial p^2} - \frac{\gamma}{R} \qquad (5.22)$$

Similarly, differentiating eqn. (5.12) partially with respect to y leads to the curvature-displacement relationship for twisting which is given by the following equation:-

$$\chi_{xy} = \frac{\partial \gamma}{\partial p} + \frac{1}{R} \quad \frac{\partial w}{\partial p} \qquad (5.23)$$

Equation (5.11) can also be used to obtain the expression for the twisting curvature, χ_{xy}. It is noticed from eqns.

(5.22) and (5.23) that the influence of the initial curvature, R, is represented by the second term on the right. This term vanishes as the radius, R, becomes infinity and the expressions for the curvatures are, then, identical to those obtained for a straight member.

5.3 The Stiffness Matrix by Assumed Displacement Functions

(i) The Displacement Functions

The assumed polynomial function, eqn. (3.1), is assigned to the out of plane displacements while the twist, γ, in the curved member is approximated by the linear function, equation (3.2).

Due to the fact that the assumed displacement functions are the same, some of the equations involved in the formulation of the stiffness matrix for the out of plane case are identical to those obtained in section 3.3 for the in-plane case. Except that u is now replaced with γ. Only the equations that are different are produced here.

(ii) The Strain-Displacement Relationships

The strain-displacement relationships for curved member suffering out of plane deformations are given in eqns. (5.22) and (5.23) but p in these equations is replaced by x . As there is only one independent variable, x , the symbol of partial differentiation can be dropped.

Differentiating the displacement functions appropriately and substituting the results into equations (5.22) and (5.23) leads to the following relationships in matrix form:-

$$
\begin{bmatrix} \chi \\ \\ \chi_{xy} \end{bmatrix} = \begin{bmatrix} 0 & 0 & 2 & 6x & -\dfrac{1}{R} & -\dfrac{x}{R} \\ \\ 0 & \dfrac{1}{R} & \dfrac{2x}{R} & \dfrac{3x^2}{R} & 0 & 1 \end{bmatrix} \begin{bmatrix} a_1 \\ a_2 \\ a_3 \\ a_4 \\ a_5 \\ a_6 \end{bmatrix} \quad (5.24)
$$

Equation (5.24) is equivalent to equation (3.24) for the in-plane case. The terms containing R represent the influence of the initial curvature. As the radius, R, of the member becomes infinity, all the terms containing R vanish and the matrix becomes the same as obtained for straight members.

(iii) The Stress-Strain Relationships

The stress-strain relationships can be found in references 1 and 2. Expressing these in matrix form :-

$$
\begin{bmatrix} M \\ \\ T \end{bmatrix} = \begin{bmatrix} EI & 0 \\ \\ 0 & GJ \end{bmatrix} \begin{bmatrix} \chi \\ \\ \chi_{xy} \end{bmatrix} \quad (5.25)
$$

where M is the out of plane bending moment in the element;

T is the twisting moment;

EI is the out of plane bending stiffness;

and GJ is the torsional rigidity of the element.

(iv) The Stiffness Terms

The elements of the stiffness matrix are calculated from the following formula obtained from equation (3.30):

$$
k_{mn} = \int_0^L (EI \; B_{1m} B_{1n} + GJ \; B_{2m} B_{2n}) \, dx \quad (5.26)
$$

The elements of the stiffness matrix are:-

$$k_{11} = EI \left(\frac{12}{L^3}\right) + GJ \left(\frac{6}{5} \frac{1}{R^2 L}\right)$$

$$k_{12} = EI \left(\frac{6}{L^2}\right) + GJ \left(\frac{1}{10R^2}\right)$$

$$k_{13} = - k_{11}$$

$$k_{14} = k_{12}$$

$$k_{15} = (EI + GJ) \frac{1}{RL}$$

$$k_{16} = - k_{15}$$

$$k_{22} = EI \left(\frac{4}{L}\right) + GJ \left(\frac{2}{15} \frac{L}{R^2}\right)$$

$$k_{23} = - k_{12}$$

$$k_{24} = EI \left(\frac{2}{L}\right) - GJ \left(\frac{1}{30} \frac{L}{R^2}\right)$$

$$k_{25} = \frac{EI}{R}$$

$$k_{26} = 0.0$$

$$k_{33} = k_{11}$$

$$k_{34} = - k_{12}$$

$$k_{35} = - k_{15}$$

$$k_{36} = k_{15}$$

$$k_{44} = k_{22}$$

$$k_{45} = 0.0$$

$$k_{46} = -k_{25}$$

$$k_{55} = EI \left(\frac{L}{3R^3}\right) + \frac{GJ}{L}$$

$$k_{56} = EI \left(\frac{L}{6R^2}\right) - \frac{GJ}{L} \qquad k_{66} = k_{55}$$

(5.27)

An examination of the stiffness matrix, eqns. (5.27), shows that the twisting moments in the members are independent of the out of plane displacements and rotations. In turn, the twist in the member does not contribute to the bending moments and the shear forces. Furthermore, it is observed that for members with the radius, R, equal to infinity, the stiffness matrix reduces to that well known for straight prismatic members.

5.4 Derivation of the Exact Displacement Functions

An element cut from a thin circular ring of radius, R, and a uniform cross-section is shown in fig. 5.2. The length of the element is dx and is measured along the curve. The angle subtended by the curved length of the element at the centre O is dθ as shown in the figure. The adjoining elements transmit the following forces to the element under consideration:-

(a) a shear force, S, at end 1 which increases along the length of the element to S + dS at end 2;

(b) a bending moment, M, at end 1 which increases to M + dM at end 2 of the element; and finally

(c) a twisting moment, T, at end 1 which increases to T + dT at end 2.

All these forces are also shown in figs. 5.2 and 5.3, the latter being another view of the element.

Summation of all the forces acting on the element along Z-axis gives:-

$$dS = 0 \tag{5.28}$$

Since the rate of change of the shear force, dS, is zero,

it is not included in the subsequent equations of static equilibrium of the element.

Considering the rotational equilibrium about the bisecting line OA and using the approximations for the trignometric functions of small angles, equations (3.36) and (3.37), yields:-

$$dM + T \, d\theta + SR \, d\theta = 0 \qquad (5.29)$$

Similarly, consideration of the rotational equilibrium about a line passing through the ends of the element leads to the following relationship:-

$$dT - M \, d\theta = 0 \qquad (5.30)$$

The second order terms involved in the derivation of equations (5.29) and (5.30) have been ignored.

From the geometry of fig. 5.2, the following relationship is obvious:-

$$d\theta = \frac{dx}{R} \qquad (5.31)$$

Substituting equation (5.31) into equation (5.29) gives:-

$$\frac{dM}{dx} + \frac{T}{R} + S = 0 \qquad (5.32)$$

Similarly from equations (5.30) and (5.31) the following equation is obtained:-

$$\frac{dT}{dx} - \frac{M}{R} = 0 \qquad (5.33)$$

Differentiating equation (5.32) with respect to x and noting that dS is equal to zero, from equation (5.28), leads to:-

$$\frac{d^2M}{dx^2} + \frac{1}{R} \frac{dT}{dx} = 0 \qquad (5.34)$$

Equations (5.33) and (5.34) are the required differential equations relating the bending and twisting moments in the curved elements.

The bending and twisting moments in the element are related to the curvatures as follows:-

The bending moment, $M = -EI \left(\dfrac{d^2w}{dx^2} - \dfrac{\gamma}{R} \right)$ (5.35)

and the twisting ", $T = GJ \left(\dfrac{1}{R} \dfrac{dw}{dx} + \dfrac{d\gamma}{dx} \right)$ (5.36)

The expressions in parenthesis in equations (5.35) and (5.36) are the strain-displacement relationships for curved members obtained in section 5.2.

Substituting equations (5.35) and (5.36) into equation (5.34) and carrying out the appropriate differentiations leads to the following equation:-

$$\frac{d^2\gamma}{dx^2} = \frac{R}{EI + GJ} \left(EI \frac{d^4w}{dx^4} - \frac{GJ}{R^2} \frac{d^2w}{dx^2} \right)$$ (5.37)

which upon integration with respect to x becomes:-

$$\gamma = \frac{R}{EI + GJ} \left(EI \frac{d^2w}{dx^2} - \frac{GJ}{R^2} w \right) + b_1 + b_2 x$$ (5.38)

Equation (5.38) relates the twist, γ, to the out of plane displacement, w, of a curved member. b_1 and b_2 are constants of integrations.

Differentiating equations (5.35) and (5.36) with respect to x and substituting the results into equation (5.33) yields:-

$$\frac{EI + GJ}{R} \frac{d^2w}{dx^2} + GJ \frac{d^2\gamma}{dx^2} - \frac{EI}{R^2} \gamma = 0$$ (5.39)

Eliminating γ from equation (5.39) by substituting equations (5.37) and (5.38) gives the required differential equation for the out of plane displacements, w. This equation is:-

$$\frac{d^4w}{dx^4} + \frac{2}{R^2} \frac{d^2w}{dx^2} + \frac{w}{R^4} = c_1 + c_2 x$$ (5.40)

where c_1 and c_2 are proportioned to b_1 and b_2 respectively.

The solution of equation (5.40) yields the required displacement function which is:-

$$w = a_1 + a_2 x + a_3 \sin \frac{x}{R} + a_4 \cos \frac{x}{R} + a_5 x \sin \frac{x}{R} +$$

$$a_6 x \cos \frac{x}{R} \tag{5.41}$$

where $a_1 - a_6$ are the arbitrary constants.

The constants c_1 and c_2 in equation (5.40) can be related to the arbitrary constants a_1 and a_2 respectively by considering the particular integrals for eqn. (5.40). Through c_1 and c_2, the constants b_1 and b_2 are related to a_1 and a_2.

The displacement function for the twisting of curved bars is obtained by substituting eqn. (5.41) into eqn. (5.38) and carrying out the necessary differentiation. The function obtained is:-

$$\Upsilon = - \frac{a_3}{R} \sin \frac{x}{R} - \frac{a_4}{R} \cos \frac{x}{R} + \tag{5.42}$$

$$a_5 \left(\frac{2EI}{EI+GJ} \cos \frac{x}{R} - \frac{1}{R} \sin \frac{x}{R} \right) - a_6 \left(\frac{2EI}{EI+GJ} \sin \frac{x}{R} + \frac{1}{R} \cos \frac{x}{R} \right)$$

Considering the displacement functions obtained, it is observed that as the radius, R, of the element increases to infinity, eqn. (5.41) degenerates into a linear equation while eqn. (5.42) gives twist, Υ , equal to a constant. Therefore, as in the case of the derived displacement functions for the in-plane case, equations (5.41) and (5.42) are expected to yield poor results for straight members.

5.5 The Stiffness Matrix by the Exact Displacement Functions

The steps involved in the development of the stiffness matrix using the derived displacement functions are the same as used for the cubic functions in section 5.3. The details

for the stiffness matrix are given in Appendix C. Equations required to discuss particular points are produced in this section.

(i) The Displacement Functions

The displacement functions are given in equations (5.41) and (5.42) for the out of plane displacements and twists respectively. These are called the exact displacement functions. The equation for slope at any point in the element is obtained by differentiating eqn. (5.41) with respect to x. Substituting the boundary conditions into the equations for the displacements, slope and the twist yields a set of simultaneous equations which express the nodal displacements in terms of the arbitrary constants, a_1 - a_6. The simultaneous equations are explicitly solved to obtain the arbitrary constants in terms of the nodal displacements. The final results from this step are expressed by eqn. (1.3).

(ii) The Strain-Displacement Relationships

The strain-displacement relationships were obtained in section 5.2 and are given in equations (5.22) and (5.23). Substituting the displacement functions, equations (5.41) and (5.42), into the expressions for the bending and the twisting curvatures, differentiating the resulting equations as required yields the following relationships in matrix form:-

$$\begin{bmatrix} \chi \\ \chi_{xy} \end{bmatrix} = \begin{bmatrix} 0 & 0 & 0 & 0 & e_1 \cos \frac{x}{R} & -e_1 \sin \frac{x}{R} \\ 0 & \frac{1}{R} & 0 & 0 & \frac{\psi}{R} \sin \frac{x}{R} & \frac{\psi}{R} \cos \frac{x}{R} \end{bmatrix} \begin{bmatrix} a_1 \\ a_2 \\ a_3 \\ a_4 \\ a_5 \\ a_6 \end{bmatrix} \qquad (5.43)$$

where $\qquad \psi = \dfrac{2EI}{EI+GJ}$; and $e_1 = \dfrac{2 + \psi}{R}$ $\qquad\qquad$ (5.44)

Equation (5.43) can be used to study the pattern of the strains in the curved elements. It is noticed that as the radius, R, is increased to infinity, the strains yielded by equation (5.43) are all equal to zero. The exact functions, therefore, cannot be used for straight members by making R equal to infinity.

(iii) The Stress-Strain Relationships.

The stress-strain relationships remain unaltered and are given in eqn. (5.25).

(iv) The Stiffness Terms

The recurssive formula, eqn. (5.26), used for the cubic functions is also valid for the exact displacement functions. The elements of the stiffness matrix are given in Appendix C. A survey of these shows that all the nodal displacements contribute to all the nodal forces of the element.

5.6 Curved Members with Variable Cross-Sections

The variations of the cross-section of an element were discussed in section 3.6. As for the in-plane case, curved elements whose cross-sections vary linearly are considered.

Several formulae, slightly differing from each other, are used to calculate the torsion constants of rectangular sections. Grashof's formula is one of these and is used in this Thesis. This expression is:-

$$J = \dfrac{b^3 t^3}{3.6(b^2 + t^2)} \qquad\qquad (5.45)$$

where J is the torsion constant of a rectangular

cross-section;

and b and t are the dimensions of the cross-sections.

(i) The Cubic Displacement Functions

As for the in-plane case, the calculation of the stiffness matrix explicitly is straight forward. Polynomial expressions for the second moment of area, I, and the torsion constant, J, are substituted into eqn. (5.26). The resulting equations are then integrated to obtain the elements of the stiffness matrix.

(ii) The Exact Displacement Functions

The variations in the second moment of area, I, and the torsion constant, J, should be taken into consideration when deriving the displacement functions. It is obvious that this makes the derivations difficult. The displacement functions obtained in section 5.4 for the elements with uniform cross-sections are, therefore, employed to formulate the stiffness matrix of a curved element with variable cross-section.

Remarks made for the in-plane case, section 3.6, also apply for the out of plane case. By using the linear variation the dimensions of the cross-section under consideration are calculated. From these it is easy to obtain the moment of inertia, I, and the torsion constant, J, expressed by eqn. (5.45). The stiffness terms are obtained by integrating equation (5.26) numerically.

5.7 Uniformly Distributed Loads

The strain energy method can easily be used to obtain the statically equivalent forces for the curved members carrying the uniformly distributed loads. Alternatively, the principle of

virtual work can be employed to obtain identical results. In this Thesis, the strain energy method is used.
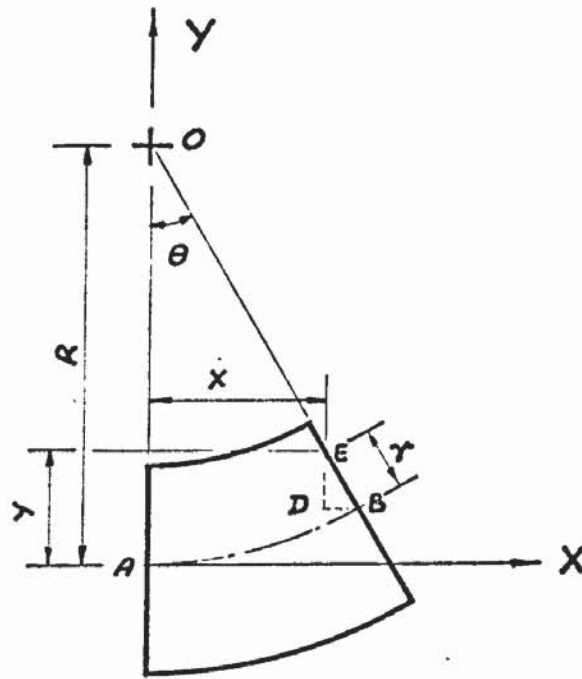
FIG. 5.1

STRAIN-DISPLACEMENT RELATIONSHIP FOR A
BOW GIRDER ELEMENT
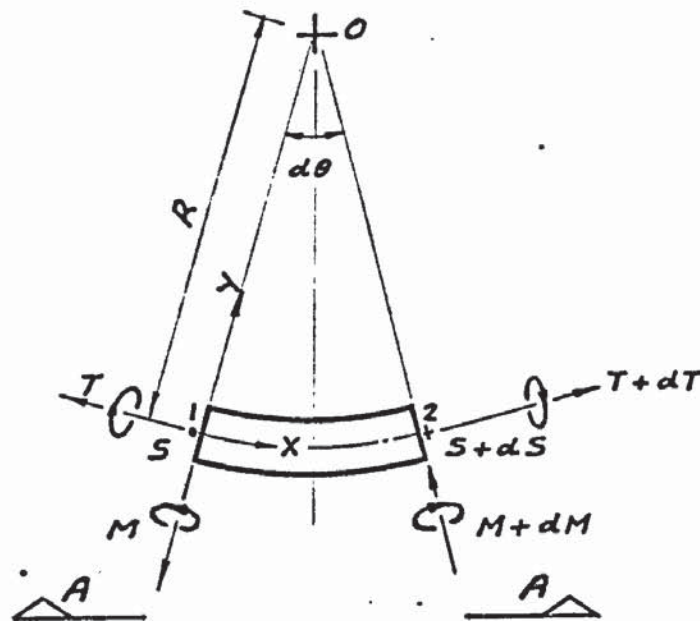
FIG. 5.2

FREE-BODY DIAGRAM OF A BOW GIRDER ELEMENT
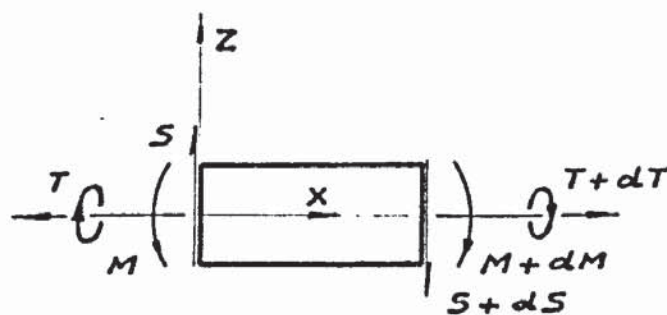
FIG. 5.3

ELEVATION A-A

C H A P T E R   6

THEORETICAL AND EXPERIMENTAL RESULTS FOR BOW GIRDERS

6.1 Introduction

The stiffness matrices for the curved elements which suffer deformations out of the plane were developed in Chapter 5. In this chapter these matrices are used to obtain the results for several bow girders under various types of loads. The bow girders with the uniform cross-section are also analysed by using the strain energy method. Some of these girders are also approximated by a number of straight prismatic members. Only the stiffness matrix obtained by using the derived displacement functions is employed to analyse the bow girders with variable cross-sections. Results for these are also obtained by experiments. The theoretical results obtained by using various methods are compared either with those yielded by the strain energy method or with those obtained by experiments. Finally, the influence of the shape of the cross-section is investigated by obtaining results for a bow girder. The ratio of the dimensions of the rectangular cross-section for this bow girder is varied.

6.2. Bow Girders of Uniform Cross-Sections

The circular bow girder shown in fig. 6.1 has the same dimensions and properties as the arch shown in fig. 4.1. In addition to those used for arches, the following properties are assumed for the material of the bow girders:-

The Poisson's ratio, $\nu = 0.3$;

and the shear modulus, $G = \dfrac{E}{2(1 + \nu)}$

The quantity E in the above expression for the shear modulus is the modulus of elasticity of the material.

The length of the bow girder subtends an angle α at the centre O as shown. Points D, C and E divide the bow girders into 4 segments of equal length. Bow girders with angle α varying from 30° to 180° are analysed by using various methods. Some of the results obtained are presented in the graphs where the curves are marked to indicate the method used to obtain the results represented by a curve. The meanings of various abbreviations used (S.E., E.F., C.F. and S.M.) have already been explained in section 4.2.

The results obtained by using various methods are compared with those yielded by the strain energy method. Thus the percentages are with respect to results obtained by using the strain energy method. From the results presented in this chapter as well as from those results that have been omitted, it is seen that the derived displacement functions and the strain energy method yield identical results. Furthermore, the exact functions do not yield improved results upon further subdivision of the bow girders.

(i) Concentrated Load at the Centre

A concentrated load equal to 1.0 kgf. is applied at the mid-point, C, of the bow girder shown in fig. 6.1. The bow girders are divided into two segments of equal lengths for analysis by the derived and the cubic displacement functions. The number of straight members used to simulate the bow girders is shown in parenthesis along the curve for the corresponding results.

The results for the bending moments under the load are

plotted in fig. 6.2. Even with the crude sub-division used, the cubic functions gave good results. For a semi-circular bow girder, these are within 10% of the results obtained by using the strain energy method. The bending moments obtained by approximating the bow girders by a number of straight members are seen to be rapidly improving upon further sub-division.

It was shown in references (27, 28) that bending moments in shallow bow girders can be assumed to be the same as in straight beams of length equal to the curved length. For bow girders carrying point loads, this assumption leads to a linear relationship between the bending moments and the lengths of bow girders. Fig. 6.2 confirms this. An almost straight line was also obtained for the bending moments at the support. These results have been left out.

The cubic functions have yielded more accurate results for twisting moments at the support than was the case for bending moments. Twisting moments are plotted in fig. 6.3. It is noticed that the results obtained by simulating the bow girder with straight members deteriorate upon further sub-division.

Consider the bow girder shown in fig. 6.1 with angle α equal to 180° and carrying a point load at the mid-point C. It is obvious from the symmetry of the structure and loading that rotation, θ_x , about an axis passing through both supports, X-axis, reaches its maximum value at C. For the same reason rotation, θ_y , about line OC must be zero at C. The displacements at the fixed ends are, of course, zero. The theoretical results obtained by using the exact functions confirmed the above observations made regarding the rotations. It was noticed that the magnitude of θ_y was of negative sign,

from A to C, as expected. The variation of both rotations was
parabolic. Simulating the bow girder with a number of straight
members the twist at an end of the member can be obtained
from the following equation:-

$$\Upsilon = \theta_x \cos\beta + \theta_y \sin\beta \qquad\qquad (6.1)$$

where β is the angle of inclination of the straight member
to the X-axis. Consider the straight member whose one end is
attached to support A. It is obvious that β increases with
the number of sub-divisions. Since θ_y is of opposite sign,
and both rotations change from point to point, it is possible,
for equation (6.1), to yield twist in the member of very small
magnitude and even of negative sign. On the other hand, a
coarser sub-division may yield, as in the present case, a
positive twist.

The twisting moment at the support was given in references
(27, 28) as proportional to the area of the bending moment
diagram. It is obvious that this yields a parabolic curve for
the twisting moments. The results in fig. 6.3 confirm this.

The results for the deflections and the angle of twist at
the mid-point of the bow girders are shown in figs. 6.4 and 6.5
respectively. The results obtained by various methods are seen
to agree very well with each other for shallow bow girders with
angle α less than 60°. The error in the results obtained for
a sime-circular bow girder by using the cubic functions is
over 20% for deflections and about 27% for the twist. Approx-
imating the bow girders with only four straight members yields
better results than the cubic functions. Straight member
approximation of arches gave better results for displacements
than for forces. It appears that the same is true in the case

of bow girders as well.

The curves for the out of plane displacements and twists are all smooth curves. This follows from the similar curves obtained for the bending and the twisting moments.

(ii) Eccentric Point Load

A load of 1.0 kgf. is applied at the quarter point, D, of the bow girder shown in fig. 6.1. The bow girders are divided into 4 equal parts for analysis by the exact and the cubic functions. As before, the number of straight members used to approximate the bow girders are given in parenthesis along the appropriate results. Table 6.1 shows the results for the bending moments at the support, M_A, the bending and the twisting moments under the point load, M_D and T_D respectively. The cubic functions are seen to have given good results. Straight member approximation yields good results for bending moments, but the results for twisting moments are poor. However, these are seen to improve upon further sub-division.

The results for the twisting moments at the support are plotted in fig. 6.6. The cubic functions have given very accurate results; being within 8% of those obtained by using the strain energy method. Simulating the bow girders with a number of straight members yields results which differ by a wide margin. Increasing the number of sub-divisions does not improve the results over the whole range of angle α.

The curves representing the strain energy and the displacement functions are smooth with the slope increasing uniformly. This is to be expected for the same reasons as given for the symmetric point load case. The slopes of the curves representing straight member approximation do not increase

uniformly as can be seen from fig. 6.6.

(iii) Skew Symmetric Point Loads

A load of 1.0 kgf. acts at each of the quarter points, D and E, of the bow girder shown in fig. 6.1. The two loads act opposite to each other. Table 6.2 shows the results obtained for the same forces as tabulated in Table 6.1 for the eccentric point load case. Once again, the cubic functions have yielded very good results, especially for the bending moments. The twisting moments are slightly under-estimated. The error varies from a negligible amount for shallow girders, to about 10% for a semi-circular one. Straight member approximation of the bow girders gives reasonable results for bending moments. There is some improvement in the results upon further sub-division. The twisting moments under the load are grossly over-estimated by the straight member simulation. The results are seen to improve upon further sub-division, but a large error persists.

The results for the twisting moments at the support are plotted in fig. 6.7. Again the curve representing the cubic functions follows that for the strain energy method very closely. Both these curves are seen to have slopes which are increasing uniformly. The curves representing the straight member approximation diverge by a wide margin. From fig. 6.7 it is seen that further sub-division does not always improve the results. Four members are inadequate to represent a semi-circular bow girder. Doubling the number of members yields nearly accurate results. Again doubling the number of members gives zero twisting moments at the support.

(iv) Uniformly Distributed Loads

Straight members have not been used to simulate bow girders carrying uniformly distributed loads. For analysis by the displacement functions, the bow girders were divided into 2 to 16 equal parts. The results presented, however, are for two sub-divisions only. All the results have been divided by the product of total load, W, and the radius, R, of the bow girders.

(a) Symmetric U.D.L.

A uniformly distributed load of 1.0 kgf./mm of the curved length is applied to the bow girder shown in fig. 6.1. The results for the bending and twisting moments, M_A and T_A respectively, and the bending moments at the mid-point, C, are tabulated in Table 6.3. It is observed that the cubic functions yield bending and twisting moments at the support which agree well with those given by the strain energy method. The results for bending moments at C are good for girders with angle α less than 90°. For a semi-circular girder, the error is about 17% which is quite reasonable considering the crude sub-division used. Increasing the number of members to 16 yields accurate results.

Deflections at the mid-point, δ_c , are plotted in fig. 6.8. It is noticed that the results obtained by various methods are very close to each other for bow girders representing up to a guardrant. For a semi-circular bow girder, the cubic functions give displacements which are about 80% of those obtained by using the strain energy method. Increasing the number of sub-divisions from 2 to 16 brings the deflections within 1%.

(b) Skew Symmetric U.D.L.

The u.d.l. in the preceding load case, (a), over half of the length of the bow girder acts in the opposite direction to that acting over the other half. Some of the results obtained are shown in Table 6.4. The cubic functions are seen to yield fairly good results for the twisting moments at the mid-point C. The results for the bending and twisting moments at the support are good for shallow girders only. Twisting moments are seen to deteriorate faster than bending moments as the bow girders become deeper. Once again, increasing the number of members representing a semi-circular bow girder improves all the results to within 2%.

6.3 The Influence of the Shape of the Cross-Section

The bow girder shown in fig. 6.1 is utilized to study the influence of the shape of the cross-section. A unit load is applied at the mid-point, C, of the bow girder. Angle a is equal to $120°$. The width, b, of the cross-section is kept constant, while the depth, d, is varied in a manner so that the ratio d/b is always an integer.

Table 6.5 shows the results for the bending and twisting moments at the support, M_A and T_A respectively, and the bending moments under the load, M_c. The girders are divided into two equal parts for analysis by the exact functions. To obtain results by the cubic functions, the girders are divided into 2 and 16 members of equal length. Four and 16 straight members are used to simulate the girders. The first row of the results for each bow girder is for the coarser sub-division, and the second row is for the finer sub-division. The ratios, r,

obtained by dividing the flexural stiffness, EI, by the torsional rigidity, GJ, of the girders appear in the second column of the table.

It is seen from the table that for the finer sub-division, the cubic functions yield results which approach those obtained by using the exact functions. A similar trend is also observed in the bending moments obtained by straight member approximation of the bow girders. However, as before, the twisting moments yielded by the latter method are seen to deviate even more upon further sub-division.

The results obtained by using the cubic and exact functions are plotted in figs. 6.9 to 6.11. Results for the strain energy method are also shown. These have been obtained from reference (6). It is seen from the graphs that the curves representing the exact functions and the strain energy method are very close to each other. The results yielded by the cubic functions are rather poor. These improve upon further sub-division as was observed from Table 6.5. However, in all the results the influence of the shape of the cross-section is seen to be fading as the ratio r increases.

7.4 Bow Girders with Variable Cross-Sections

The separation of strains and, therefore, of stresses into those due to bending and those due to twisting becomes complicated. Consequently, the strain gauges have not been used for

the bow girders. The stiffness matrix developed in the preceding chapter for curved elements with variable cross-sections is used to obtain the theoretical results.

(i) Tests on the Bow Girders

The arch with both ends fixed was tested as a bow girder. The deflections obtained were linear for small loads, but became non-linear as the load was increased. This non-linearity was traced to the hollow sections to which the ends of the arch were welded. Similar observations were also made in the case of the two curved cantilevers when tested as half bow girders. The hollow sections were, therefore, cut off and both ends of the bow girder were welded to 250 x 250 x 19.1 mm thick mild steel plates which can be seen in Plate 7. An isometric sketch of the base plate and the end of the bow girder is shown in Drawing No. 1.

Three 4.8 x 15.9 x 270.0 mm long bars of mild steel were welded to the girder in the radial directions. One of these bars is near the centre and the other two are near the quarter points. Slight offsets from the centre and the quarter points are to avoid the loading brackets. By measuring the displacements of two points on a bar, the angle of twist of the girder can be calculated. The radial bars and some deflection dial gauges are visible in Plate 7.

The loading pins required to test the structure as an arch were removed in order to apply the out of plane loads exactly at the centre and quarter points. The bow girder was tested in an upright position. The loads were, therefore, applied horizontally. Triangular frames were made from dexian. To each of these a pully was fixed at the required height. One end of

a rope was tied to the loading bracket and the other to a hanger. The rope passed over the pully. Care was taken to ensure that the rope between the loading bracket and the pully was horiztonal. Otherwise, the applied load will have a component in the plane of the structure. The loading arrangement can be seen in Plate 7 which is a general view of the bow girder. Other loading brackets and deflection dial gauges were removed for clarity. The dimensions and details of the loading brackets are shown on Drawing No. 5.

Three tests were carried out on the bow girder. In each test the load was applied in 7 increments of 8.0 kgf. and a final one of 4.0 kgf. After reaching 60.0 kgf., the load was decreased in the reverse order. At each stage of the load readings of all the deflection dial gauges were recorded. From the readings for the loading and unloading cycles, the average readings at each load stage were calculated. These average readings were plotted against the load and the best line drawn through each set of points. From the graphs thus obtained, the deflections corresponding to the 60.0 kgf. load were calculated.

(ii) Results for Bow Girders with Variable Cross-Sections

Table 6.6 shows the results obtained for the bow girder carrying a 60.0 kgf. load at the mid-point, C. Points D and E are the quarter points of the bow girder. The results are for the deflections at D and C and the angle of twist at the latter point. The bending and the twisting moment diagrams are shown in figs. 6.12 and 6.13. As mentioned earlier no results have been obtained for the forces by experiments. The bending and the twisting moment diagrams are, therefore, of academic interest only.

The results for the eccentric and the skew symmetric point
loads are tabulated in Tables 6.7 and 6.8 respectively. Theor-
etical displacements were divided by the corresponding results
obtained by experiments. The ratios thus obtained appear in
the rows for computer results in Tables 6.6 to 6.8.

It is noticed from the tables that the two sets of results
differ from each other by a wide margin. Some of the factors
which may have contributed to the discrepancies were discussed
in section 4.4(ii). Other reasons for the errors could be:-

(a) Since the loads were applied to the bow girder via pullies,
a part of the load was resisted by the friction in the
pullies. This in turn reduces the displacements obtained
by experiment. The influence of the friction, however,
appears to be small as can be seen from the results in
Table 6.7. Theoretical displacements obtained for the
skew symmetric case are smaller than those obtained by ex-
periment. One reason for this is that the two increments
of load were not added exactly at the same time. Load at
one point was increased first causing the bow girder to
displace in one direction. Then the load was added to other
hanger . This should have, theoretically, brought the
girder to the correct position but the friction may have
prevented this. This could be one of the reasons for the
non-zero displacement and twist at c shown in Table 6.8.

(b) The torsion constant, J, for the cross-section is calcul-
ated by using an approximate formula for rectangular cross-
sections. The depth to width ratio of the cross-section
varies from 6 at the supports to 24 at the centre. It
appears that the torsion constant for thin rectangular

sections is under-estimated. Under the eccentric and skew symmetric loads, the thin portion of the bow girder twists less. Consequently, the difference between the two sets of results for these two load cases is markedly reduced.

(c) It is observed that the magnitude of the displacements is very small. Small values obtained by experiments are usually more error prone. Large loads were not applied to obtain reasonable displacements due to the possibility of the base plates or the girder itself buckling.

6.5 Conclusions

From the results presented in this chapter for various bow girders, the following conclusions are drawn:-

(i) Bow Girders with Uniform Cross-Sections

(a) The displacement functions derived in the preceding chapter describe the deformed shape of curved bars almost exactly. The strain energy of the structures composed of curved bars obtained by using the derived displacement functions is the same as obtained by using the strain energy method. Consequently, as seen from the results presented, both methods yield identical results.

(b) The bow girders were divided into a number of sub-divisions for analysis by the exact functions. It was observed that the results did not improve for finer sub-divisions. This is to be expected because the displacement functions represent the out of plane displacements of curved bars accurately. Upon further sub-division, the displacements of a point in the member do not change. As a result of this the strains and, therefore, the strain energy of the structure remains the same for all sub-divisions. It is obvious that

the use of the stiffness matrix formulated by using the derived displacement functions results in the saving of core space and solution time without sacrificing accuracy.

(c) In contrast to the results obtained for arches, the cubic functions have yielded reasonable results for bow girders, even with a crude sub-division. These results were seen to improve upon further sub-division. For example, dividing semi-circular bow girders into 16 equal parts brought the results within 2% of those obtained by using the strain energy method. However, it was noticed that the twisting moments did not always converge monotonically. The reason for this is that the cubic functions are accurate for straight prismatic members only. Here these were applied to curved members.

From the improved results obtained for displacements, it is obvious that the strain energy of the structure is better approximated with a finer sub-division. The elements of the member stiffness matrix also vary with the sub-division. Those affecting the twisting moments seem to fluctuate a little while the other elements converge towards the accurate values.

(d) The approximation of bow girders with a number of straight prismatic members yields good results for displacements and bending moments. The results obtained for twisting moments are poor. Sub-dividing the bow girders further improved the results for displacements and bending moments. Twisting moments are seen to deteriorate for some cases. An examination of the stiffness matrix for a straight member shows that the out of plane displacements and rotations do

not contribute to the twisting moments. From the results,
it is seen that this contribution is substantial. The
twist in turn does not contribute to the shear forces and
bending moments in straight members. Again the results for
these forces show that the influence of twist is negligible.

(e) The influence of the shape of the cross-section was seen to
diminish as the cross-section changed from a square into a
thin rectangle. The shape of various curves was seen to
be the same as the one for the strain energy method. The
reason for this is that the same expression was employed
to calculate the torsion constant, J, for all methods. A
larger difference may occur between the theoretical results
and those obtained by experiments.

(ii) Bow Girders with Variable Cross-Sections

The theoretical and experimental results obtained for the
bow girder were not so conclusive as those obtained for the
arches. The reasons for this were discussed in section 6.4(ii).
The following observations and recommendations are made for
model bow girders:-

(a) In order to obtain reasonable displacements, the bow gir-
ders should be made more flexible. This also helps to
achieve complete fixity of the ends more easily.

(b) A better agreement exists between the theoretical and ex-
perimental results obtained for the eccentric and skew
symmetric point load cases than for the symmetric point load
case . This is in spite of the larger displacements ob-
tained for the latter case than for the other two cases.
From Tables 6.6 to 6.8 it is observed that in the symmetric
point load case, the thin part of the bow girder twists more

than it does in the other two load cases. It is,therefore, obvious that the error in the calculation of the torsion constant, J, is passed on to the displacements. Better agreement between the two sets of results may be obtained by using the torsional rigidity, GJ, obtained by experiment, or that obtained by pure application of Sain Venant's theory of torsion although this will involve more complex calculations.

(c) Where possible, thin sections should be avoided. Alternatively, appropriate formulae should be employed to calculate the torsion constant of such sections. An expression for this can be found in reference (1).

(d) Strain gauges should be used in model tests. The bending and twisting moments obtained by experiments should be compared with those obtained theoretically to ascertain the accuracy of the latter.
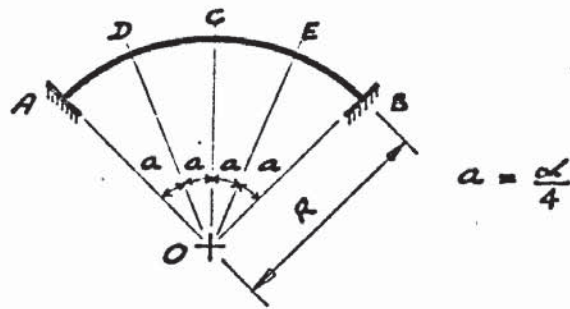
CIRCULAR BOW GIRDER OF UNIFORM CROSS-SECTION

FIG. 6.1
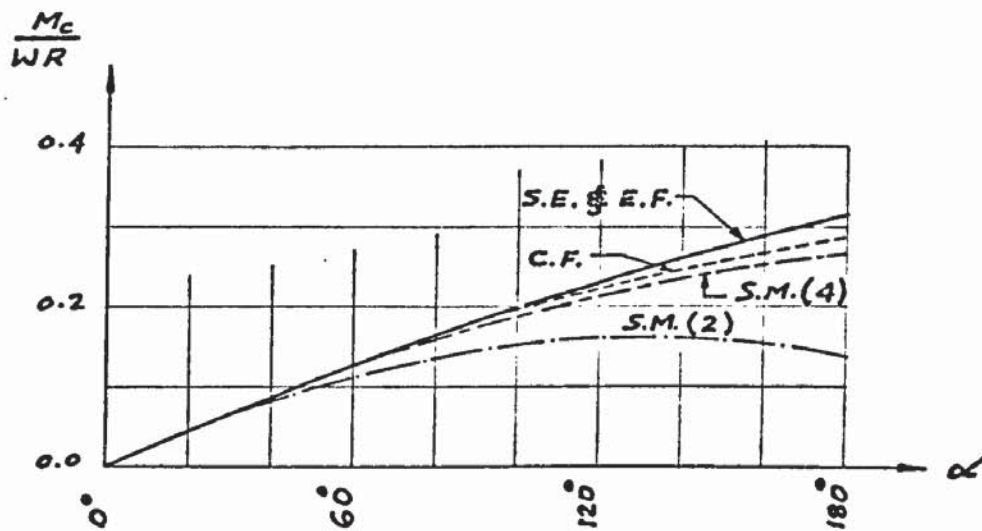
BENDING MOMENTS AT MID-POINT OF BOW GIRDERS
UNDER A SYMMETRIC UNIT LOAD

FIG. 6.2
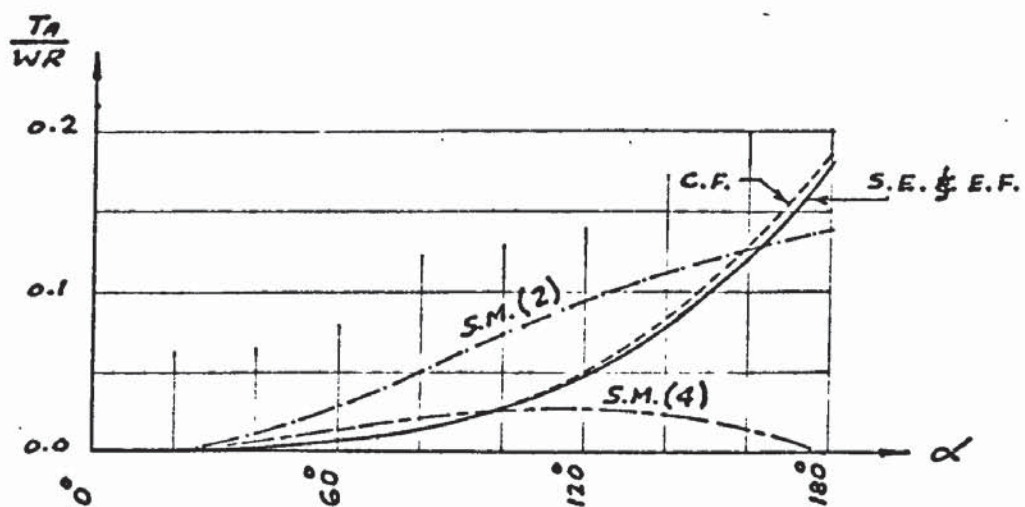
TWISTING MOMENT AT SUPPORT OF BOW GIRDERS
UNDER A SYMMETRIC UNIT LOAD

FIG. 6.3
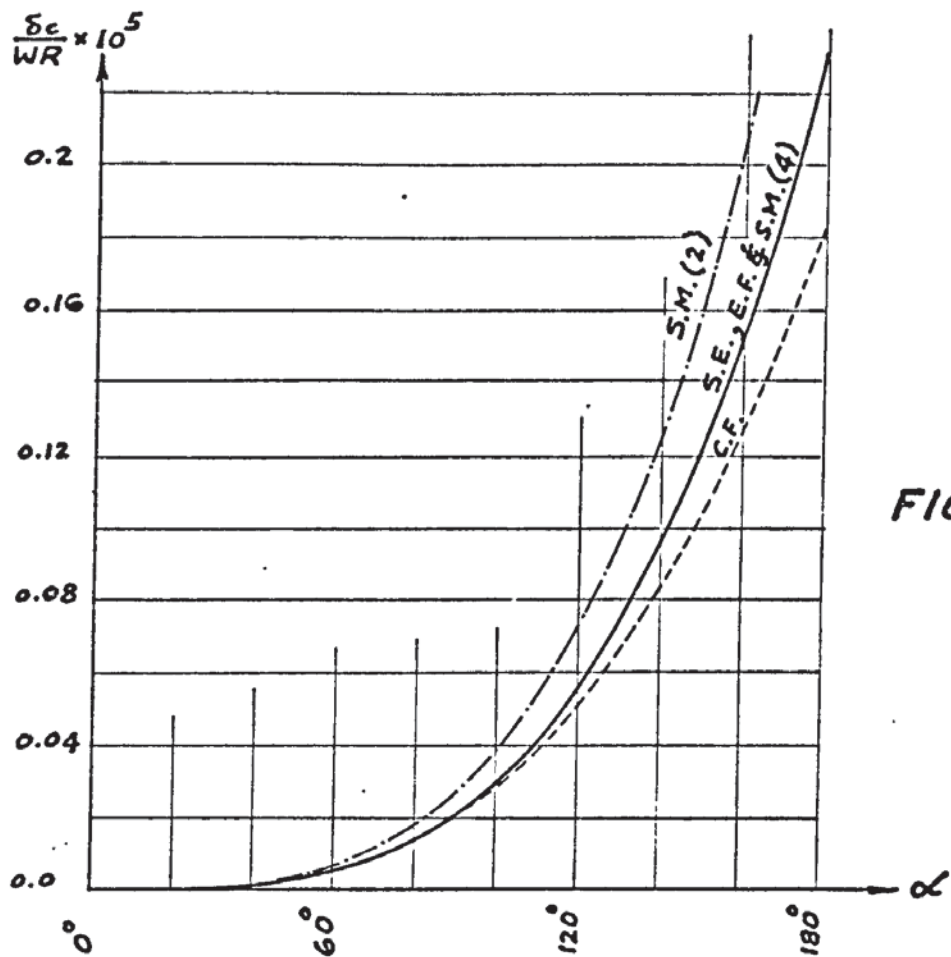
FIG. 6.4

DISPLACEMENTS AT MID-POINT OF BOW GIRDERS
UNDER A SYMMETRIC UNIT LOAD
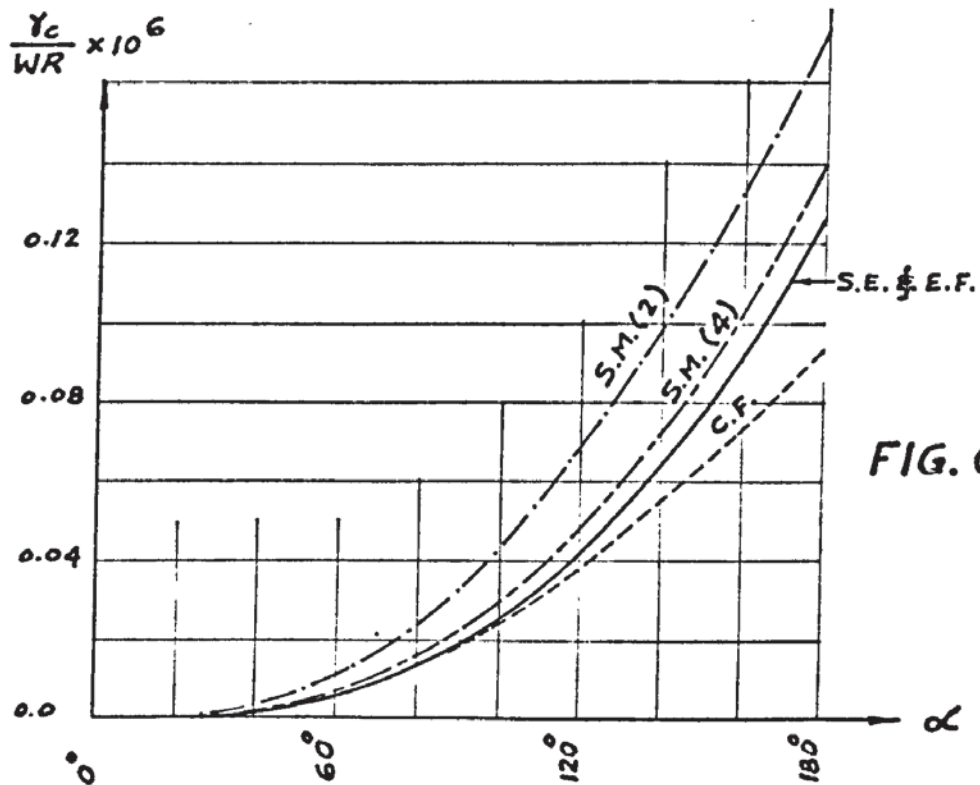
FIG. 6.5

TWIST AT MID-POINT OF BOW GIRDERS
UNDER A SYMMETRIC UNIT LOAD
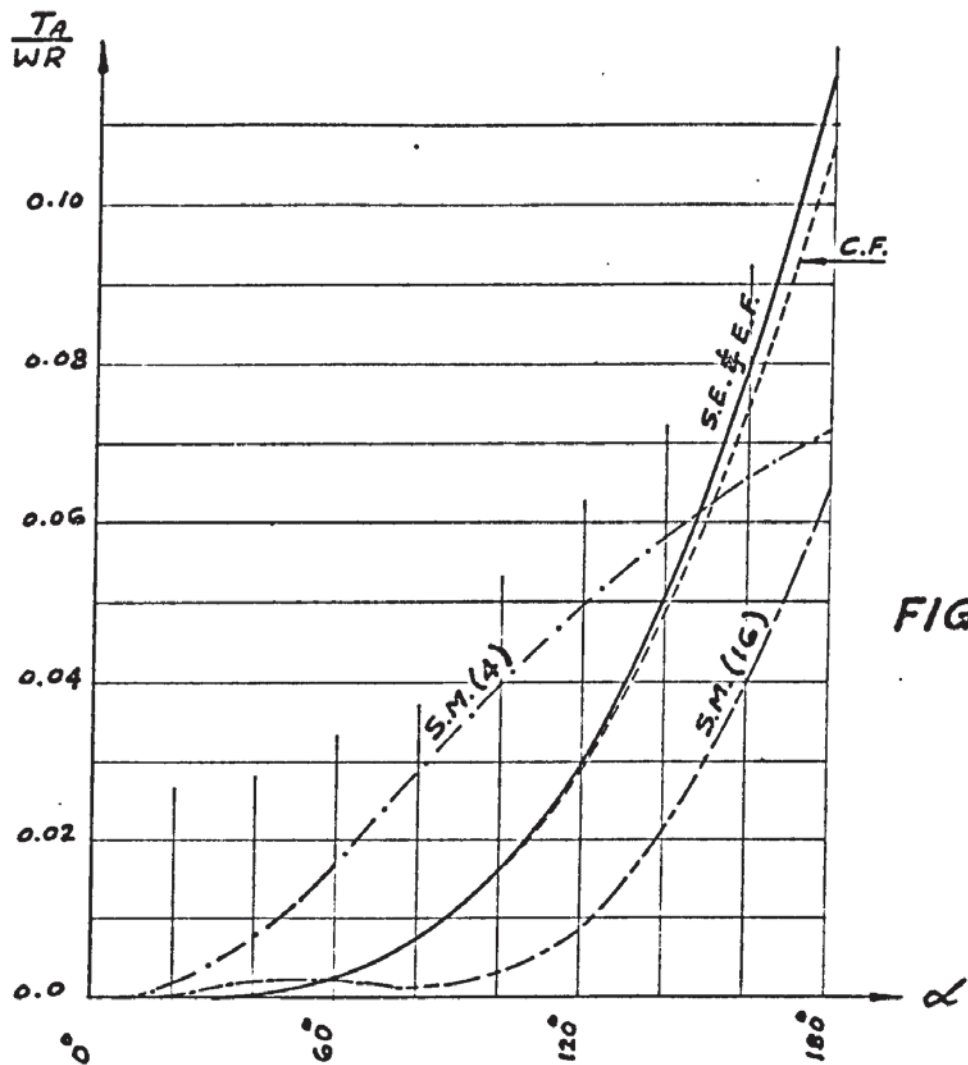
FIG. 6.6

TWISTING MOMENTS AT SUPPORT OF BOW GIRDERS
UNDER ECCENTRIC POINT LOAD
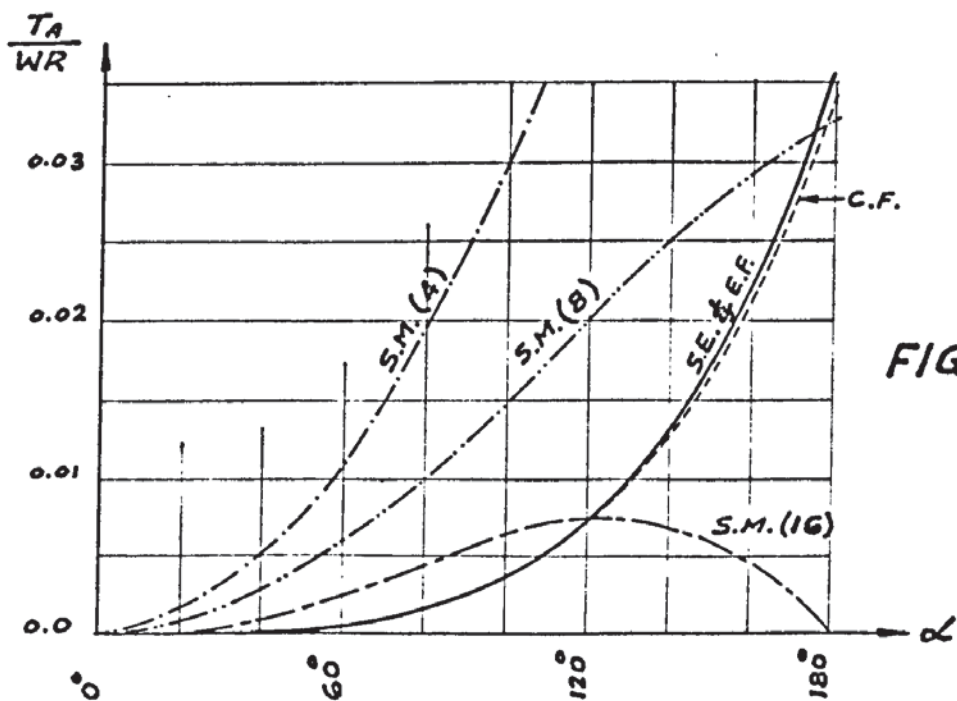
FIG. 6.7

TWISTING MOMENTS AT SUPPORT OF BOW GIRDERS
UNDER SKEW SYMMETRIC POINT LOADS
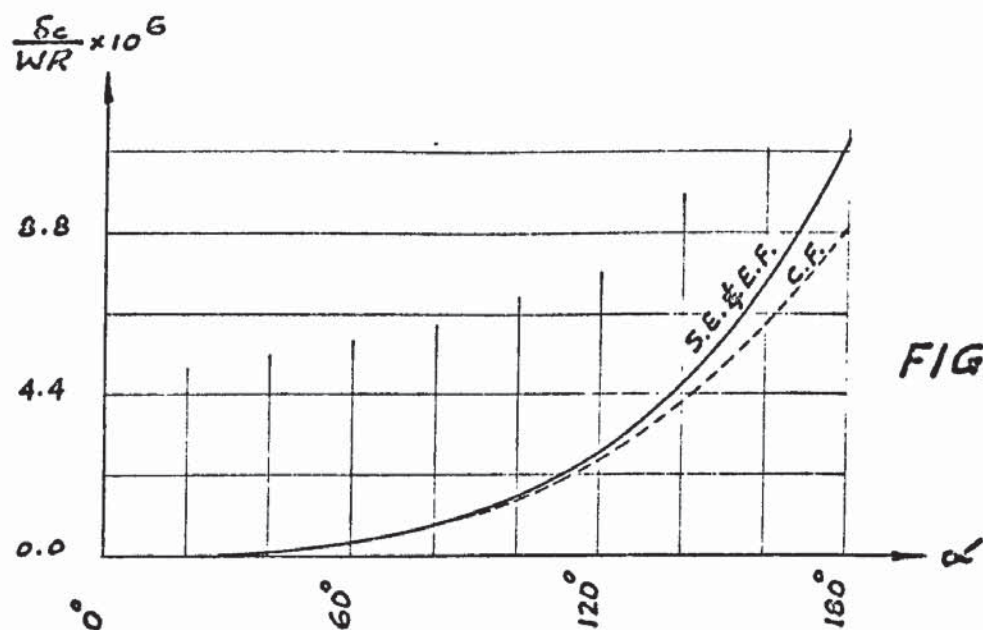
FIG. 6.8

DISPLACEMENTS AT MID-POINT OF BOW GIRDERS
UNDER UNIFORMLY DISTRIBUTED LOAD
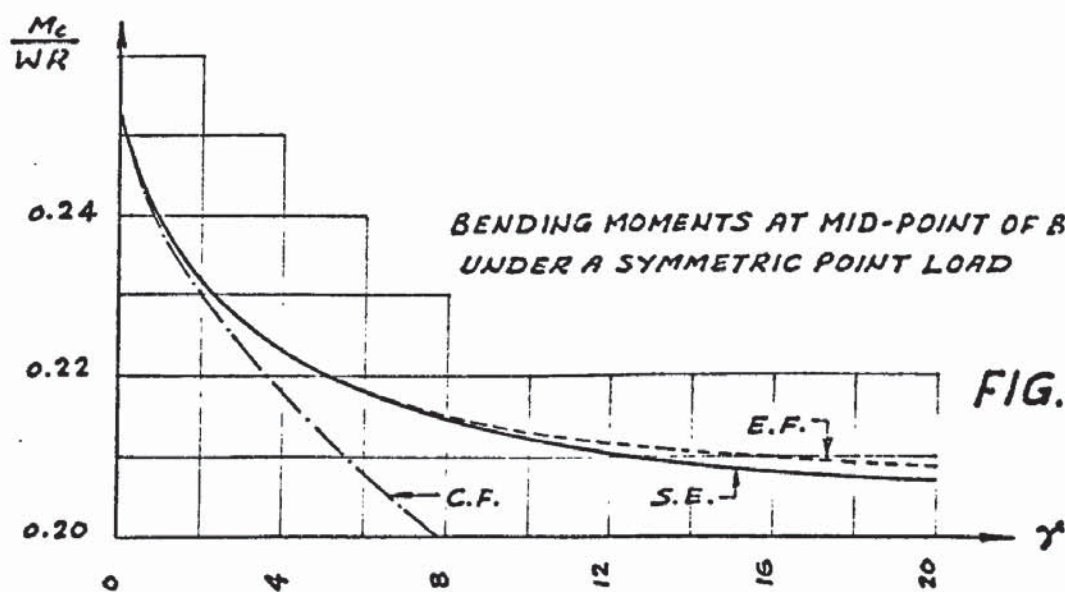
BENDING MOMENTS AT MID-POINT OF BOW GIRDERS
UNDER A SYMMETRIC POINT LOAD

FIG. 6.9
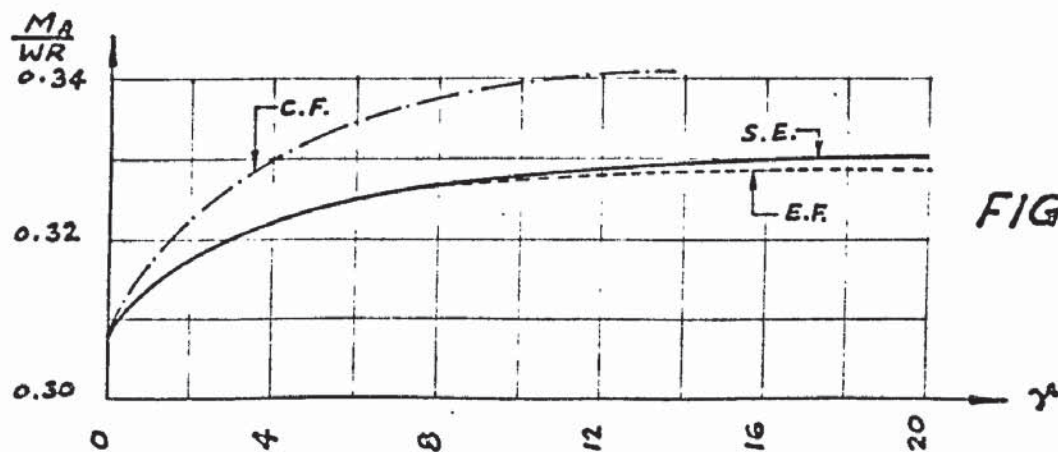
FIG. 6.10

BENDING MOMENTS AT SUPPORT OF BOW GIRDERS
UNDER A SYMMETRIC POINT LOAD
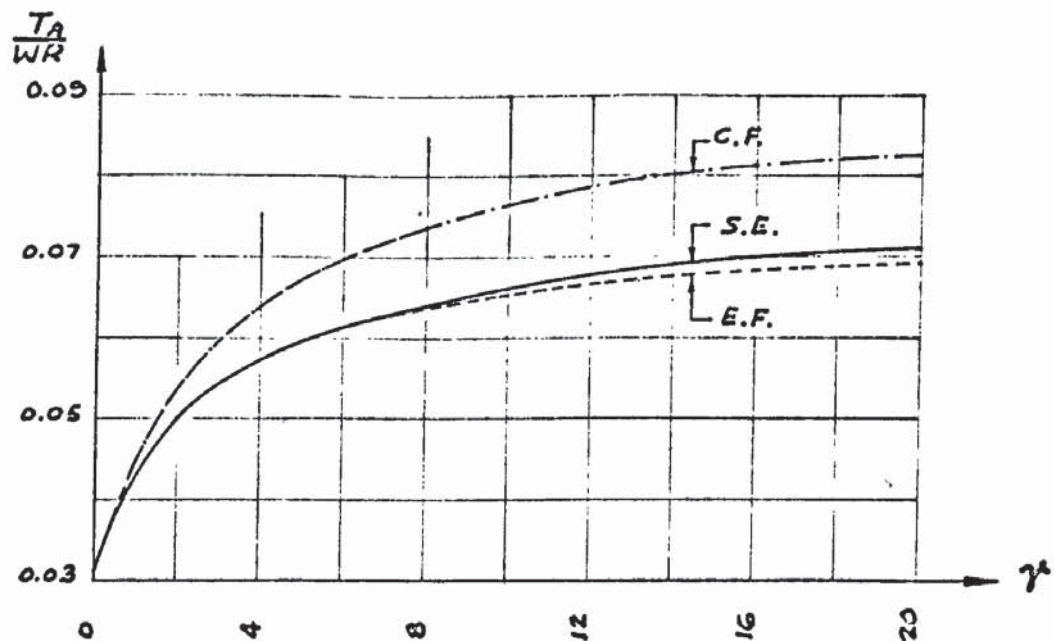
TWISTING MOMENTS AT SUPPORT OF BOW GIRDERS
UNDER A SYMMETRIC POINT LOAD

FIG. G.11
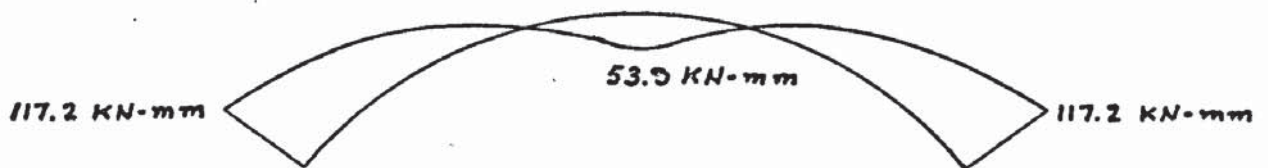
BENDING MOMENT DIAGRAM FOR FIXED BOW GIRDER
WITH VARIABLE CROSS-SECTION UNDER 60.0 Kgf. LOAD
AT MID-POINT

FIG. 6.12

TWISTING MOMENT DIAGRAM FOR FIXED BOW GIRDER
WITH VARIABLE CROSS SECTION UNDER 60.0 Kgf. LOAD
AT MID-POINT

FIG. 6.13

TABLE 6.1

BOW GIRDERS UNDER ECCENTRIC POINT LOADS

|	Method	M_A/WR	M_D/WR	T_D/WR
30°	S.E. + E.F.	0.075	0.036	0.0025
	C.F.	"	"	"
	S.M. (4)	"	"	0.005
	S.M. (16)	"	"	0.003
60°	S.E. + E.F.	0.155	0.07	0.009
	C.F.	"	"	"
	S.M. (4)	"	0.067	0.017
	S.M. (16)	0.154	0.07	0.011
90°	S.E. + E.F.	0.24	0.098	0.018
	C.F.	"	"	0.0175
	S.M. (4)	"	0.09	0.033
	S.M. (16)	"	0.097	0.0227
120°	S.E. + E.F.	0.335	0.120	0.0285
	C.F.	"	"	0.027
	S.M. (4)	0.345	0.102	0.050
	S.M. (16)	0.34	0.118	0.0360
150°	S.E. + E.F.	0.44	0.138	0.039
	C.F.	"	"	0.0355
	S.M. (4)	0.455	0.108	0.063
	S.M. (16)	0.445	0.133	0.049
180°	S.E. + E.F.	0.545	0.15	0.0475
	C.F.	"	"	0.042
	S.M. (4)	0.57	0.107	0.072
	S.M. (16)	0.554	0.142	0.06

TABLE 6.2

BOW GIRDERS UNDER TWO SKEW-SYMMETRIC POINT LOADS

	Method	M_A/WR	M_D/WR	T_E/WR
30°	S.E. + E.F. C.F. S.M. (4) S.M. (16)	0.05 " " "	0.04 " " "	0.0005 " 0.0028 0.0012
60°	as above	0.105 " 0.102 "	0.08 " " "	0.0022 " 0.00227 0.0048
90°	"	0.16 " " "	0.12 " 0.116 0.12	0.0052 " 0.0112 0.011
120°	"	0.225 " 0.23 0.224	0.16 " 0.148 0.158	0.010 0.0096 0.025 0.020
150°	"	0.295 " 0.31 0.30	0.196 " 0.174 0.194	0.0176 0.0157 0.066 0.032
180°	"	0.353 " 0.40 0.38	0.214 " 0.194 0.226	0.0268 0.0238 0.0914 0.0483

TABLE 6.3

BOW GIRDERS UNDER U.D.L.

	Method	M_A/WR	T_A/WR	M_C/WR
30^0	S.E.+E.F.	0.0443	0.1307×10^{-3}	0.0215
	C.F.	0.0443	0.131×10^{-3}	0.0215
60°	S.E.+E.F.	0.0923	0.002	0.0412
	C.F.	0.0925	"	0.0412
90°	S.E.+E.F.	0.146	0.009	0.0578
	C.F.	0.147	0.0093	0.0566
120°	S.E.+E.F.	0.2033	0.0251	0.0709
	C.F.	0.206	0.026	0.0674
150°	S.E.+E.F.	0.2623	0.0532	0.0806
	C.F.	0.267	0.0545	0.072
180°	S.E.+E.F.	0.3183	0.0947	0.087
	C.F.	0.326	0.0945	0.072

TABLE 6.4

BOW GIRDERS UNDER SKEW-SYMMETRIC U.D.L.

	Method	M_A/WR	T_A/WR	T_C/WR
30°	S.E.+E.F.	0.0165	0.0834×10^{-4}	0.071×10^{-2}
	C.F.	0.0164	"	"
60°	S.E.+E.F.	0.0338	0.0138×10^{-2}	0.0028
	C.F.	0.0332	0.0065 "	"
90°	S.E.+E.F.	0.0525	0.067×10^{-2}	0.0063
	C.F.	0.0504	0.032 "	"
120°	S.E.+E.F.	0.0736	0.0021	0.011
	C.F.	0.0685	0.098×10^{-2}	"
150°	S.E.+E.F.	0.097	0.0051	0.0167
	C.F.	0.087	0.002	0.0164
180°	S.E.+E.F.	0.124	0.0105	0.0234
	C.F.	0.105	0.0045	0.0226

TABLE 6.5

THE INFLUENCE OF SHAPE OF CROSS-SECTION ON FORCES

d/b	r	Exact Displacement Fen.			Cubic Displacement Fen.			Straight Members		
		M_c/R	M_A/R	T_A/R	M_c/R	M_A/R	T_A/R	M_c/R	M_A/R	T_A/R
1.0	1.56	0.2338	0.3161	0.04755	0.2263	0.3207	0.0495			
2.0	3.9	0.2226	0.3217	0.05727	0.2090 0.2225	0.3304 0.3217	0.06357 0.05719	0.194 0.2208	0.341 0.3255	0.0126 0.0372
4.0	13.26	0.2112	0.3274	0.06711	0.1893 0.21111	0.3411 0.3275	0.0795 0.06709	0.1714 0.2087	0.3575 0.3322	0.00394 0.04723
6.0	28.86	0.2074	0.3293	0.07042	0.1821 0.2072	0.3450 0.3294	0.0853 0.07043	0.1637 0.2047	0.3631 0.3345	0.0096 0.05061
8.0	50.7	0.2058	0.3301	0.07179	0.1790 0.2056	0.3466 0.3302	0.08777 0.07181	0.1605 0.203	0.3655 0.3354	0.01192 0.052
10.0	78.78	0.2050	0.3305	0.07246	0.1775 0.2048	0.3475 0.3306	0.08901 0.07249	0.1589 0.2022	0.3666 0.3359	0.0131 0.0527
15.0	176.28	0.2042	0.3309	0.07316	0.1759 0.2040	0.3483 0.331	0.09030 0.07319	0.1573 0.2013	0.3678 0.3364	0.01429 0.05341
20.0	312.78	0.2039	0.3311	0.07342	0.1753 0.2037	0.3487 0.3311	0.09077 0.07345	0.1567 0.201	0.3683 0.3365	0.01472 0.05367
25.0	488.28	0.2038	0.3311	0.07353	0.1750 0.2036	0.3488 0.3312	0.09099 0.07357	0.1564 0.2008	0.3685 0.3366	0.01492 0.05379

Note: for E.F. & C.F. results are for 2 divisions

The second figure for C.F. for each girder is for 16 divisions

Note: First figure is for 4 divisions followed by 16 divisions

TABLE 6.6

DISPLACEMENTS OF THE BOW GIRDER UNDER A SYMMETRIC
POINT LOAD

	δ_D	δ_C	Υ_C
Experimental Results	0.089mm	0.265mm	3.5×10^{-3} rad.
Computer results for 4 sub-divisions	1.31	1.26	1.39
Computer results for 8 sub-divisions	1.41	1.48	1.63
Computer results for 16 sub-divisions	1.51	1.52	1.85

TABLE 6.7

DISPLACEMENTS OF THE BOW GIRDER UNDER AN ECCENTRIC
POINT LOAD

	δ_D	δ_C	δ_E	Υ_C
Experimental Results	0.082mm	0.11mm	0.02mm	9.0×10^{-4} rad
Computer results for 4 sub-divisions	0.96	1.09	1.56	1.28
Computer results for 8 sub-divisions	1.0	1.16	1.64	1.48
Computer results for 16 sub-divisions	1.03	1.21	1.68	1.63

TABLE 6.8

DISPLACEMENT OF THE BOW GIRDER UNDER SKEW SYMMETRIC
POINT LOADS

	δ_D	δ_C	Υ_C
Experimental results	0.059mm	0.014mm	2.24×10^{-4} rad.
Computer results for 4 4 sub-divisions	0.81	0.0	0.0
Computer results for 8 sub-divisions	8.84	0.0	0.0
Computer results for 16 sub-divisions	0.87	0.0	0.0

C H A P T E R   7

DISPLACEMENT TRANSFORMATION MATRICES FOR CURVED MEMBERS
WITH OFFSETS AND HINGES

7.1 Introduction

The load-displacement relationships for the curved members were obtained in their local co-ordinates in Chapters 3 and 5. The capacity of a structural member to carry loads depends not only on its properties, but also on its position relative to the loads. The applied loads and the resulting joint displacements are specified in the global co-ordinates. When assembling the overall stiffness matrix for the structure, the stiffness matrices for the individual members are transformed from their local axes into the global axes by using a displacement transformation matrix.

The displacement transformation matrices were tacitly used to obtain the results presented in Chapters 4 and 6. In this chapter, these matrices are constructed for a curved element both for the in-plane and the out of plane case. As already mentioned in Chapter 1, irregularities such as offsets and hinges are unavoidable in civil engineering structures. Provisions are made in the displacement transformation matrices to allow for the effects of these practical features.

7.2 In-Plane Displacement Transformation Matrix

Figures 7.1 and 7.2 show the two positions a curved member of a plane frame can occupy when connecting two joints of a structure. The positive directions of the local axis, P and Q , and the displacements, u, w and θ , at end 1 of the member are also shown in both figures. In both cases, end 1 of the member

must move through the same displacements in the global co-ordinates as joint i. Let the displacements for this joint be given by the column vector:-

$$\{x\}_i = \{x_i \quad y_i \quad \theta_i\} \tag{7.1}$$

where x_i is the displacement in the x-direction;

y_i " " " " " y- " ;

and θ_i " " rotation.

The end displacements of the member in its local co-ordinates are related to the joint displacements through angle a which the P-axis makes with the X-axis. Considering the two cases shown in figures 7.1 and 7.2, it can be easily shown that the displacements are related as follows:-

The tangential displacements, $u_1 = x_i l_p + y_i m_p$ (7.2)

" radial " , $w_1 = r (x_i l_Q + y_i m_Q)$ (7.3)

and the end rotation , $\theta_1 = r \theta_i$ (7.4)

where $lp = \cos a$; $mp = \sin a$;

$l_Q = -\sin a$ and $m_Q = \cos a$ (7.5)

The constant r is equal to -1.0 when the arrow drawn from end 1 to end 2 of the member is clockwise as shown in fig. 7.1. For the case shown in fig. 7.2, the constant r is equal to 1.0.

(i) The Effect of Offsets

Only the in-plane offsets are considered here but similar considerations also apply to the out of plane case. The two cases for the curved members with the in-plane offsets are shown in figs. 7.3 and 7.4. The offsets are assumed to be positive if the end of the member is displaced in the positive

direction of the local axes from the joint of the structure. Thus the offsets, p_c and q_c, are positive as shown in the figures. Also shown in both figures is the positive joint rotation θ_i.

Due to the offset p_c and the joint rotation θ_i, the end of the member is displaced parallel to the Q-axis. Similarly, the offset q_c contributes to the end displacement along the P-axis of the member as joint i rotates through θ_i. Considering the two cases shown in figs. 7.3 and 7.4, it is evident that the contributions to end displacements of the member are given by the following equations:-

For the tangential displacements, $u_1 = -r.q_c\,\theta_i$ (7.6)

and for the radial   "   , $w_1 = r.p_c\,\theta_i$ (7.7)

Similarly equations can be obtained for end 2 of the member which is connected to joint j of the structure. Writing these for both ends of the member in the matrix form gives:-

$$
\begin{bmatrix} u_1 \\ w_1 \\ \theta_1 \\ u_2 \\ w_2 \\ \theta_2 \end{bmatrix}
=
\begin{bmatrix}
l_{p1} & m_{p1} & -rq_{c1} & & & \\
rl_{Q1} & rm_{Q1} & rp_{c1} & & 0 & \\
0 & 0 & r & & & \\
& & & l_{p2} & m_{p2} & -rq_{c2} \\
& 0 & & rl_{Q2} & rm_{Q2} & rp_{c2} \\
& & & 0 & 0 & r
\end{bmatrix}
\begin{bmatrix} x_i \\ y_i \\ \theta_i \\ x_j \\ y_j \\ \theta_j \end{bmatrix}
\quad (7.8)
$$

or $\{Z\} = [A]\ \{X\}$ (7.9)

where $\{Z\}$ is the vector of the nodal displacements in the local co-ordinates of the member;

{X}   is the vector of global displacements
       of joints i and j to which the member
       is connected.

and   [A]   is the displacement transformation matrix
       for the member.

Equations (7.8) and 7.9) are the compatibility equations for the member.

(ii) The Effect of Hinges

The hinge rotations are assumed to conform to the sign convention in the same manner as the joint rotations. Consequently the column in matrix [A] corresponding to the hinge rotation is identical to the column for the end rotation. For further information, reference (5) can be consulted.

7.3 The Effect of Offsets on Equivalent Loads

In the matrix analysis of structures, equivalent loads are used to represent the effect of the uniformly distributed loads. These equivalent loads are obtained in the local co-ordinates and act at the ends of the members. To obtain the joint loads for the structure, the equivalent loads are transformed from the local axes of the members to the global axes. In the case of the members with offsets, the thrusts and the shears at the ends of the members also contribute to the joint moments. By resolving forces, it is noticed that:-

The force parallel to the X-axis, $F_x = P.l_p + S.r.l_Q$ (7.10)

" " " " " Y- ; $F_y = P.m_p + S.r.m_Q$ (7.11)

and the joint moment   , $M_i = r(M - P.q_c + S.p_c)$ (7.12)

where P is the thrust in the member due to a uniform load, S is the shear and M is the fixed end moment in the member.

7.4 Out of Plane Displacement Transformation Matrix

An orthogonal set of global axes X, Y and Z is shown in fig. 7.5. The origin of these axes is assumed to be at joint i of the structure. A curved member which lies in the XY plane is shown to be connected to joint i. Local axes for the member are also shown in the figure. Fig. 7.6 shows the same set of global axes but the member is curved opposite to that in fig. 7.5. The local P-axis in each case makes the same angle, α, with the X-axis. It is seen from the figures that the local Q and R axes in fig. 7.5 are opposite to those in fig. 7.6. The joint and member forces and the corresponding rotations are also shown, in the positive sense, in both figures.

For each case of the curved members shown in figs. 7.5 and 7.6 a set of equations is obtained which express the end displacements in terms of the joint displacements and the direction cosines. A comparison of the two sets of equations leads to the following general equations:-

The displacement along R-axis, $w_R = r.Z_i$ (7.13)

the rotation about the P-axis, $\theta_p = \theta_x.l_p + \theta_y m_p$ (7.14)

and the rotation about the

Q-axis, $\theta_Q = r(\theta_x.l_Q + \theta_y m_Q)$ (7.15)

where Z_i is the displacement of joint i along Z-axis;

θ_x " " rotation " " " about X-axis;

and θ_y " " " " " " " " Y-axis.

(i) The Effect of Offsets

The contributions of offsets to the out of plane displacements are obtained by multiplying the offsets by the appropriate

end rotations of the member. As seen from equations (7.14)
and (7.15), the end rotations are themselves functions of the
joint rotations. Therefore, intermediate displacement trans-
formation matrices are used to obtain the final relationships
between the displacements at the member end and the joint.
Reference (11) adopts similar procedure for the case of straight
members.

Fig. 7.7 shows the offsets p_c, q_c and r_c for a member in
the positive directions. The joint of the structure is at A
and the end of the member is at B. Through A a set of ortho-
gonal axes is drawn parallel to the local axes of the member.
The out of plane rotations, θ_P and θ_Q, are shown in the positive
sense. The contribution of the offsets to the out of plane
end displacement of the member is:-

$$w_R = \theta_P \cdot q_c - \theta_Q \times p_c \qquad (7.16)$$

Writing equations (7.13) to (7.15) for both ends of the
member in matrix form:-

$$
\begin{bmatrix} w_{R1} \\ \theta_{P1} \\ \theta_{Q1} \\ w_{R2} \\ \theta_{P2} \\ \theta_{Q2} \end{bmatrix}
=
\begin{bmatrix}
r & o & o & & & \\
l_{p1} & m_{p1} & & & 0 & \\
r \cdot l_{Q1} & r \cdot m_{Q1} & & & & \\
& & & r & o & o \\
& & & o & l_{p2} & m_{p2} \\
& & & o & r \cdot l_{Q2} & r \cdot m_{Q2}
\end{bmatrix}
\begin{bmatrix} z_i \\ \theta_{xi} \\ \theta_{yi} \\ z_j \\ \theta_{xj} \\ \theta_{yj} \end{bmatrix}
\qquad (7.17)
$$

Writing equation (7.17) in compact form:-

$$\{y\} = [V] \{x\} \qquad (7.18)$$

where $\{y\}$ is an intermediate vector for member
displacements;

and $[V]$ is an intermediate displacement transformation
matrix

The end displacements for the member in its local co-ordinates can be expressed in terms of the intermediate vector of displacements, $\{Y\}$. These relationships in matrix form are:-

$$
\begin{bmatrix} w_1 \\ \theta_1 \\ \Upsilon_1 \\ w_2 \\ \theta_2 \\ \Upsilon_2 \end{bmatrix} = \begin{bmatrix} 1.0 & q_{c1} & -p_{c1} & & & \\ 0 & 0 & -1.0 & & 0 & \\ 0 & 1.0 & 0 & & & \\ & & & 1.0 & q_{c2} & -p_{c2} \\ & 0 & & 0 & 0 & -1.0 \\ & & & 0 & 1.0 & 0 \end{bmatrix} \begin{bmatrix} w_{R1} \\ \theta_{P1} \\ \theta_{Q1} \\ w_{R2} \\ \theta_{P2} \\ \theta_{Q2} \end{bmatrix}
\qquad (7.19)
$$

where w_1 is the out of plane displacement of end 1;

θ_1 is the out of plane rotation of end 1;

and Υ_1 is the twist of end 1 of the member.

Similarly, the other quantities are for end 2.

Equations (7.19) can be written more concisely as:-

$$\{Z\} = [U]\{Y\} \qquad (7.20)$$

where $\{Z\}$ is the vector of the end displacements for the member in its local co-ordinates;

and $[U]$ is another intermediate displacement transformation matrix.

Substituting eqn. (7.18) into eqn. (7.20) yields:-

$$\{Z\} = [U][V]\{X\} \qquad (7.21)$$

Comparing eqn. (7.21) with eqn. (7.9) it is seen that the displacement transformation matrix, $[A]$, for the out of plane case is equal to the matrix product, $[U][V]$. Carrying out

the matrix multiplication in equation (7.21) and writing the results in full:-

$$
\begin{bmatrix} w_1 \\ \theta_1 \\ \Upsilon_1 \\ w_2 \\ \theta_2 \\ \Upsilon_2 \end{bmatrix}
=
\begin{bmatrix}
r & F_1 & H_1 & & & \\
o & -rl_{Q1} & -rm_{Q1} & & 0 & \\
o & l_{p1} & m_{p1} & & & \\
& & & r & F_2 & H_2 \\
& 0 & & o & -rl_{Q2} & -rm_{Q2} \\
& & & o & l_{p2} & m_{p2}
\end{bmatrix}
\begin{bmatrix} z_1 \\ \theta_{xi} \\ \theta_{yi} \\ z_j \\ \theta_{xj} \\ \theta_{yj} \end{bmatrix}
\qquad (7.22)
$$

where $F_1 = q_c \cdot l_{p1} - p_{cl} \cdot rl_{Q1}$ (7.23)

and $H_1 = q_c \cdot m_{p1} - p_{cl} \cdot rm_{Q1}$ (7.24)

Similarly, F_2 and H_2 are for end 2 of the member.

Writing equations (7.22) in compact form leads to eqn. (7.9)

(ii) The Effect of Hinges

In the out of plane case hinges can be introduced with their axes parallel to the global axes. Alternatively, the rotational restraints about the local axes, P and Q, of the member may be released. Each one of these assumptions influences the displacement transformation matrix, [A] , in a different manner. It is assumed here that the axes of the hinges are parallel to either of the in-plane global axes, X and Y. A hinge with its axis parallel to the X-axis contributes a column to matrix [A] which is identical to the column corresponding to the joint rotation, θ_x. Similarly for a hinge with its axis parallel to the Y-axis, the corresponding

columns of matrix [A] are identical.

7.5 The Effect of Offsets on Equivalent Loads

In section 7.3 the uniformly distributed loads were considered for the in-plane case. The uniformly distributed loads for the out of plane case are dealt with in the same manner. Thus the force along the Z-axis is:-

$$F_Z = r \cdot S, \qquad (7.25)$$

the moment about the X-axis is:-

$$M_x = M_p \cdot l_p + M_Q \cdot l_Q r + S (l_p \cdot q_c - p_c \cdot r \cdot l_Q) \qquad (7.26)$$

and the moment about the Y-axis is:-

$$M_Y = M_p \cdot m_p + M_Q \cdot r \cdot m_Q + S(m_p \cdot q_c \cdot - p_c \cdot r \cdot m_Q) \qquad (7.27)$$

where S is the shear force due to out of plane uniform load;

M_p is the fixed end moment about P-axis;

and M_Q is the fixed end moment about Q-axis of the member.

7.6 The Out-of-Plane Offset

From fig. 7.7 it is obvious that the out of plane offset, r_c, contributes to the in-plane displacements. This contribution is proportional to the offset and the out of plane rotations, θ_p and θ_Q, of the member. However, for the in-plane case these rotations are suppressed. Consequently, there is no contribution of offset r_c to the in-plane displacements.

In the case of space frames, where all the degrees of freedom are available, the out of plane offset r_c should be taken into consideration.

IN-PLANE DISPLACEMENTS
OF A CURVED MEMBER

FIG.7.1

IN-PLANE DISPLACEMENTS
OF A CURVED MEMBER

FIG.7.2

IN-PLANE OFFSETS OF A
CURVED MEMBER

FIG.7.3

IN-PLANE OFFSETS OF A
CURVED MEMBER

FIG.7.4

JOINT i OF THE STRUCTURE
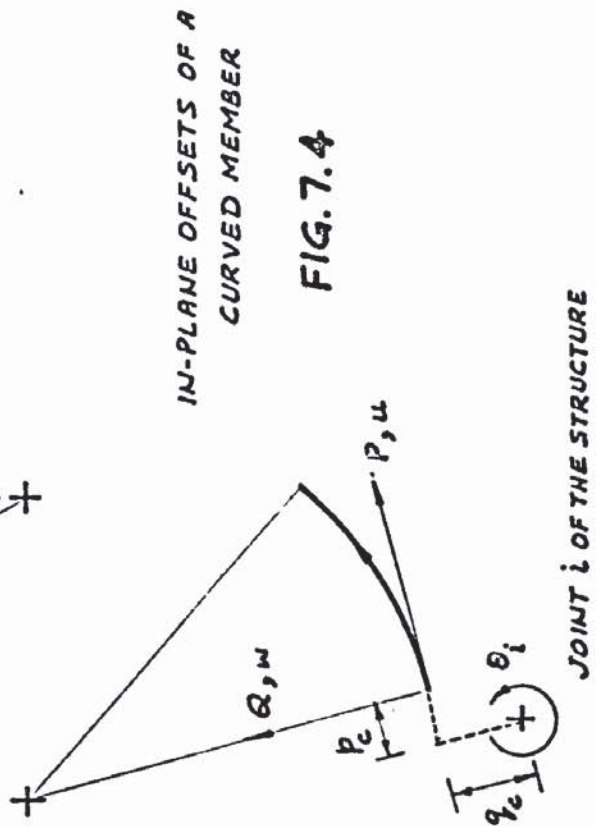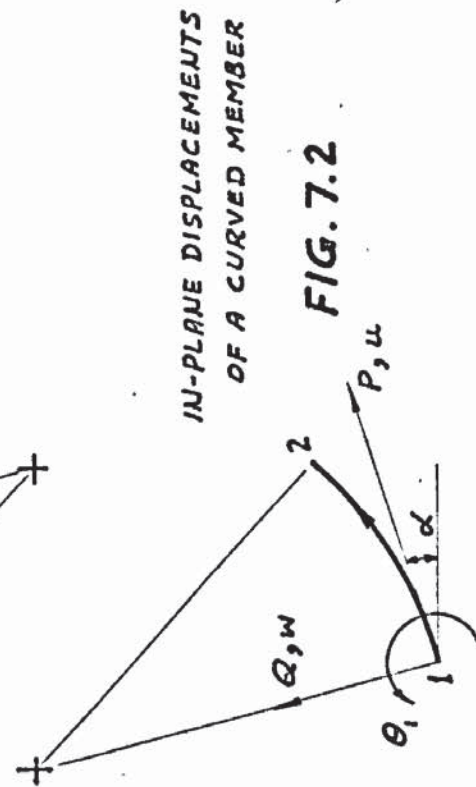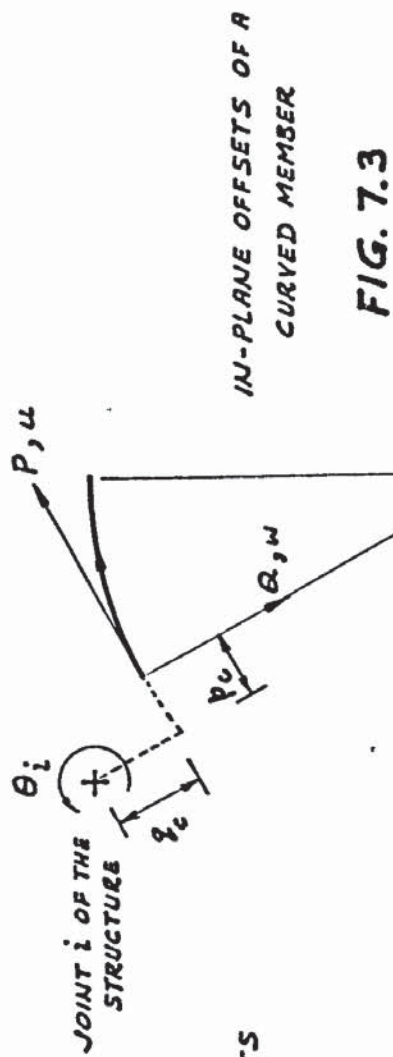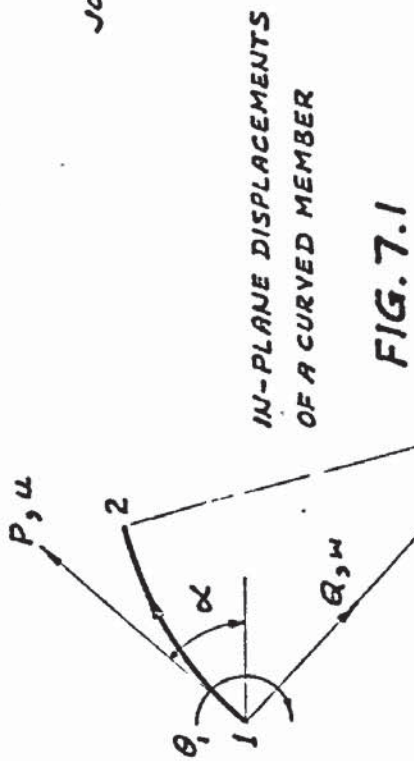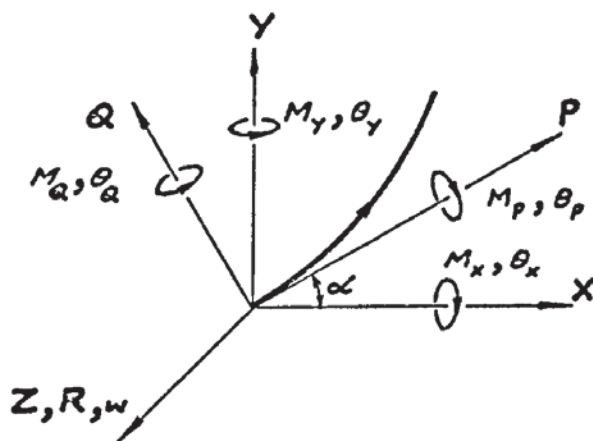
OUT OF PLANE FORCES AND DISPLACEMENTS

FIG. 7.5
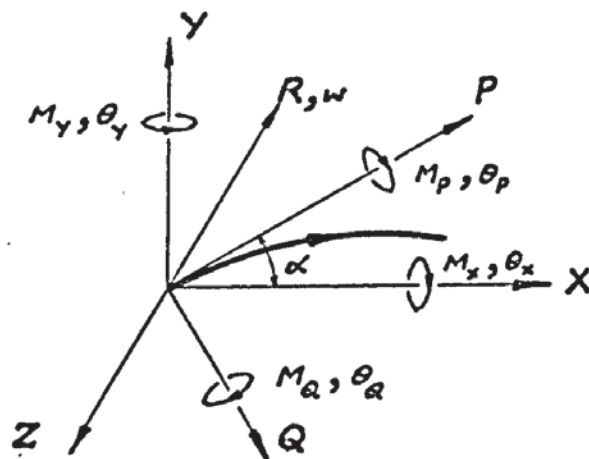
OUT OF PLANE FORCES AND DISPLACEMENTS

FIG. 7.6
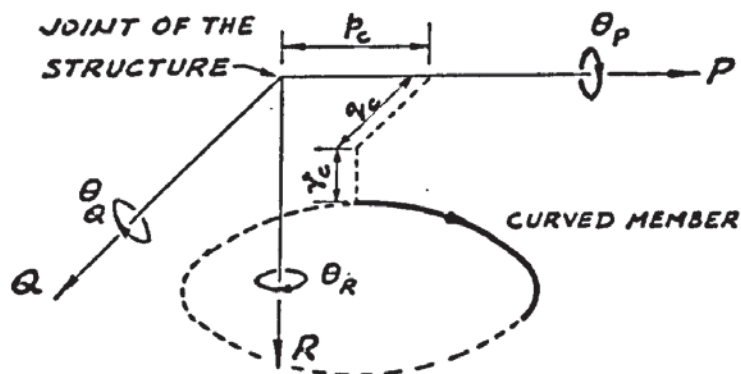
OUT OF PLANE DISPLACEMENTS DUE TO OFFSETS

FIG. 7.7

C H A P T E R   8

RESULTS FOR STRUCTURES WITH OFFSETS AND HINGES

8.1 Introduction

The displacement transformation matrices for the in-plane
and the out of plane case were constructed in the preceding
chapter. These matrices allow for the effect of offsets as well
as hinges. For reasons explained in section 7.6 only in-plane
offsets have been considered. Two structures with offsets and
hinges were analysed by using the stiffness matrices developed
in Chapters 3 and 5 together with the displacement transform-
ation matrices obtained in Chapter 7. The details and the re-
sults obtained for these structures are presented in this chapter.

8.2 The Arch Bridge

The details and dimensions for the arch bridge are shown
in Drg. No. 4. For further details, reference 15 may be con-
sulted from which this structure has been obtained. The arch
shown in Drg. No. 4 forms part of a three dimensional bridge
and was analysed as such. Here the structure is treated as a
plane frame only. Some of the dimensions were scaled from a
drawing which showed the elevation of the bridge. The loads and
moments applied at the joints were calculated for an approximate
dead load only. The idea was to analyse a structure with real-
istic dimensions and loads using the theory developed in this
Thesis rather than perform a rigorous analysis of the actual
problem for which only a three dimensional analysis is justified.

The vertical hangers are of mild steel and the rest of the
structure is composed of reinforced concrete. Values of

207.0 KN/mm^2 and 53.3 KN/mm^2 were assumed for the modulus of elasticity of steel and reinforced concrete respectively. The effective length of a hanger was taken equal to the vertical distance between the centre lines of the tie beam and the arch. The cross-sections of the hangers are very small compared to the cross-sections of the rest of the members of the structure. Therefore, the bending stiffness, EI, of the hangers was ignored throughout the analysis. Finally, it was assumed that between two consecutive joints, the arch describes a segment of a circle.

Fig. 8.1 shows the structure diagramatically. The joints of the structure are numbered consecutively from 1 to 44 and are enclosed in circles. Similarly, the members of the structure are numbered from 1 to 54. An arrow is drawn along each member pointing towards the second end of the member. The co-ordinates of all the joints, up to joint 38, are tabulated in Table 8.1. Table 8.2 shows the loads applied at the joints of the structure. As can be seen from Drg. No. 4, the longitudinal axes of all the members meeting at the springing of the arch do not meet at a single point and thus give rise to irregularities. In order to study the influence of the offsets, the same have been varied from zero to their respective full values in 10 equal increments.

8.3 Results for the Arch Bridge

Two sets of results were obtained for comparison. For the first set of results the arch was approximated by straight prismatic members. The second set of results was obtained by assuming that the arch is composed of circularly curved members of uniform cross-sections. The cross-section of a member was assumed to be equal to that obtaining at its mid-point. This is

quite a reasonable assumption since the variation of the cross-section of a member is very small. It should be stressed that it is the effect of the offsets which is being investigated and not the stiffness matrices of curved members developed in Chapter 3.

Various results obtained are plotted against the offset ratio which is equal to the current values of the offsets divided by their respective maximum values. The vertical deflections of joint 18 which is adjacent to the centre line of the structure are plotted in fig. 8.2. It is seen that the two sets of results are very close to each other. The difference being less than 1% with the offsets equal to zero. The deflection is seen to decrease almost linearly with the increase in the offsets. Total decrease in the deflection is about 11%.

Increasing the offsets decreases the flexible lengths of the members with the offsets. The displacements are, therefore, expected to decrease with the increase in the offsets. Fig. 8.2 shows that this is so. Using the curved members makes the structure a little more flexible than straight member approximation. Both curves are close to each other as expected because the radius is very large and a straight member is a good approximation of a curved one.

Both methods yielded approximately the same thrust in the arch at the springing. The thrust obtained by straight member approximation was seen to be insensitive to the change in the offsets. On the other hand, the thrust obtained by representing the arch by curved members increased slightly with the increase in the offsets. The radius of the arch being large, the direction of thrust in a straight member nearly coincides with that

in the corresponding curved member. The external loads are the same for both cases. Therefore, nearly the same thrust is to be expected for both cases.

In curved members, both offsets contribute to the thrust in the member in proportion to their magnitudes and the joint rotation. However, the contribution of offset p_c decreases with the increase in the radius and vanishes for straight members. From Drwg. No. 4 it can be seen that offset q_c is small for the arch. Consider the straight member approximation first. The results showed that, as expected, the joints rotate less as the structure becomes more stiff due to the increase in the offsets. The axial strain due to increase in offset q_c is cancelled by the decrease in joint rotation. Hence the constant thrust obtained for this case.

Representing the arch with curved members gave rotations at the springing which increased with the increase in the offsets. This is possible. Results obtained for simple arches showed that the support moment was reversed as the arch became deeper. It is obvious that rotations of the ends of an arch with elastic supports vary with the change in the moments. With the increase in offsets a shallow arch becomes still shallower. This increases the support moments which, in turn, cause greater rotations at the supports. In the present case, the influence of offset p_c is small. Offset q_c is itself small as already remarked. The effect of both offsets is to increase the thrust, though by a small amount.

The results for the shear force at the springing are plotted in fig. 8.4. For offsets equal to zero, straight member approximation yields a shear force which is not only small in

magnitude, but is opposite in direction to that obtained by using curved members for the arch. This is not so strange. Consider a semi-circular arch under a symmetric point load. The shear force at the support is towards the centre. Replace the arch with two straight members which connect the mid-point to the supports. Shear force at the supports of this structure is in the general opposite direction to that in the arch. Increasing the number of straight members representing the arch to infinity should give identical results to those obtained for the arch. The shear force, in changing its direction, must pass through zero value. Therefore, the shear force in a member can be of any magnitude and sign depending on the geometry of the structure.

It is interesting to note that the two curves in fig. 8.3 have opposite slopes to each other. This is to be expected. As the offsets become larger, the adjoining members become smaller. It is obvious that a straight member represents a short curved member better than a longer one of the same radius. Furthermore, the directions of the shear vectors converge as the lengths of the members is reduced.

The influence of offset q_c on the shear forces and bending moments in curved members fades away with the increase in the radius and becomes zero for straight members. For the present case the contribution of q_c can be assumed to be negligible. Only offset p_c, therefore, affects the shear forces and bending moments. Consider the straight member approximation first. The displacements of joints 2 and 3 are such that the member rotates clockwise as the offsets are increased. This tends to increase the shear force in the member. Offset p_c produces a transverse

displacement which tends to decrease the shear force. From the results obtained it is clear that the contribution of offset is greater than that of the displacements of joints 2 and 3. The curved member rotates clockwise more than the corresponding straight one. The transverse displacement due to offset p_c is approximately the same for both cases. The cord length between joints 2 and 3 increases due to their displacements. This produces shear force in the curved member. The direction of this shear force is radially away from the centre, the same as due to rotation of the member. The net decrease in shear force shows that the effect of offsets is smaller than the combined effect of the other two factors mentioned above. It is noticed that both curves are nearly straight for small offsets. For large offsets, the assumptions made in formulating the equations which allow for the influence of offsets are violated. The maximum value of offset p_c is greater than the length of the adjoining member.

The results for the bending moments in the arch at the support are plotted in fig. 8.4. For small offsets it is seen that the straight member approximation has yielded bending moments which are small and of opposite sign to those obtained by representing the arch with curved members. The reasoning used to explain similar results for shear force is equally applicable to bending moments. Considering the results when offsets are small, the structural member designed for forces obtained by representing the arch with straight members will be grossly inadequate. However, in practice a curved member is approximated by a number of straight members instead of the only one used here. From the results obtained for simple arches, it can be

assumed that generally the accuracy of results improves upon
further sub-division.

The curve representing curved members for the arch is seen
to droop a little before rising with the increase in the offsets.
On the other hand, the results obtained by straight member
approximation lie along an approximately straight line with a
positive slope. The various factors which affect the shear forces
in members also affect the bending moments. In addition to
these, the transverse displacement in curved bars also contri-
butes to the bending curvature and, therefore, to bending moments.
For reasons discussed for the shear force, the two sets of
results for bending moments are expected to converge with the
increase in the offsets.

Like the thrust in the arch at the springing, both methods
yielded the same tensile force in the tie beam. The influence
of offsets on the results obtained by straight member approxi-
mation is negligible. The axial force obtained by representing
the arch with curved members increases by about 4%. The ten-
sile force in the tie beam is caused by the thrust in the arch
which increases slightly as was noted earlier. This is to be
expected. The offsets decrease the length of the arch thus
making it shallower. It was observed from the results for simple
arches that the thrust increased as the arches became shallower.
Furthermore, with the increase in the offsets, the line of
action of the thrust rotates towards the tie beam, thus in-
creasing the horizontal component of thrust even further.

The tie beam has offsets. Of these, q_c is very small and
p_c does not contribute to axial forces in straight members.

The results for the shear force in the tie beam at the

support are plotted in fig. 8.5. The two sets of results are
seen to be fairly close to each other over the whole range of
offsets. The maximum difference between the results is within
15%. The curve representing the straight member approximation
is seen to rise gradually with the increase in offsets. Sev-
eral factors influence the shear force. The net difference
between the vertical displacements of joints 2 and 4 decreases
with the increase in offsets. The contribution of offset p_c
decreases this difference even further. The two effects should
decrease the shear force in the member. However, the member
becomes shorter with the increase in offsets. A short member
offers a greater resistance to transverse displacement than a
longer one. The rotations at the ends of the member also con-
tribute to the shear force. The results showed that these end
rotations decreased slightly. Due to the increased stiffness
of the shorter member, the rotations tend to reduce the shear
force. It is noticed from fig. 8.5 that the net result of all
these factors is an increase in the shear force. The curve
obtained by representing the arch with curved members is fairly
level over a wide range of offsets. All the factors disucssed
for straight members also apply in this case. Joint 2 now
rotates more. Offset p_c, therefore, decreases the transverse
displacement more than it did in the case of straight member
approximation of the arch. From the results it is seen that the
increase in shear force is balanced by the decrease. For reasons
already given, results for large offsets are not reliable.

Fig. 8.6 shows the results for the bending moments in the
tie beam at the support. For offsets equal to zero, the straight
member approximation yields bending moment which is about 80%

of that obtained by representing the arch with curved members.
The bending moments are seen to be decreasing proportionally
to the increase in offsets. At the extreme end of the range
bending moments obtained by both methods are approximately the
same in magnitude but opposite in sign to each other.

Consider the straight member approximation first. As was
noted in the case of shear force in the tie beam, the trans-
verse displacement decreases with the increase in offsets. The
increased stiffness due to shortening of the member tends to
increase the bending moment. The change in joint rotations was
observed to be small. Bigger moments are required to maintain
the same end rotations as the member becomes smaller. The nature
of contribution due to end rotations is to reduce the bending
moment in the tie beam. From the results it is seen that the
influence of factors tending to reduce the bending moments is
greater than of those which tend to increase these forces. All
the above factors also influence the bending moments obtained
by representing the arch with curved members. In addition to
these it was noticed that the rotation of joint 2 increased with
the increase in offsets. The reduction in the transverse dis-
placement due to offset p_c becomes bigger. The result of these
is that bending moment in the tie beam at the support decreases
faster than in the case of straight member approximation. To-
wards the extreme limit of offsets, the bending moment is re-
versed. It may not happen in practice. The reason for this is
that the offsets are no longer small compared to the lengths of
the adjoining members.

The bending moments in the arch at the joint adjacent to
the crown decrease gradually as the offsets increase. The

maximum decrease is about 15%. The straight member approx-
imation of the arch yields bending moments which are approximatel
55% of those obtained by representing the arch with curved mem-
bers. There are two reasons for this. The first is the slight-
ly different end rotations obtained for curved members instead
of the same rotations expected in a symmetric structure. This
is perhaps due to the rounding off error. The second is the
bending moment caused in the curved member by its ends moving
towards each other. In the straight member representation, this
movement causes axial force only.

The bending moments in the tie beam at a joint adjacent to
the centre line also decrease gradually with the increase in
the offsets. The maximum difference between the bending moments
for the extreme limits of offsets is about 24%. With the offsets
equal to zero, the straight member approximation yields slightly
lower bending moment than that obtained by using curved members.
This is to be expected. Straight member approximation over-
estimates the stiffness of the arch and thus over-estimates the
load carried by it. The load carried by the tie beam is, there-
fore, under-estimated. This is confirmed by the results. The
middle portion of the tie beam remains horizontal in both cases.
The end rotations of member 44 obtained by representing the arch
with curved members decrease faster. This yields a higher rate
of decrease in the bending moments. The smaller change of
rotations obtained by straight member approximation is also
reflected in the bending moments.

From the graphs plotted for various quantities, it can be
seen that, as expected, the influence of the offsets fades with
the distance of the member from the supports. The results for

the tension in the hangers most affected by the offsets, the
shortest ones, are plotted in fig. 8.7. With the offsets equal
to zero, the straight member approximation yields results which
are about 80% of those obtained by using curved members for the
arch. However, the curve for the latter case is seen to dip
more than that for the former case.

The force in the hanger is expected to decrease. Consider
the extreme case where the offsets are equal to the lengths of
members 3 and 36. The joints at the ends of the hanger, by
being connected to a rigid piece, cannot displace. The force in
the hanger in that case will obviously be zero.

To explain different slopes of the curves in fig. 8.7, con-
sider the curved member and the corresponding straight member.
It is obvious that the axial force in the straight member is
constant throughout its length while in the curved member this
is not so. Similarly, the bending moment in the straight member
varies linearly from one end to the other. In the curved member
this variation is non-linear. As the offset is increased, the
contribution to the strain energy due to axial thrust decreases
faster for the curved member than for the straight one. On the
other hand, the contribution due to bending decreases faster for
the straight member than for the curved member. The strain
energy due to bending is usually greater than that due to axial
forces. This causes the vertical displacement of the second end
of the curved member to decrease less than is the case for the
straight member. It was noticed from the results obtained that
both methods yielded the same vertical displacement for the
joint at the lower end of the hanger. The result is a higher
rate of decrease of axial strain and, therefore, of axial force

in the hanger obtained by representing the arch with curved members.

The method used in catering for the offsets is valid for small offsets only. The accuracy of results towards the higher range of offsets is, therefore, doubtful. More representative results may be obtained by treating the piece of concrete which gives rise to offsets as a straight member with variable cross-section.

8.4 Bow Girder with Offsets

The dimensions of the bow girder with the offsets are shown in Drwg. No. 5. Further details can be seen from Plates 8 to 10. For reasons given for the arches, the bow girder was formed from a bar of bright milk steel with a rectangular cross-section of 12.7 x 6.35 mm. Bright milk steel was used because of smaller deviation in dimensions of the cross-section permitted than that allowed for sections of black mild steel. The bar was bent cold to a radius of 600.0 mm with a roller. The curved length of the bar forms a quadrant. A plate of bright mild steel with dimensions of 50.0 x 19.0 x 300.0 mm was welded to each end of the curved bar as shown in the drawing and plates.

Also shown in the drawing and plates are the dimensions and details of two brackets which were fabricated from bright mild steel. Two 6.35 x 35.0 x 55.0 mm long knife edges made from hardened steel were welded to each bracket. These knife edges

provide pinned supports to the end plates of the bow girder as can be seen from the drawing and plates. An end of the bow girder is effectively clamped by reversing the top plate with the knife edge as shown in Plate 10.

The arrangement used to provide pinned supports for arches was considered for the bow girder but was rejected for two reasons. The first was the possibility of some play in the axle and the bearings. Small displacements at the support are magnified along the length of the bow girder. The second reason was that the bow girder was to be tested for various offsets and end conditions. This would have required the fabrication of several bow girders. It is impossible to make two girders identical and this would have contributed to discrepancies in results. The method adopted here eliminated the above-mentioned possible causes of errors but itself introduced new ones. These are discussed later in this chapter.

When deciding the dimensions of the bow girder and end plates, advantage was taken of the experience gained by testing the bow girders with variable cross-section, Chapter 6. A reasonably flexible bow girder was chosen. The dimensions of the end plates are such that their contribution to the deflections of the bow girder is negligible. Larger plates would have presented difficulties when aligning the knife edges to obtain a hinge effect. No strain gauges were employed to measure the strains from which to calculate the bending and twisting moments. Therefore, only theoretical deflections can be compared with those obtained by experiment.

The same loading bracket was used as for the bow girder with variable cross-section. The dimensions of this bracket are also

shown in drwg. No. 5.

8.5 Test Specimen

A test specimen was cut from the same bar as the bow girder. Two 6.35 mm electrical strain gauges were fixed to the opposite faces of the test specimen to measure the longitudinal strain. Similarly, two strain gauges were used to measure the transverse strain. The load was applied to the test specimen with a Denison machine in 7 increments of 250.0 kgf. After reaching the full load, it was reduced in the reverse order. At each stage of the load, the strain gauge readings were recorded.

From the strain gauge readings, the average readings were calculated as was done for the test specimens for the arches, Chapter 4. These average readings were plotted against the load. Through each set of points for a strain gauge the best straight line was drawn. From the graphs the strains corresponding to the maximum test load were calculated. The average of the longitudinal strains was assumed to be the required longitudinal strain. Similarly, the average of the transverse strains was taken to be the required strain in that direction.

The area of the cross-section of the test specimen is computed from its dimensions. With the load, area and the strains known, it is easy to calculate the following properties of the material:-

The modulus of elasticity, E $\quad$ = $\quad$ 198.0 KN/mm^2

and the Poisson's ratio, ν $\quad$ = $\quad$ 0.274

8.6 Experiments on the Bow Girder

The load was applied at the mid-point of the bow girder. The offsets were varied in steps of 50.0 mm. Three types of tests were carried out. In the first test the offset in the

radial direction, q_c, at end A was varied whilst end B was clamped. For the second test end A was fixed whilst the offset along the tangential direction, p_c, at end B was varied. In the final test both offsets q_c at end A and p_c at end B, were varied.

The knife edges were seen to bite into the end plates as the nuts were tightened. As a result the end plates behaved as clamped for small loads. Some yielding of the plates occurred in the region adjacent to the knife edges as the load was increased. Therefore, the load was applied in a single increment of 5.0 kgf. Furthermore, to ensure that the nuts were tightened to the same degree, a torque wrench was used.

8.7 Results for the Bow Girder

For the analysis by computer the bow girder was divided into two segments of equal lentgh. The exact stiffness matrix for the bow girder element developed in Chapter 5, together with the displacement transformation matrix constructed in the preceding chapter was utilized in the analysis. The results for the deflection at the mid-point of the bow girder are tabulated in Table 8.3. It is seen that the theoretical results for offset p_c and offset q_c agree reasonably well with those obtained by experiments. The difference between the two sets of results varies from 10% to 20%, even for large offsets. The deflections obtained by experiment for the third case, both offsets p_c and q_c vary, are far below those obtained theoretically; being only about 50%. The reasons for the discrepancies between the two sets of results are discussed in the next section.

Theoretical results for the deflections at the mid-point c are plotted in fig. 8.8. It is noticed that as the offsets are increased, the deflections also increase, though at different

rates for the three cases considered. This is to be expected. In the case of the tied arch bridge, the offsets increased at the expense of the flexible part of the structure. The deflections of the arch bridge, therefore, decreased. On the other hand, in the case of the bow girder, the flexible part is not affected by the offsets.

Consider the case when offset p_c alone increases whilst the other end is clamped. Two factors contribute to the displacements: the strain energy due to bending and the strain energy due to twisting. It was noticed from the results, not produced here, that all these forces gently increased with the increase in the offset p_c. Consequently, the strain energy of the structure also increased thus resulting in greater displacements.

For the case of the offset q_c alone, the twisting moments at the two ends of the bow girder were seen to increase more than in the previous case. The twisting moments at the mid-point were not affected by offset q_c. Therefore, it can be said that the strain energy due to twisting increased. The magnitude of the bending moment at the fixed end increased whilst at the other end it was seen to decrease. The bending moment at mid-point c remained unchanged. It can, therefore, be assumed that the strain energy due to bending remained approximately the same for all values of offset q_c. The greater rate of increase in the deflections obtained for offset q_c than that obtained for offset p_c, therefore, suggests that the bow girder is more flexible to twisting than it is to bending.

The third curve in fig. 8.8 shows the deflections at the mid-point as both offsets, p_c and q_c, are varied. It is noticed that deflections increase more steeply than in the other two

cases considered. Fig. 8.9 shows the bending moments at both ends and at mid-point. It is noticed that the bending moment at end A decreases whilst at the other two points it is increasing. Therefore, it can be concluded that on the whole the strain energy due to bending increases with the increase in the offsets.

Results for twisting moments are plotted in fig. 8.10. It is seen that the magnitude of all the twisting moments increases with the increase in the offsets. The increase in the bending and twisting moments is greater for the present case than for the other two cases considered previously. This fact is also reflected in the greater deflections obtained for the present case.

It must be pointed out that the results for the third case, both offsets increasing, cannot be obtained by combining the results for the other two cases. This is because the three structures are not the same.

In the third case, the shear force in the bow girder can be calculated by considering the rotational equilibrium of the whole structure about the axis of one hinge. With the shear force known, the twisting moment at end A and the bending moment at end B can be determined. This was the reason for plotting the bending and twisting moments for this case only. A check of the twisting moments at end A and the bending moments at end B showed that the results plotted in figs. 8.9 and 8.10 were correct. It can, therefore, be assumed that the results for other forces shown in the two figures are also correct.

8.8 Conclusions

From the results obtained, it can be concluded that the influence of small offsets is easily allowed for through the

displacement transformation matrices constructed in the preceding chapter. The theoretical results become unreliable as the offsets increase beyond a certain limit. More tests on simple arches and bow girders are needed to establish the limit of small offsets. Furthermore, strain gauges should be used to measure the strains. These can, then, be converted into forces and moments which should be compared with those obtained theoretically.

It was noticed from the results obtained for the arch that the two sets of results agreed, sometimes even for large offsets. The reason for this is that both are theoretical results and the same assumptions were made to obtain the equations which allow for the influence of offsets. On the other hand, the theoretical results for the bow girder differed always by more than 10%.

Some factors which can cause discrepancies between theoretical results and those obtained by experiment were discussed in Chapter 6. Other factors which may have contributed to errors in the results for the bow girder are:-

(a) Any misalignment of the knife edges causes the end plate to behave as partially clamped. The knife edges were made sharp and slightly longer than the width of the end plates to help align them more accurately. In spite of this, some misalignment may have occurred. The fixity of the end plates is proportional to the misalignment of the knife edges and the degree to which the nuts were tightened. To reduce the error due to latter cause a torque wrench was used to tighten the nuts to the same degree for all offsets.

(b) As mentioned earlier, the knife edges were seen to bite into the end plates. As a plate rotates, two points on the

opposite horizontal faces of the plate which were origin-
ally on the same vertical line move horizontally in the
opposite direction to each other. The knife edges, having
bitten into the plate, resist this type of movement. The
resistance is proportional to the thickness of the plate
and its angle of rotation. It is obvious that large deflec-
tions are usually accompanied by large rotations. It
appears that this cause greatly reduced the deflections ob-
tained for the case where both offsets were varied.

Retrospectively, more accurate results may be obtained for
the bow girder by using the type of pin supports used for the
arches instead of the knife edges employed here.
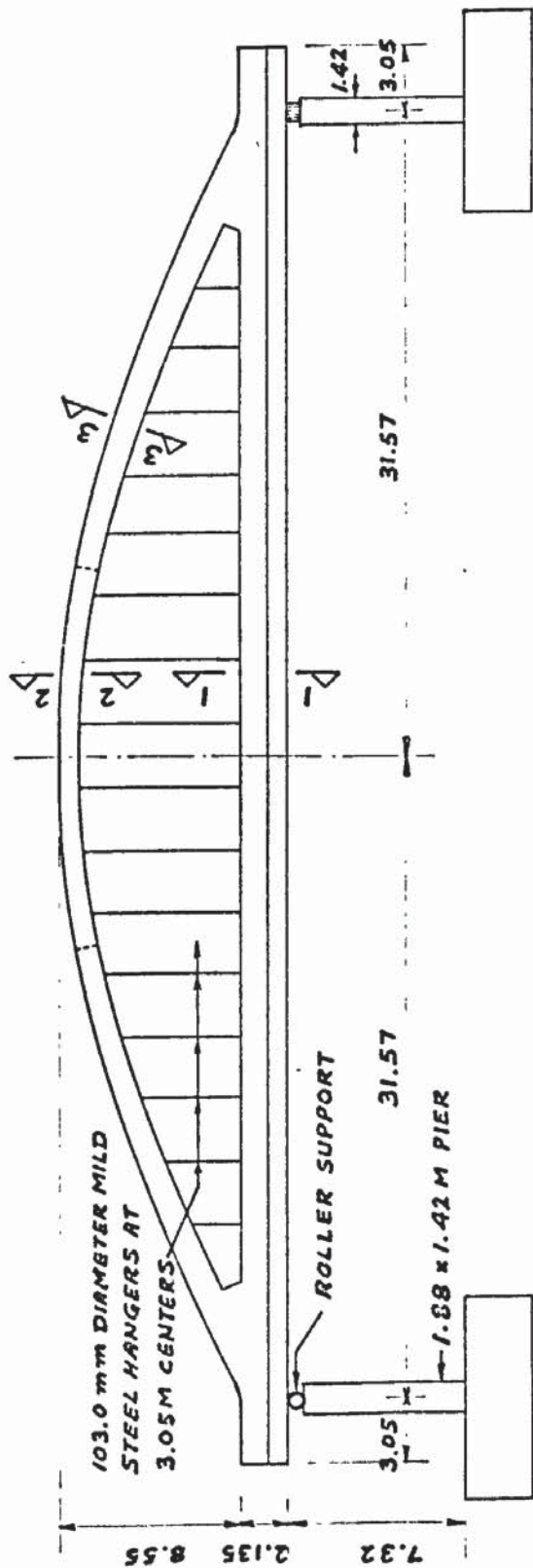
ELEVATION OF THE TIED-ARCH BRIDGE

NOTE: ALL DIMENSIONS ARE IN METERS UNLESS SPECIFIED OTHERWISE.
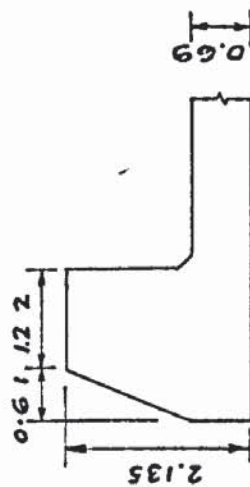
SECTION 1-1
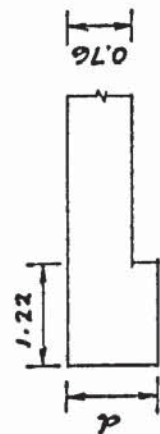
SECTION 2-2

DIMENSION d VARIES FROM 1.45 M
AT SPRINGING TO 0.76 M AT CROWN OF ARCH

SECTION 3-3

DRAWING NO. 4

103.0 mm DIAMETER MILD
STEEL HANGERS AT
3.05 M CENTERS

ROLLER SUPPORT

1.88 x 1.42 M PIER

1.42

3.05

31.57

31.57

3.05

8.55

2.135

7.32

0.69

0.61 1.12 2

2.135

1.22

0.76

d

1.22

d
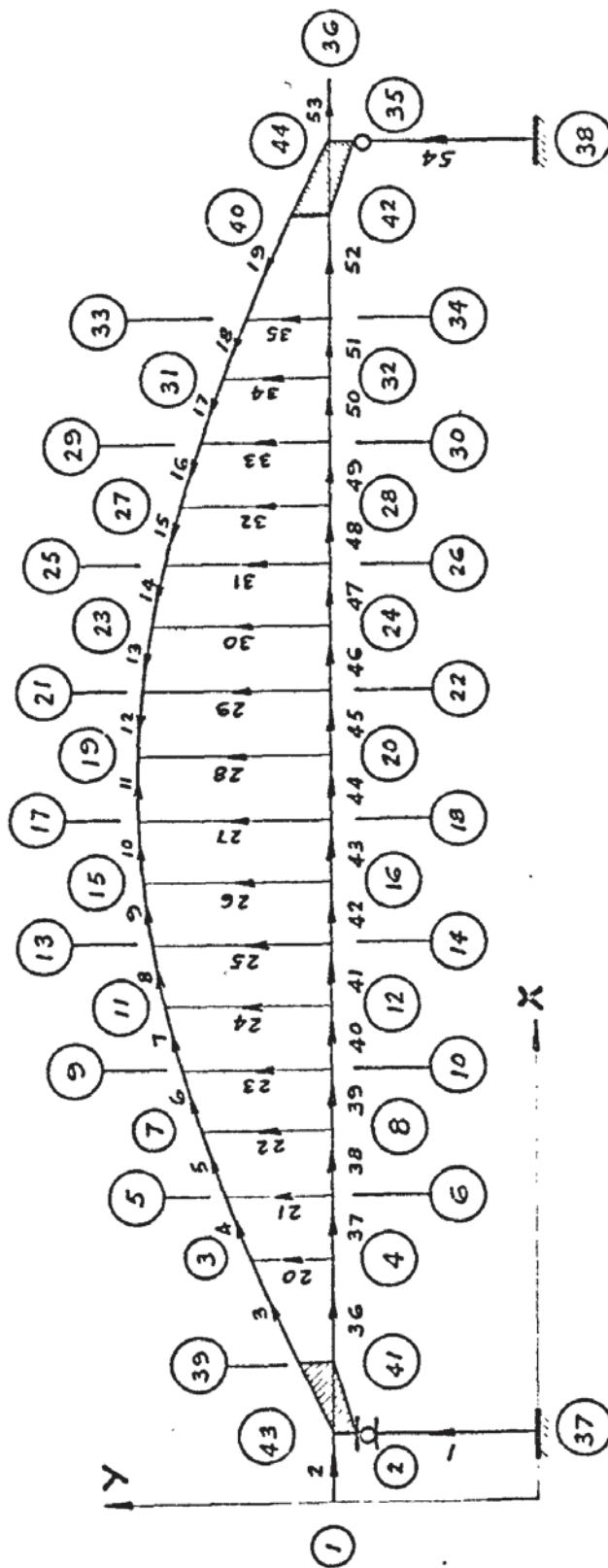
ELEVATION OF TIED-ARCH BRIDGE SHOWN DIAGRAMATICALLY

FIG. 8.1

TABLE SHOWING DEPTH OF CURVED MEMBERS

3	1.334	4	1.169	5	1.068	6	0.991	7	0.991	8	0.891	9	0.839	10	0.788	11	0.763
12	0.788	13	0.839	14	0.891	15	0.940	16	0.991	17	1.068	18	1.169	19	1.334		

NOTE: IN EACH ROW MEMBER NO. IS INDICATED BY THE INTEGER FOLLOWED BY ITS DEPTH IN METERS

Table 8.1

Co-ordinates of the Joints of the Bridge Frame

Joint No.	X-co-ord. (mm)	Y-co-ord. (mm)	Joint No.	X-co-ord. (mm)	Y-co-ord. (mm)
1	0.0	838.2	20	3611.9	838.2
2	304.8	"	21	3916.7	1745.0
3	1173.5	1257.3	22	"	838.2
4	"	838.2	23	4221.5	1706.9
5	1478.3	1379.2	24	"	838.2
6	"	838.2	25	4526.3	1645.9
7	1783.1	1485.9	26	"	838.2
8	"	838.2	27	48310.1	1577.3
9	2087.9	1577.3	28	"	838.2
10	"	838.2	29	5135.9	1485.9
11	2392.7	1645.9	30	"	838.2
12	"	838.2	31	5440.7	1379.2
13	2697.5	1706.9	32	"	838.2
14	"	838.2	33	5745.5	1257.3
15	3002.3	1745.0	34	"	838.2
16	"	838.2	35	6614.2	"
17	3307.1	1760.2	36	6919.0	"
18	"	838.2	37	304.8	0.0
19	3611.9	1760.2	38	6614.2	0.0

Table 8.2

Loads for the Bridge Frame

Joint No.	Vert.Load (KN)	Moment (KN-M)	Joint No.	Vert.Load (KN)	Moment (KN-M)
1	1627.9	–	19	178.4	–
2	1262.2	-140.1	20	602.1	–
3	191.8	13.5	21	178.4	–
4	1083.8	109.1	22	602.1	–
5	100.4	–	23	127.1	2.7
6	602.1	–	24	602.1	–
7	100.4	–	25	100.4	–
8	602.1	–	26	602.1	–
9	100.4	–	27	100.4	–
10	602.1	–	28	602.1	–
11	100.4	–	29	100.4	–
12	602.1	–	30	602.1	–
13	127.1	– 2.7	31	100.4	–
14	602.1	–	32	602.1	–
15	178.4	–	33	191.8	– 13.5
16	602.1	–	34	1083.8	-109.1
17	178.4	–	35	1262.2	140.1
18	602.1	–	36	1627.9	–

Note: The moments not shown are equal to zero.
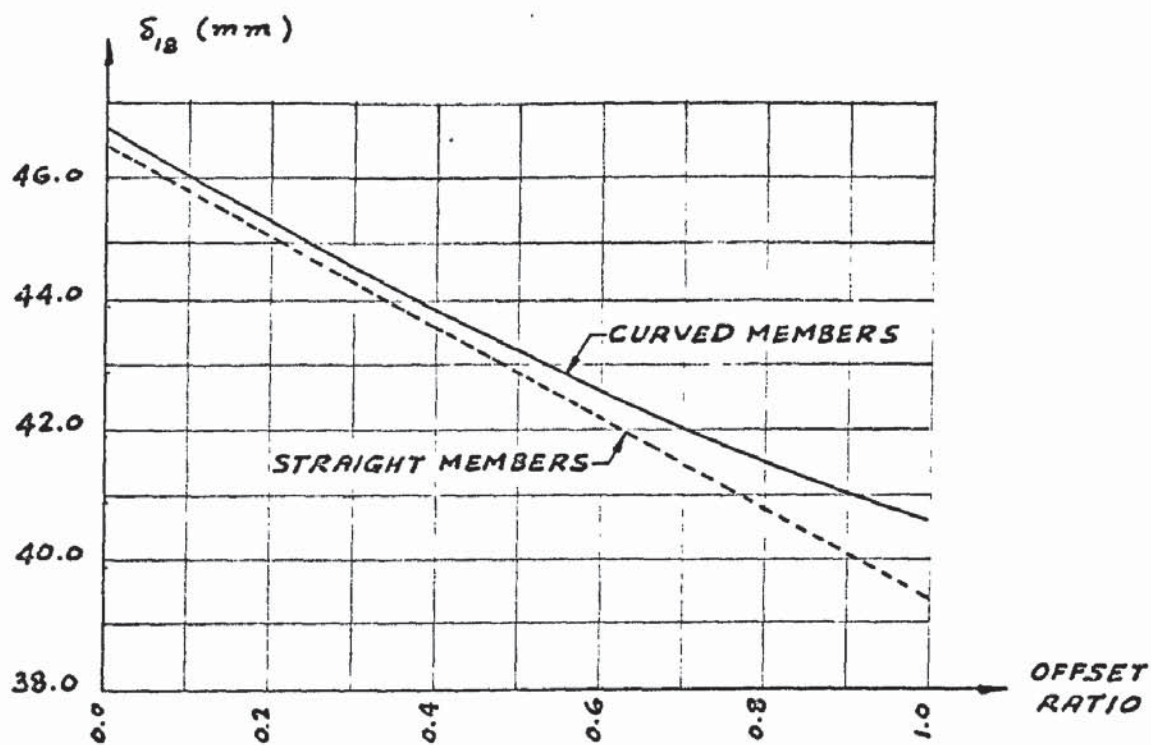
VERTICAL DISPLACEMENTS OF JOINT 18

FIG. 8.2
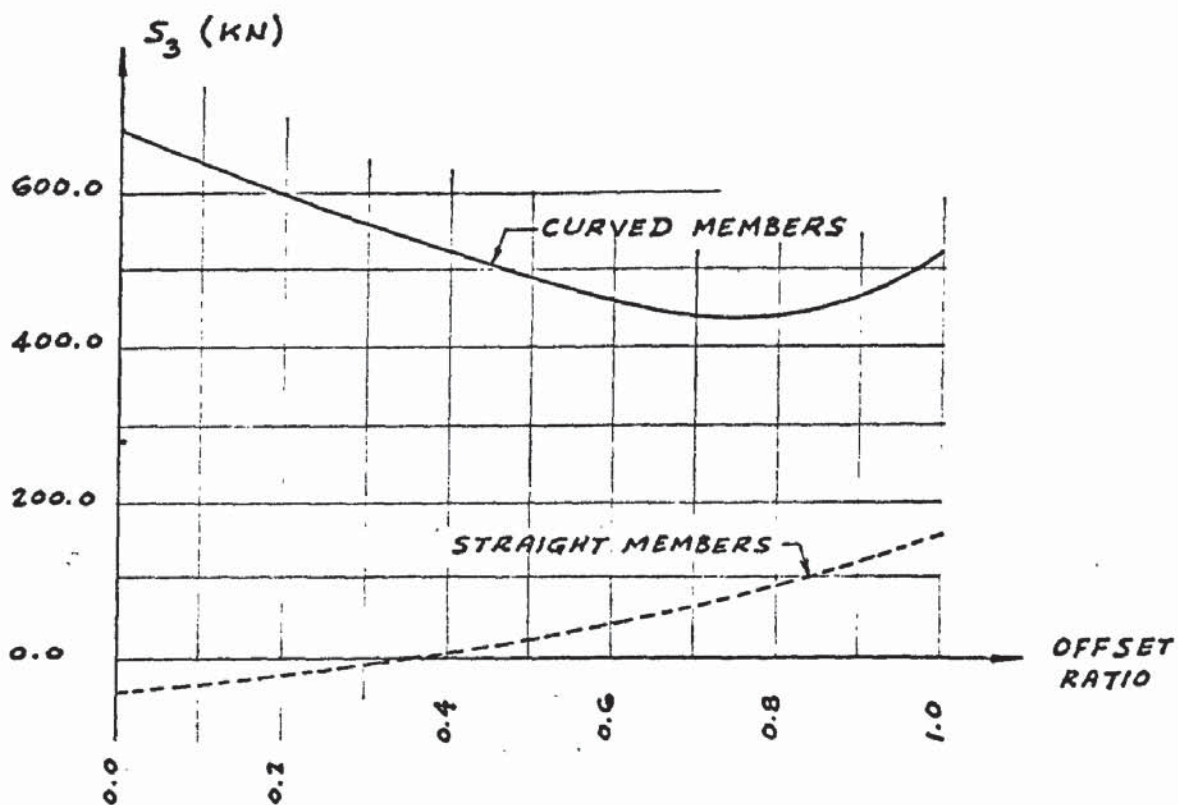
SHEAR FORCE IN THE ARCH AT THE SPRINGING

FIG. 8.3

BENDING MOMENTS IN THE ARCH AT THE SPRINGING

FIG. 8.4

SHEAR FORCE IN THE TIE BEAM AT THE SUPPORT

FIG. 8.5

M_{36} (KN-M)

CURVED MEMBERS

STRAIGHT MEMBERS

OFFSET RATIO

BENDING MOMENTS IN THE TIE BEAM AT THE SUPPORT

FIG. 8.6

P_{20} (KN)

CURVED MEMBERS

STRAIGT MEMBERS

OFFSET RATIO
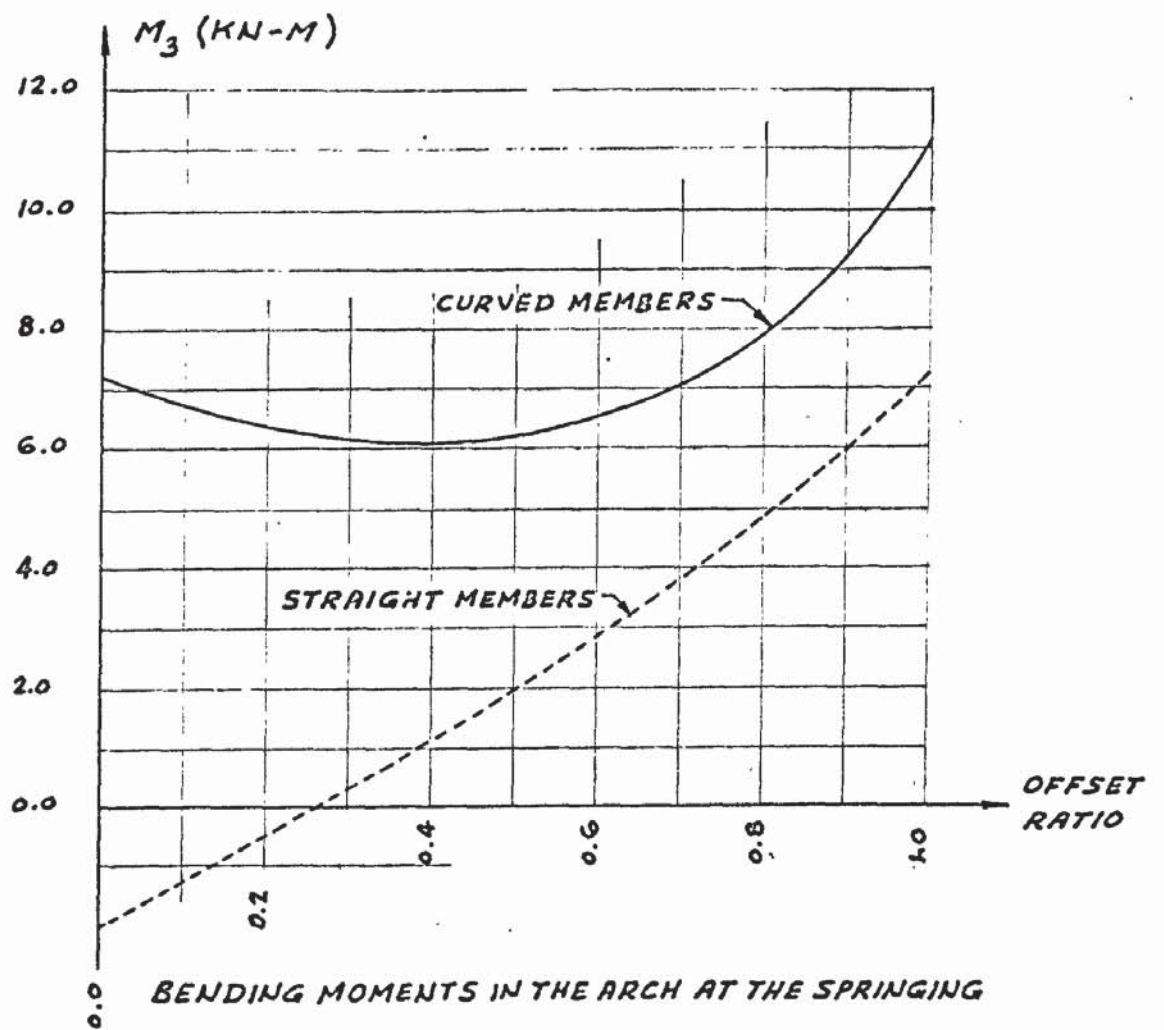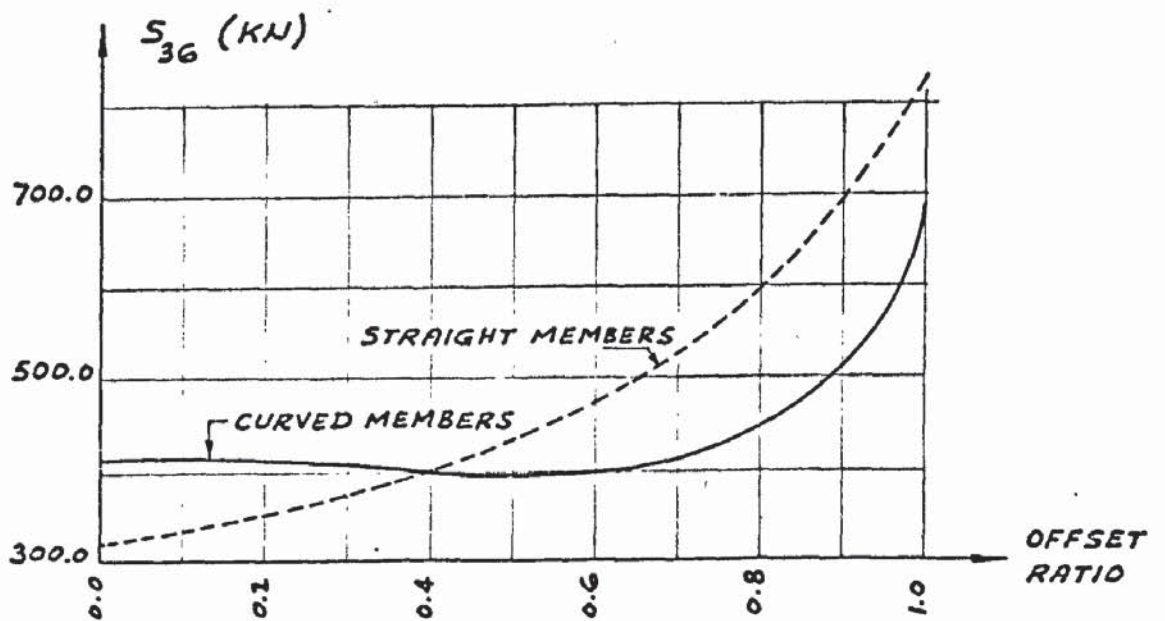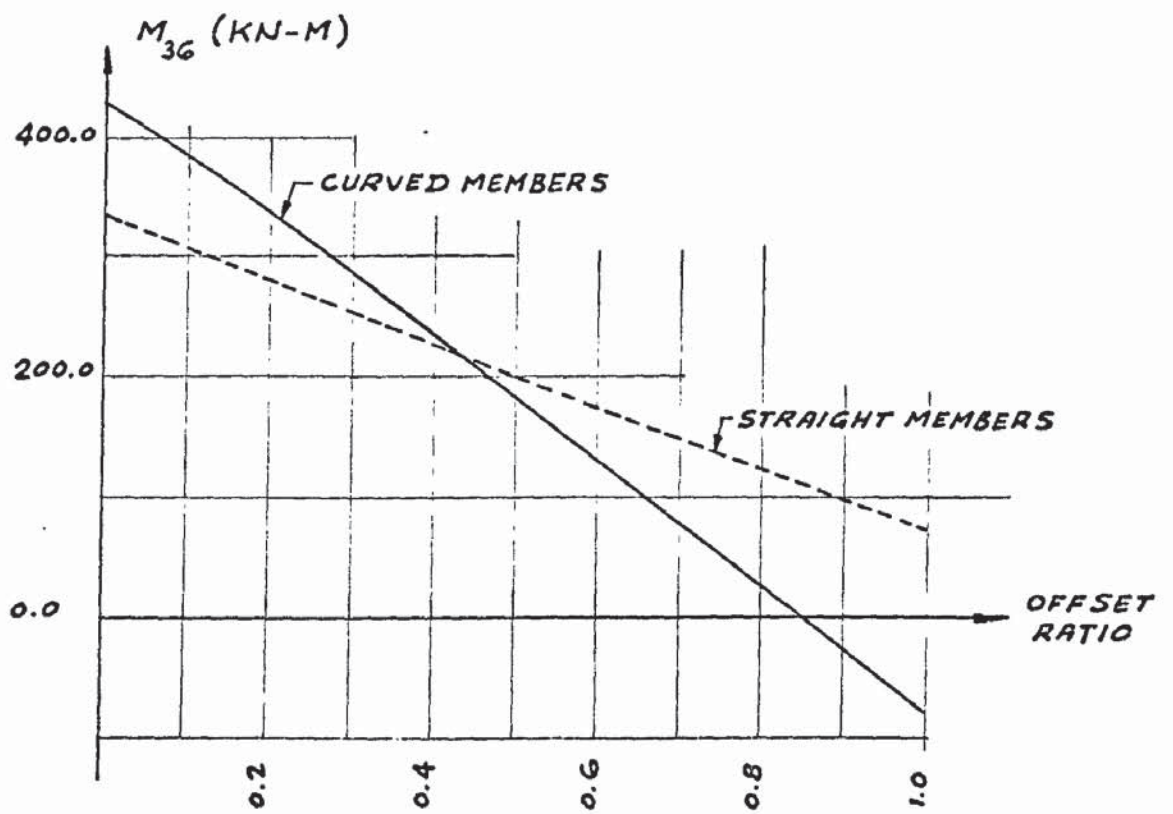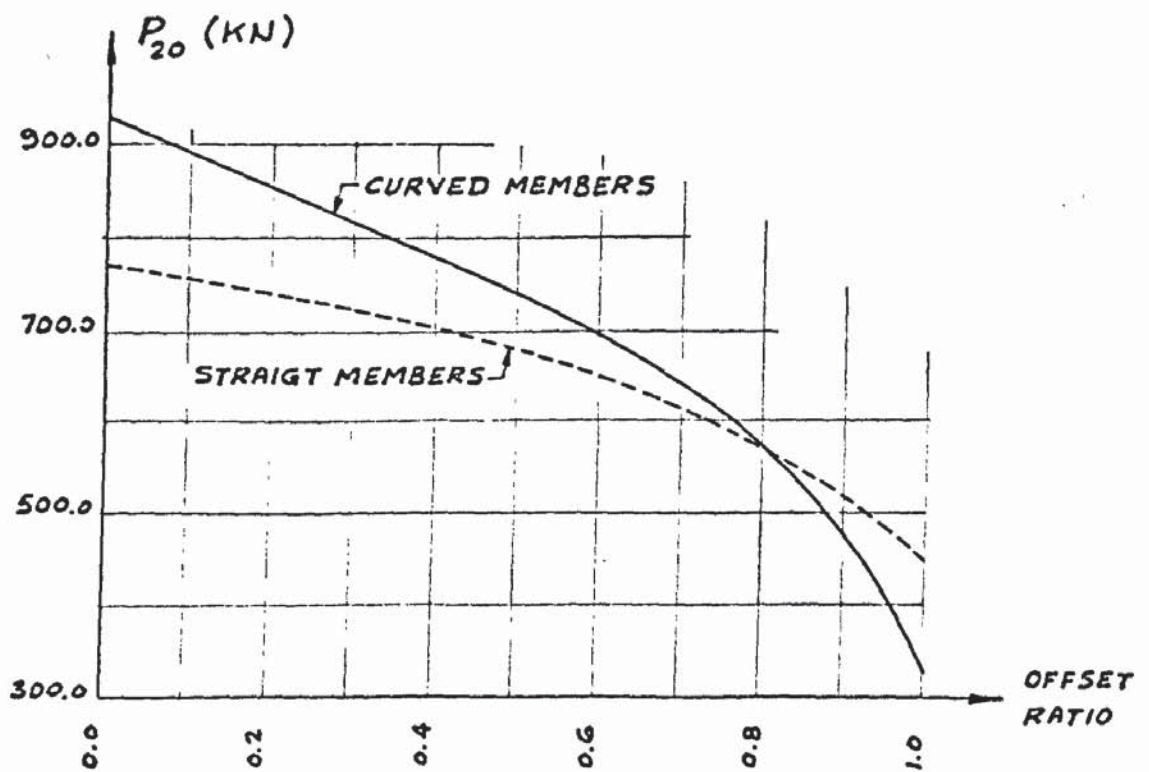
TENSILE FORCE IN THE SHORTEST HANGER

FIG. 8.7

6.35

12.7

SECTION 1-1

203.0

50.0
100.0
203.0

100.0

300.0

203.0

100.0

600.0

300.0

2   2

PLAN OF BOW GIRDER WITH
OFFSETS AND HINGES

NOTE: ALL DIMENSIONS ARE IN mm.

16.0
35.0
19.0
35.0
16.0

3

3

ELEVATION 2-2

6.35 x 35.0 x 55.0
mm LONG HARDEN-
ED KNIFE EDGES

SECTION 3-3

140.0

85.0

19.0
13.0
19.0

6.35

19.0
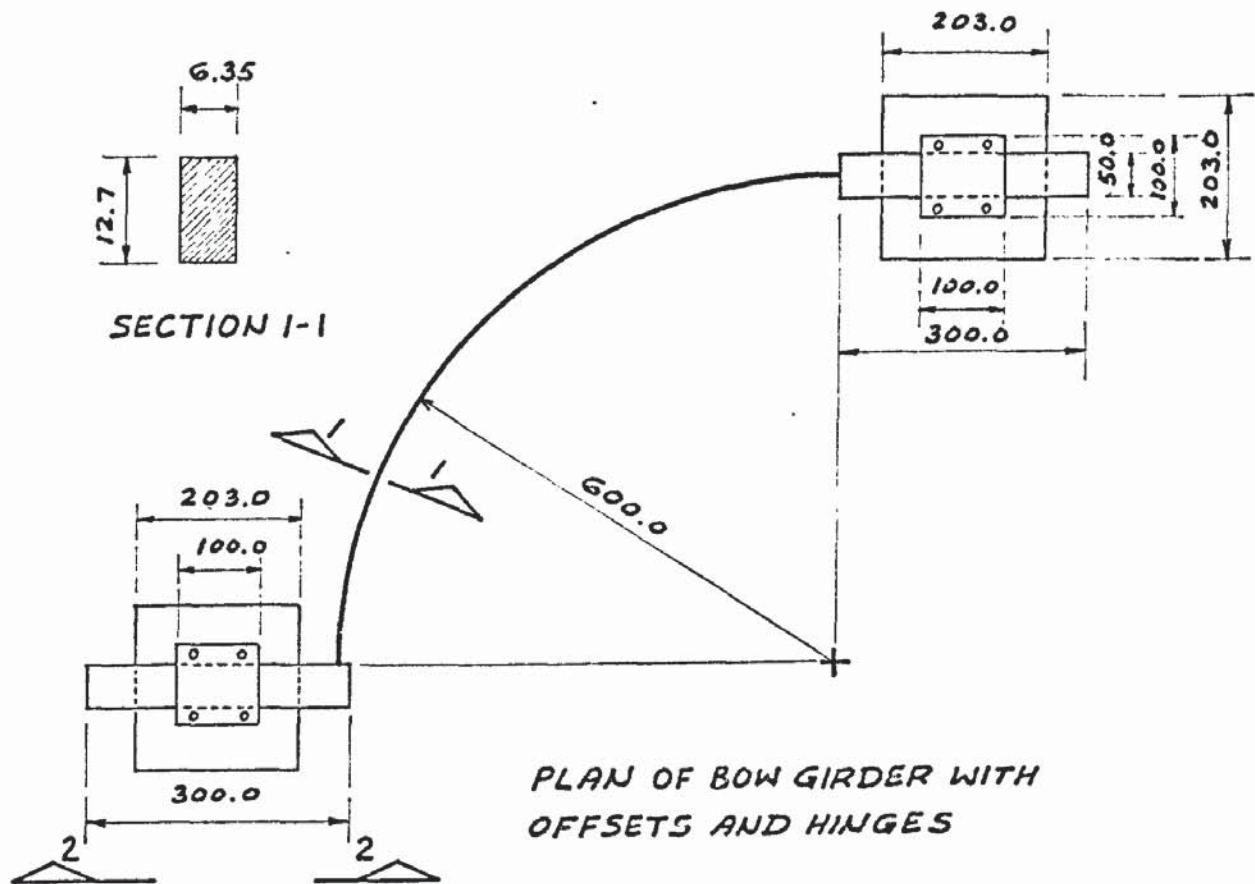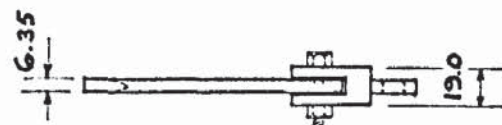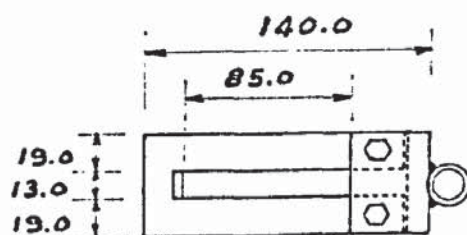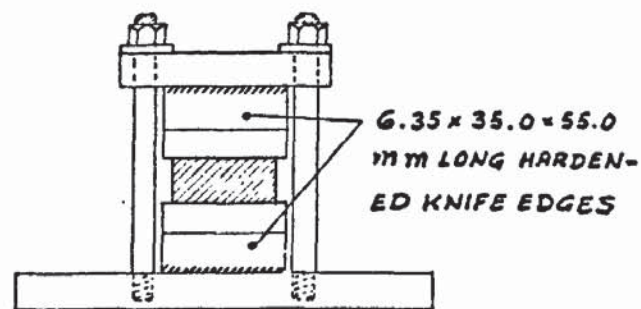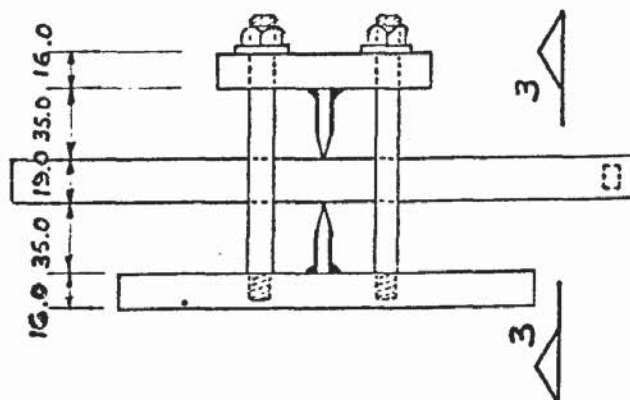
DETAILS OF BRACKET TO LOAD BOW GIRDERS

DRAWING NO. 5

Table 8.3

Deflections at the Mid-Point of Bow Girder with Offsets

Offsets	P_c		Q_c		P_c & Q_c	
mm	Exp.	Comp.	Exp.	Comp.	Exp.	Comp.
0.0		2.8		1.33		3.065
25.0		2.93		1.45		3.66
50.0	2.52	3.05	1.34	1.61	2.48	4.45
75.0		3.16		1.79		5.43
100.0	2.96	3.27	1.49	1.98	3.35	6.59
125.0		3.36		2.17		7.87
150.0	3.05	3.46	1.93	2.36	4.70	9.33
175.0		3.54		2.54		10.93
200.0	3.30	3.62	2.47	2.71	5.40	12.66
225.0		3.69		2.87		14.52
250.0	3.42	3.75	3.33	3.02	6.17	16.51

Note: All the deflections are in mm.

FIG.8.8
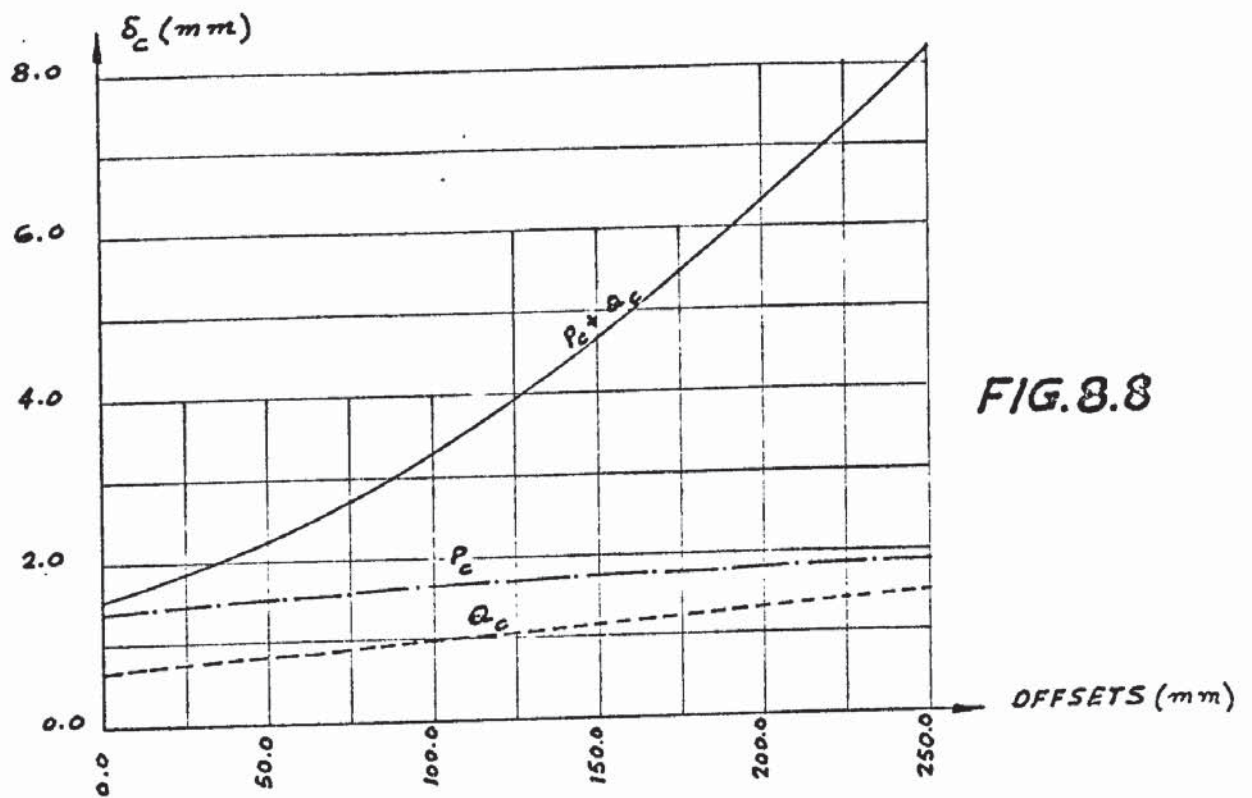
DEFLECTIONS AT MID-POINT OF BOW GIRDER

FIG.8.9

BENDING MOMENTS IN THE BOW GIRDER

FIG.8.10
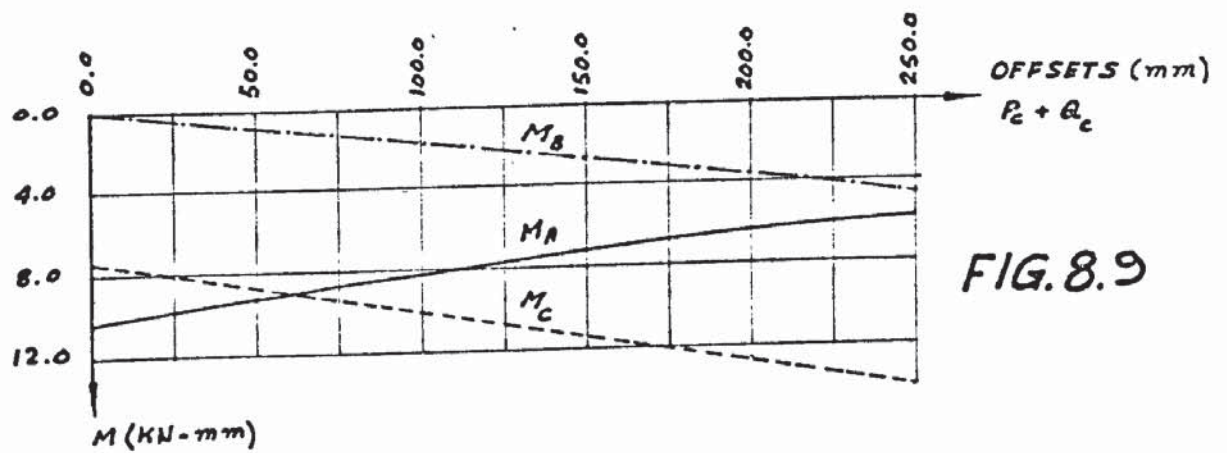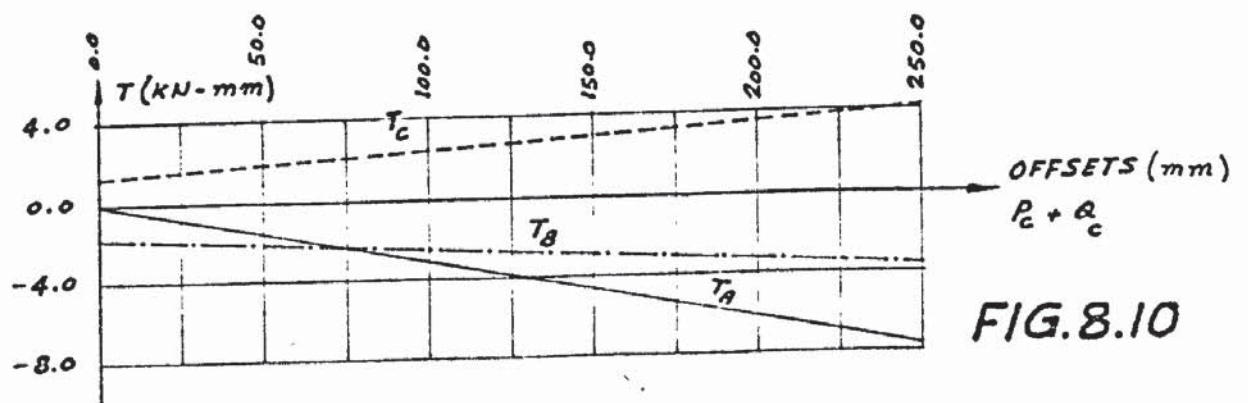
TWISTING MOMENTS IN THE BOW GIRDER

C H A P T E R   9

GENERAL CONCLUSIONS

The method of storage adopted for the coefficients of the variables of simultaneous symmetric equations in Chapter 2, has been shown (33) to be efficient in use of core space and solution time of the computer. The sub-routine for the solution of equations uses the backing store facilities, thus enabling large problems to be solved. The computer time required to transfer the information to and from the backing store is minimised by making the block size as large as possible. The efficiency of the sub-routine can be further improved by the following modifications:-

(a)   At present the RHS are reduced separately. This requires the transfer of some blocks from the backing store. Eliminating both sides at the same time uses those blocks in the reduction of the RHS as they are formed. Furthermore, the contents of the temporary store need not be stored in the backing store at all.

(b)   The coefficients of the LHS matrix are stored row by row. However, the elimination process is carried out column by column. This combination of storage and elimination requires searching operations to determine whether or not a coefficient is stored. These searching operations can be greatly reduced by storing the coefficients of the LHS matrix column by column. Such a method of storage has been claimed (58) to require less computer time to solve a set of simultaneous equations.

The inadequacy of the polynomial displacement functions to allow for the rigid body movements without straining the curved elements was pointed out by Cantin and Clough (24). This has been confirmed by the results obtained for arches which were presented in Chapter 4. It is commonly assumed that the finite element technique yields results which converge to the correct solution as the mesh size is refined. This, however, was not so for some of the results obtained for the arches by using the cubic displacement functions.

A scrutiny of the polynomial displacement functions reveals that the two functions are independant of each other. This condition is obtained in the axi-symmetric shells of revolution under symmetric radial loads because the tengential displacements vanish. This could be the reason why, in spite of the inadequacy of the polynomial displacement functions, very good results were obtained for such structures (22, 23, 40, 42). It is, therefore, likely that the cubic functions may yield good results for arches or circular rings under radial loads. Hydrostatic pressures in liquid containers give rise to radial loads. Stiffening ribs in such structures can be treated as rings.

Simulating semi-circular arches with only eight straight prismatic members yielded results which were very close to those obtained by using the classical theory of strain energy. Furthermore, these results were seen to be improving upon further subdivision. Cantin and Clough's assertion (24) that equally good results can be obtained by using flat elements for structures divided into large number of elements, therefore, seems to be correct.

More accurate displacement functions were derived in

Chapter 3 for arch elements with uniform cross-section. Two types of curvature-displacement relationships were utilized in the derivation. This yielded two sets of displacement functions called the approximate and the exact functions. The approximate functions were obtained by using the curvature formula for straight beams. The exact functions were obtained by using Flügge's formula for curvature for curved beams. The results obtained by using both sets of derived displacement functions show the influence of the initial curvature, R. It is seen that for arches which subtend an angle less than 60° at the centre, both sets of functions yield similar results. As the arches become deeper the results diverge. However, the exact functions always yielded results identical to those obtained by the strain energy method. For the analysis by using the derived displacement functions, the arches were divided into the minimum number of sub-divisions. It was found as expected, that the results did not improve upon further sub-division. Therefore, it is concluded that the use of the exact displacement functions derived here leads to saving in the core space and solution time without sacrificing accuracy.

The influence of Timoshenko's and Flügge's theories yielded similar results. It is possible that the difference in the results, if any, was lost due to the crude nature of the assumed displacement functions. Therefore, to obtain more conclusive evidence, the displacement functions should be derived by using Timoshenko's formula for curvature of curved bars. The results obtained by using these functions should, then, be compared with those obtained by using the exact displacement functions derived in this Thesis.

The exact displacement functions derived for curved element of uniform cross-sections were employed to formulate the stiffness matrix for a curved element with variable cross-section. This presupposes that the pattern of strain in both types of elements is the same. In spite of this assumption, good results have been obtained for the arches with variable cross-sections. However, more accurate results can be obtained by deriving the displacement functions for curved elements with variable cross-section.

From the experiments on the arches with fixed ends the difficulties in achieving complete fixity were realised. In spite of the corrections applied to account for the end rotations, some discrepancies lingered. The use of more flexible arches for the experiments, if possible, is, therefore, recommended. The strength of hollow steel sections to provide the fixity is deceptive and, therefore, such sections should be avoided altogether.

In reference (61) displacement functions for cylindrical shell element were reduced to beam element. The displacement functions derived in this Thesis can be extended to cylindrical shell elements. This can be achieved by adding terms to the displacement functions so that the displacement along a line parallel to the longitudinal axis of the shell varies as a polynomial.

The strain-displacement relationships for curved elements suffering out of plane deformations were derived in Chapter 5. These relationships were used in conjunction with the polynomial displacement functions to obtain the stiffness matrix for a bow girder element. Results obtained by using this stiffness matrix

for some bow girders under various loads were presented in
Chapter 6. It is observed that the polynomial displacement
functions yield good results for bow girders, even with crude
sub-division. From the results obtained it appears that for
arch elements the influence of the displacement functions is
predominant while the curvature-displacement relationships play
only a minor role. For the bow girder elements, however, the
reverse seems to be the case.

Simulation of arches with a number of straight members
yielded good results which improved upon further sub-division.
On the other hand, the twisting moments obtained by approxim-
ating the bow girders with a number of straight members de-
teriorated as the mesh was refined. Reasons for this were given
in Chapter 6.

More accurate displacement functions were derived in
Chapter 5 for the bow girder elements of uniform cross-section.
These functions yielded results for bow girders identical to
those obtained by using the strain energy method. The bow
girders were divided into the minimum number of sub-divisions.

The stiffness matrix for a bow girder element with variable
cross-section was developed by using the displacement functions
derived for elements of uniform cross-section. The theoretical
deflections obtained for bow girders with variable cross-
sections agree reasonably well with those obtained by experi-
ments. It was not possible to compare the results obtained for
the bending and the twisting moments because no strain gauges
were fixed to the bow girders. To assess the accuracy of the
stiffness matrix more conclusively, the forces obtained theor-
etically should be compared with those obtained from experiments.

However, more accurate displacement functions can be derived by considering the static equilibrium of bow girder elements with variable cross-section.

The torsion constant of the cross-section, J, was calculated from an approximate formula for rectangular cross-sections. The reason that the strain energy method and the derived displacement functions yielded identical results was that the same formula was employed in both to compute the torsion constant. The cross-section of the experimental bow girder varies from a thin rectangle at the supports to a very thin rectangle at the mid-point. The validity of the formula to calculate the torsion constant of these sections is questionable. It is possible that the error in the torsion constant is the major contributor to the errors in the results for the bow girders. Therefore, the recommendation of reference (6) that where possible the stiffness, GJ, of a member should be obtained by experiment has merits.

Finally, if possible, the bow girders should be made reasonably flexible. This helps to achieve full fixity of the ends more easily.

The displacement functions were derived for the curved elements with the forces acting at their ends only. No difficulty arises when dealing with uniformly distributed loads. Using the equivalent loads and the derived displacement functions, results were obtained which were identical to those yielded by the strain energy method. For the matrix analysis, the arches and the bow girders were divided into two segments only. The equivalent loads were calculated by strain energy method. The same results can be obtained by employing the principle of virtual work

The latter method is more attractive from the viewpoint of the finite element technique.

Following the procedure adopted in reference (11), the displacement transformation matrices were constructed which allow for the effect of the offsets and hinges. The results for the arch bridge seems to be reasonable over the whole range of the offsets, but this is to be expected as both sets of results obtained are theoretical. The results for the bow girder, however, show that the theoretical method of catering for the offsets is valid for small offsets only. More experiments are needed on simple arches and bow girders with the offsets to establish the limit of small offsets. Furthermore, in these experiments strain gauges should be used. The moments computed from the strains should be compared with those obtained theoretically.

For reasons explained in section 7.6, only in-plane offsets can be considered for plane frames. For a member in three dimensional space the in-plane and the out of plane stiffness matrices cannot be assembled simply. The out of plane offset, r_c, contributes coupling terms to the stiffness matrix in three dimensional space.

APPENDIX A

```
SUBROUTINE CDM (A,B,C,IB,IR,IS,NG,NT,NIS,MA,MB,MXA,MXB,LQ)
INTEGER P, Q, R, S
DIMENSION A(MXA),B(MXB),C(MA),IS(NIS),IR(NT),IB(NG)
P = 1

Q = 2
2   IQ = Q - 2
Q = IB(P)
IF (Q .EQ. P .OR. Q .EQ. IQ) GO TO 1
IF (Q .EQ. P - 1) GO TO 4
K = (Q - 1) * MA + 1
CALL GETPART (10, K, A, A(MA + 1), A(2 * MA))
GO TO 1
4   DO 5 I = 1, MA
5   A(MA + I) = A(I)
1   K = (P - 1) * MA + 1
CALL GETPART (10, K, A, A(1), A(MA))
MP = IR(P) + 1
NP = IR(P + 1)
MQ = IR(Q) + 1
NQ = IR(Q + 1)
NA = - IS(MP)
ND = MA - IS(MQ)
MQ = MP
DO 7 I = MP, NP
J = I - IS (I + 1) + IS (I) + 1
IF (MQ . GT. J) MQ = J
7   CONTINUE
IF (P .EQ. Q) ND = NA
DO 8 J = MQ, NQ
MJ = J - IS(J + 1) + IS(J) + 1
R = MP
IF (J .GT. MP) R = J
DO 8 I = R, NP
MI = I - IS(I + 1) + IS(I) + 1
IF (J .LT. MI) GO TO 8
```

```
        IF (J .EQ. 1) GO TO 9
        L = J - 1
        IF (I .GT. J) GO TO 10
        S = IS (I + 1) + NA
        IF (L .LT. MJ) GO TO 11
        DO 11 M= MJ, L
        K = IS (I + 1) - I + M + NA
        A(S) = A(S) - C(K) * A(K)
11      CONTINUE
        C(S) = A(S)
        GO TO 8
10      IF (MI .LT. MJ) MI = MJ
        S = IS(I + 1) - I + 1 + NA
        IF L .LT. MT) GO TO 12
        DO 12 M = MI, L
        K = IS(I + 1) - I + M + NA
        N = IS(J + 1) - J + M + ND
        A (S) = A(S) - C(K) * A(N)
12      CONTINUE
        N = IS(J + 1) + ND
        C(S) = A(S)
         A(S) = C(S) * A(N)
        GO TO 8
 9      K = IS(I + 1) - I + 1 + NA
        C(K) = A(K)
        IF (I .GT. 1) GO TO 13
        A(K) = 1.0 / C(K)
        GO TO 8
13      N = IS(J + 1) + ND

        A(K) = C(K) * A(N)
 8      CONTINUE
        Q = Q + 1
        IF ( Q .EQ. P) GO TO 3
        IF (Q .GT. P) GO TO 16
        K = (Q - 1) * MA + 1
        CALL GETPART (10, K, A, A(MA + 1), A(2 * MA))
 3      MQ = IR(Q) + 1
```

```
        NQ = IR (Q + 1)
        ND = MA - IS(MQ)
        GO TO 7
  16    K = (P - 1) * MA + 1
        CALL PUTPART (10, K, A, A(1), A(MA))
        K = (NG + P - 1) * MA + 1
        CALL PUTPART (10, K, C, C(1), C(MA))
        P = P + 1
        IF (P .LE. NG) GO TO 2
        P = 1
  26    CONTINUE
        MP = IR(P) + 1
        NP = IR(P + 1)
        K = 2 * NG * MA + IR(P) * LQ + 1
        NE = ( NP - MP + 1 ) * LQ
        CALL GETPART (10, K, B, B(1), B(NE))
        K = (P - 1) * MA + 1
        CALL GETPART (10, K, A, A(1), A(MA))
        K = (NG + P - 1) * MA +1
        CALL GETPART (10, K, C, C(1), C(MA))
        Q = IB(P)
        IF (Q .EQ. P) GO TO 17
        K = 2 * NG * MA + IR(Q) * LQ + 1
        NE = (IR(Q + 1) - IR(Q)) * LQ
        CALL GETPART (10, K, B, B(MB + 1), B(MB + NE))
  17    NA = - IS(MP)
        NB = - IR(P) * LQ
  20    ND = MB - IR(Q) * LQ
        IF (Q .EQ. P) ND = NB
        MQ = IR(Q) + 1
        DO 18 I = MP, NP
        NQ = IR(Q + 1)
        MI = I - IS(I + 1) + IS(I) + 1
        IF (MI .GT. NQ) GO TO 18
        DO 18 J = 1, LQ
        IF (I .GT. 1) GO TO 19
        B(J) = B(J) * A(1)
        GO TO 18
```

```
19    MJ = MQ
      R = (I - 1) * 10 + J + NB
      IF (MJ .LT. MI) MJ = MI
      IF (Q .EQ. P) NQ = I -1
      IF (MJ .GT. NQ) GO TO 18
      DO 21 M = MJ. NQ
      K = (M - 1) * LQ + J + ND
      L = IS(I + 1) - I + M + NA
      B(R) = B(R) - C(L) * B(K)
21    CONTINUE
      IF (NQ .LT. I - 1) GO TO 18
      L = IS(I + 1) + NA
      B(R) = A(L) * B(R)
18    CONTINUE
      IF (Q E.Q. P) GO TO 24

      Q = Q + 1
      IF (Q .EQ. P) GO TO 20
      K = 2 * NG * MA + IR(Q) * LQ + 1
      NE = (IR(Q + 1) IR(Q)) * LQ
      CALL GETPART (10, K, B, B(MB + 1), B(MB + NE))
      K = 2 * NG * MA IR(P) * LQ + 1
      GO TO 20
24    IF (P .EQ. NG) GO TO 25
      NE = (IR(P + 1) - IR(P)) * LQ
      CALL PUTPART (10, K, B, B(1), B(NE))
      P = P + 1
      GO TO 26
25    CONTINUE
      I = NIS - 1
      IF(I .EQ. MP) GO TO 99
30    I = I - 1
      DO 29 J = 1, LQ
      N = (I - 1) * LQ + J + NB
      DO 29 L = I+1, NP
      IF(I .LT. L - IS(L + 1) + IS(L) + 1) GO TO 29
      K = IS(L + 1) - 1 + I + NA
      M = (L - 1) * LQ + J + NB
      B(N) = B(N) - A(K) * B(M)
```

```
29    CONTINUE
      IF (I .GT. MP) GO TO 30
99    CONTINUE
      K = 2 * NG * MA + IR(P) * LQ + 1
      NE = (IR(P + 1) - IR(P)) * LQ
      CALL PUTPART (10, K, B, B(1), B(NE))
      IF (P .EQ. 1) GO TO 100
47    P = P - 1
      Q = Q - 1
      MP = IR(P) + 1
      NP = IR(P + 1)
      NA = - IS(MP)
      NB = - IR(P) * LQ
      IQ = Q
      Q = NG
32    IF (P .GE. IB(Q)) GO TO 31
      Q = Q - 1
      GO TO 32
31    MQ = IR(Q) + 1
      NQ = IR(Q + 1)
      NC = MB - IR(Q) * LQ
      ND = MA - IS(MQ)
      IF (Q .EQ. IQ) GO TO 33
      IF (Q .EQ. P) GO TO 33
      IF (* .NE. P. + 1) GO TO 34
      DO 35 I = 1, MA
35    A(MA + I) = A(I)
      NE = (NQ - MQ + 1) * LQ
      DO 36 I = 1, NE
36    B(MB + I) = B(I)
      GO TO 33
34    K = (Q - 1) * MA + 1
      CALL GETPART (10, K, A, A(MA + 1), A(2 *MA))
      K = 2 * NG * MA + IR(Q) * LQ + 1
      NE = (IR(Q + 1) - IR(Q)) *LQ
      CALL GETPART (10, K, B, B(MB + 1), B(MB + NE))
33    K = (P - 1) * MA + 1
      CALL GETPART (10; K, A, A(1), A(MA))
```

```
            K = 2 * NG * MA + IR(P) * LQ + 1
            NE = (IR(P + 1) - IR(P)) * LQ
            CALL GETPART (10, K, B, B(1), B(NE))
            IF (Q .NE. P) GO TO 37
            ND = NA
            NC = NB
   37       CONTINUE
            MJ = MQ
            DO 38 I = MQ, NQ
            J = I - IS(T + 1) + IS(I) + 1
            IF (MJ .GT. J) MJ = J
   38       CONTINUE
            IF (MP .GT. MJ) MJ = MP
   45       I = IR(P +1)
   41       DO 39 J = 1, LQ
            IF (I .EQ. NQ) GO TO 39
            N = (I -1) * LQ + J + NB
            IF (Q .EQ. P) MQ = I + 1
            DO 39 L = MQ, NQ
            IF(I .LT. L - IS(L + 1) + IS(L) + 1) GO TO 39
            K = IS(L + 1) - L + I + ND
            M = (L - 1) * LQ + J + NC
            B(N) = B(N) - A(K) * B(M)
   39       CONTINUE
            I = I - 1
            IF (I .GE. MJ) GO TO 41
            IF (Q .EQ. P) GO TO 43
            Q = Q - 1
            IF (Q .EQ. P) GO TO 44
            K = (Q - 1) + MA + 1
            CALL GETPART (10, K, A, A(MA + 1), A(2 * MA))
            K = 2 * NG * MA + IR(Q) * LQ + 1
            NE = (IR(Q + 1) - IR(Q)) * LQ
            CALL GETPART (10, K, B, B(MB + 1), B(MB + NE))
            MQ = IR(Q) + 1
            NQ = IR(Q + 1)
            ND = MA - IS(MQ)
            NC = MB - IR(Q) * LQ
```

```
            GO TO 37
     44     MQ = MP
            NQ = NP
            ND = NA
            NC = NB
            MJ = MP
            GO TO 45
     43     K = 2 * NG * MA * + IR(P) * LQ + 1
            NE = (IR(P +1) - IR(P)) * LQ
            CALL PUTPART (10, K, B, B(1), B(NE))
            IF (P .GT. 1) GO TO 47
    100     CONTINUE
            RETURN
            END
```

APPENDIX B

Stiffness Matrix for Curved Members with Uniform Cross Section.

1.   The Displacement Functions.

The displacement functions were derived in Chapter 3 and are given by equations (3.56) and (3.57). The equation for the slope at any point in the member is obtained by differentiating equation (3.56) with respect to x. This equation is:

$$\frac{dw}{dx} = a_2 \cdot \frac{1}{R} \cos \frac{x}{R} - a_3 \cdot \frac{1}{R} \sin \frac{x}{R} + a_4 \left(\sin \frac{x}{R} + \frac{x}{R} \cos \frac{x}{R} \right) + a_5 \left(\cos \frac{x}{R} - \frac{x}{R} \sin \frac{x}{R} \right) \quad (1)$$

Substituting the boundary conditions into equations (3.56), (3.57) and (1) the nodal displacements become:

$$w_1 = a_1 + a_3 \quad (2)$$

$$u_1 = -a_2 + a_5 \cdot a + a_6 \quad (3)$$

$$\theta_1 = a_2 \cdot b + a_5 \quad (4)$$

$$w_2 = a_1 + a_2 \cdot c + a_3 \cdot d + a_4 \cdot e + a_5 \cdot f \quad (5)$$

$$u_2 = a_1 \cdot g - a_2 \cdot d + a_3 \cdot c + a_4 \cdot h + a_5 \cdot i + a_6 \quad (6)$$

and $\theta_2 = a_2 \cdot j + a_3 \cdot k + a_4 \cdot m + a_5 \cdot n \quad (7)$

where:

$$a = R - \frac{2I}{AR} \quad ;$$

$$b = \frac{1}{R} \quad ;$$

$$c = \sin \frac{L}{R} \quad ;$$

$$d = \cos \frac{L}{R} \quad ;$$

$$e = L \cdot \sin \frac{L}{R} \quad ;$$

$$f = L \cdot \cos \frac{L}{R} \quad ;$$

$$g = \frac{L}{R} \qquad ;$$

$$h = \left(R - \frac{2I}{AR}\right) \sin \frac{L}{R} - L \cos \frac{L}{R} \quad ;$$

$$i = \left(R - \frac{2I}{AR}\right) \cos \frac{L}{R} + L \sin \frac{L}{R} \quad ;$$

$$j = \frac{1}{R} \cos \frac{L}{R} \qquad ;$$

$$k = \frac{-1}{R} \sin \frac{L}{R} \quad ;$$

$$m = \sin \frac{L}{R} + \frac{L}{R} \cos \frac{L}{R} \quad ;$$

and $\quad n = \cos \frac{L}{R} - \frac{L}{R} \sin \frac{L}{R}$

Solving the set of eqns. (2) to (7) and writing the results in matrix form yields: (the equations shown on the following page).

Equations (8) have been obtained by making the following substitutions during the solution process:

$$\alpha = c - g - \frac{h}{e}(d - 1) \quad ;$$

$$\beta = \frac{d}{b} + i - a - \frac{1}{b} - \frac{h}{e}\left(f - \frac{c}{b}\right);$$

$$\lambda = k - \frac{m}{e}(d-1) \quad ;$$

$$\gamma = n - \frac{j}{b} - \frac{m}{e}\left(f - \frac{c}{b}\right);$$

$$B = \alpha\gamma - \beta\lambda \quad ;$$

$$D = \lambda\left(g - \frac{h}{e}\right) + \frac{\alpha m}{e} \quad ;$$

$$E = \frac{1}{b}\left[\lambda\left(1 - d - \frac{ch}{e}\right) - \alpha\left(j - \frac{cm}{e}\right)\right] \quad ;$$

$$F = \frac{1}{e}(\lambda h - m) \quad ;$$

$$G = \gamma\left(g - \frac{h}{e}\right) + \frac{\beta m}{e} \quad ;$$

$$H = \frac{1}{b}\left[\gamma\left(1 - d - \frac{ch}{e}\right) - \beta\left(j - \frac{cm}{e}\right)\right] \quad ;$$

$$
\begin{bmatrix} a_1 \\ a_2 \\ a_3 \\ a_4 \\ a_5 \\ a_6 \end{bmatrix}
= \frac{1}{b}
\begin{bmatrix}
\gamma & B+G & H & \gamma & J & \beta \\[4pt]
-\dfrac{\lambda}{b} & -\dfrac{D}{b} & \dfrac{1}{b}(B-E) & \dfrac{\lambda}{b} & -\dfrac{F}{b} & -\dfrac{\alpha}{b} \\[6pt]
-\gamma & -G & -H & \gamma & -J & -\beta \\[4pt]
K & M & N & -K & P & Q \\[4pt]
\lambda & D & E & -\lambda & F & \alpha \\[6pt]
\dfrac{B-\lambda}{b}(ab+1) & -\dfrac{D}{b}(ab+1) & \dfrac{1}{b}[B-E(ab+1)] & \dfrac{\lambda}{b}(ab+1) & -\dfrac{F}{b}(ab+1) & -\dfrac{\alpha}{b}(ab+1)
\end{bmatrix}
\begin{bmatrix} u_1 \\ w_1 \\ \theta_1 \\ u_2 \\ w_2 \\ \theta_2 \end{bmatrix}
\qquad (8)
$$

$$J = \frac{1}{e} (\gamma h - \beta m) \ ;$$

$$K = \frac{1}{e} \left[\gamma (d - 1) - \lambda \left(f - \frac{c}{b}\right) \right] \ ;$$

$$M = \frac{1}{e} \left[G(d - 1) - D \left(f - \frac{c}{b}\right) - B \right] \ ;$$

$$N = \frac{1}{e} \left[H (d - 1) - E \left(f - \frac{c}{b}\right) - \frac{Bc}{b} \right] \ ;$$

$$P = \frac{1}{e} \left[J (d - 1) - F \left(f - \frac{c}{b}\right) + B \right] \ ;$$

and $\quad Q = \frac{1}{e} \left[\beta (d - 1) - \alpha \left(f - \frac{c}{b}\right) \right] \ ;$

2.   The Strain - Displacement Relationships.

The strain - displacement relationships are expressed by eqns. (3.58) and (3.59).

3.   The Stress - Strain Relationships.

The stress - strain relationships are given in eqns. (3.26) to (3.29).

4.   The Strain Matrix.

The strain matrix is obtained by substituting into eqn (3.58) for the arbitrary constants from eqn (8). Carrying out the matrix multiplication yields the elements of the strain matrix. The following recurrsive formula is obtained for the strain elements:

$$B_{1i} = b_{i1} \psi_1 + b_{i2} \psi_2 \tag{10}$$

and $\quad B_{2i} = d_{i1} + b_{i1} \psi_3 + b_{i2} \psi_4 \qquad$ where $i = 1, 2 \ldots\ldots 6.$ $\tag{11}$

The coefficients b_{ij} and d_{ij} are derived below:

$b_{11} = \frac{K}{B} \ ; \quad b_{12} = \frac{\lambda}{B} \ ; \quad b_{21} = \frac{M}{B} \ ; \quad b_{22} = \frac{D}{B} \ ; \quad b_{31} = \frac{N}{B} \ ; \quad b_{32} = \frac{E}{B} \ ; \quad b_{41} = -b_{11} \ ;$

$b_{42} = -b_{12} \ ; \quad b_{51} = \frac{P}{B} \ ; \quad b_{52} = \frac{F}{B} \ ; \quad b_{61} = \frac{Q}{B}$ and $b_{62} = \frac{d}{B}$

$d_{11} = \frac{\gamma}{BR^2} \ ; \quad d_{21} = \frac{B + G}{BR^2} \ ; \quad d_{31} = \frac{H}{BR^2} \ ;$

$d_{41} = -d_{11} \ ; \quad d_{51} = \frac{J}{BR^2}$ and $d_{61} = \frac{\beta}{BR^3}$

The following integrations are needed to obtain the elements of the stiffness matrix:

$$\lambda_1 = \int \psi_1{}^2 \, dx = c_1 \left(\frac{L}{2} + \frac{R}{4} \sin \frac{2L}{R} \right);$$

$$\lambda_2 = \int \psi_1 \cdot \psi_2 \, dx = -c_1 \cdot \frac{R}{2} \sin^2 \left(\frac{L}{R} \right);$$

$$\lambda_3 = \int \psi_2{}^2 \, dx = c_1 \left(\frac{L}{2} - \frac{R}{4} \sin \frac{2L}{R} \right);$$

$$\lambda_4 = \int \psi_3 \, dx = 2 \sin \frac{L}{R};$$

$$\lambda_5 = \int \psi_4 \, dx = 2 \left(\cos \frac{L}{R} - 1 \right);$$

$$\lambda_6 = \int \psi_3{}^2 \, dx = c_2 \left(\frac{L}{2} + \frac{R}{4} \sin \frac{2L}{R} \right);$$

$$\lambda_7 = \int \psi_3 \cdot \psi_4 \, dx = -c_2 \cdot \frac{R}{2} \sin^2 \frac{L}{R};$$

$$\text{and} \quad \lambda_8 = \int \psi_4{}^2 \, dx = c_2 \left(\frac{L}{2} - \frac{R}{4} \sin \frac{2L}{R} \right)$$

where: $c_1 = \left(\frac{2I}{AR^2} \right)^2$;

and $c_2 = \frac{4}{R^2}$

All the above integrations are from 0 to L, the length of the curved member.

The elements of the stiffness matrix are obtained by substituting the strain matrix into eqn.(3.30) and carrying out the integrations. It can be easily shown that the following reccurssive formula is obtained for the stiffness terms:

$$K_{ij} = EA \left[b_{ji} \left(b_{i1} \lambda_1 + b_{i2} \lambda_2 \right) + b_{j2} \left(b_{i1} \lambda_2 + b_{i2} \lambda_3 \right) \right]$$

$$+ EI \left[d_{ji} \left(d_{t1} + b_{i1} \lambda_4 + b_{i2} \lambda_5 \right) + b_{j1} \left(d_{i1} \lambda_4 + b_{i1} \lambda_6 + b_{i2} \lambda_7 \right) \right.$$

$$\left. + b_{j2} \left(d_{i1} \lambda_5 + b_{i1} \lambda_7 + b_{i2} \lambda_8 \right) \right]$$

where:

EA is the extensional stiffness of the member;

and EI " " bending " " " "

APPENDIX C

Stiffness Matrix of Curved Members with Uniform Cross Section.

1. The Displacement Functions.

The displacement functions were obtained in section 5.4 and are given by equations (5.39) and (5.40). Differentiation of eqn. (5.39) yields the following equation for the slope at any point in the curved member:

$$\frac{dw}{dx} = a_2 + a_3 \cdot \frac{1}{R} \cos \frac{x}{R} - a_4 \cdot \frac{1}{R} \sin \frac{x}{R} + a_5 \left(\sin \frac{x}{R} + \frac{x}{R} \cos \frac{x}{R} \right)$$

$$+ a_6 \left(\cos \frac{x}{R} - \frac{x}{R} \sin \frac{x}{R} \right) \tag{1}$$

Substituting the boundary conditions into the equations for the displacements and the slope, eqns. (5.39), (5.40) and (1) respectively yields the following set of simultaneous equations:

For end 1;

$$w_1 = a_1 + a_4 \tag{2}$$

$$\gamma_1 = -\frac{a_4}{R} - a_5 \psi \tag{3}$$

$$\text{and } \theta_1 = a_2 + \frac{a_3}{R} + a_6 \tag{4}$$

Similarily for end 2;

$$w_2 = a_1 + a_2 \cdot L + a_3 \cdot b + a_4 \cdot c + a_5 \cdot d + a_6 \cdot e \tag{5}$$

$$\gamma_2 = a_3 \cdot f - a_4 \cdot g + a_5 \cdot h + a_6 \cdot i \tag{6}$$

$$\text{and } \theta_2 = a_2 + a_3 \cdot g + a_4 \cdot f + a_5 \cdot j + a_6 \cdot k \tag{7}$$

where:

$$\psi = -\frac{2EI}{EI+GJ} \quad ;$$

$$b = \sin \frac{L}{R} \quad ;$$

$$c = \cos \frac{L}{R} \quad ;$$

$$d = L \cdot \sin \frac{L}{R} \quad ;$$

$$e = L \cdot \cos \frac{L}{R} \quad ;$$

$$f = -\frac{1}{R} \sin \frac{L}{R} \quad ;$$

$$g = \frac{1}{R} \cos \frac{L}{R} \quad ;$$

$$h = -\frac{L}{R} \sin \frac{L}{R} - \psi \cdot \cos \frac{L}{R} \quad ;$$

$$i = \psi \cdot \sin \frac{L}{R} - \frac{L}{R} \cdot \cos \frac{L}{R} \quad ;$$

$$j = \sin \frac{L}{R} + \frac{L}{R} \cdot \cos \frac{L}{R} \quad ;$$

$$\text{and} \quad k = \cos \frac{L}{R} - \frac{L}{R} \cdot \sin \frac{L}{R}$$

Solving eqns. (2) to (7) yields the arbitrary constants in terms of the nodal displacements. These relationships, in matrix form, are:

$$
\begin{bmatrix} a_1 \\ a_2 \\ a_3 \\ a_4 \\ a_5 \\ a_6 \end{bmatrix}
= \frac{1}{B}
\begin{bmatrix}
B + D & E & -F & -D & \beta & -\phi \\
N & P & Q & -N & T & U \\
-R(N+H) & R(B-P-J) & R(K-Q) & R(H+N) & -R(T+\alpha) & R(\Delta-U) \\
-D & -E & F & D & -\beta & \phi \\
Dq & Eq & -\frac{B}{\psi} -Fq & -Dq & \beta q & -\phi q \\
H & J & -K & -H & \alpha & -\Delta
\end{bmatrix}
\begin{bmatrix} w_1 \\ \theta_1 \\ \Upsilon_1 \\ w_2 \\ \theta_2 \\ \Upsilon_2 \end{bmatrix}
\quad (8)
$$

where:

$$m = \frac{1}{bR-L} \quad ;$$

$$q = \frac{1}{\psi R} \quad ;$$

$$n = m(c - 1.0 - dq) \quad ;$$

$$p = m(c - bR) \quad ;$$

$$\alpha = -nfR - g - hq \quad ;$$

$$\beta = i - pfR - fR \quad ;$$

$$\Delta = n(1.0 - gR) + f - jq \quad ;$$

$$\phi = p(1.0 - gR) + k - gR \quad ;$$

$$B = \alpha\phi - \Delta\beta \quad ;$$

$$D = -\phi.mfR - \beta m(1.0 - gR) \quad ;$$

$$E = \phi.fr (1.0 - mbR) - \beta[mbR (1-gR) + gR] \quad ;$$

$$F = \{\phi (h - mdfR) - \beta [md (1.0 - gR) + j]\} /\psi \quad ;$$

$$H = -\Delta mfR - \alpha m (1.0 - gR) \quad ;$$

$$J = \Delta.fR (1.0 - mbR) - \alpha[mbR (1.0 - gR) + gR] \quad ;$$

$$K = \{\Delta (h - mdfR) - \alpha[md (1.0 - gR) + j]\} /\psi \quad ;$$

$$N = B.m - D.n + H.p \quad ;$$

$$P = B.mbR - E.n + J.p \quad ;$$

$$Q = F.n - k.p - \frac{Bmd}{\psi} \quad ;$$

$$T = \alpha.p - \beta.n \quad ;$$

and $U = \phi.n - \Delta.p$

2. The Strain Displacement Relationships

The strain displacement relationships are given by eqns. (5.43) and (5.44). Substituting eqn. (5.43) into eqn. (8) yields the strain matrix. The elements of this matrix are:

$$B_{1i} = b_{i1} \cos \frac{x}{R} + b_{i2} \sin \frac{x}{R} \qquad (9)$$

and

$$B_{2i} = d_{i1} + d_{i2} \sin \frac{x}{R} + d_{i3} \cos \frac{x}{R} \qquad (10)$$

where i in eqns. (9) and (10) varies from 1 to 6.

The coefficients b_{ij} and d_{ij} in eqns. (9) and (10) are as follows:

$$b_{11} = -\frac{e_1}{B} . Dq \quad ; \qquad\qquad b_{12} = \frac{e_1}{B} . H \quad ;$$

$$b_{21} = -\frac{e_1}{B} . Eq \quad ; \qquad\qquad b_{22} = \frac{e_1}{B} . J \quad ;$$

$$b_{31} = \frac{e_1}{B} \left(fq + \frac{B}{\psi}\right) ; \qquad\qquad b_{32} = -\frac{e_1}{B} . K \quad ;$$

$$b_{41} = -b_{11} \quad ; \qquad\qquad b_{42} = -b_{12} \quad ;$$

$$b_{51} = -\frac{e_1}{B} . \beta q \quad ; \qquad\qquad b_{52} = \frac{e_1}{B} . \alpha \quad ;$$

$$b_{61} = \frac{e_1}{B} \cdot \phi q \; ; \qquad\qquad b_{62} = \frac{-e_1}{B} \; ;$$

$$d_{11} = \frac{-N}{BR} \; ; \qquad d_{12} = \frac{-\psi\, Dq}{BR} \; ; \qquad d_{13} = \frac{-\psi H}{BR} \; ;$$

$$d_{21} = \frac{-P}{BR} \; ; \qquad d_{22} = \frac{-\psi Eq}{BR} \; ; \qquad d_{23} = \frac{-\psi J}{BR} \; ;$$

$$d_{31} = -\frac{Q}{BR} \; ; \qquad d_{32} = \frac{\psi}{BR}\left(\frac{B}{\psi} + Fq\right) ; \qquad d_{33} = \frac{\psi K}{BR} \; ;$$

$$d_{41} = -d_{11} \; ; \qquad d_{42} = -d_{12} \; ; \qquad d_{43} = -d_{13} \; ;$$

$$d_{51} = \frac{-T}{BR} \; ; \qquad d_{52} = \frac{-\psi\beta q}{BR} \; ; \qquad d_{53} = \frac{-\psi\alpha}{BR} \; ;$$

$$d_{61} = \frac{-U}{BR} \; ; \qquad d_{62} = \frac{\psi\phi q}{BR} \qquad \text{and} \qquad d_{63} = \frac{\psi\Delta}{BR} \; .$$

3. Integrations:

The following integrations are required to obtain the elements of the stiffness matrix:

$$\lambda_1 = \int_0^L \sin \frac{x}{R} \, dx = R\left(\cos \frac{L}{R} - 1.0\right)$$

$$\lambda_2 = \int \cos \frac{x}{R} \, dx = R \sin \frac{L}{R}$$

$$\lambda_3 = \int x \sin \frac{x}{R} \, dx = R^2 \sin \frac{L}{R} - RL \cos \frac{L}{R}$$

$$\lambda_4 = \int x \cos \frac{x}{R} \, dx = RL \sin \frac{L}{R} - R^2 \left(\cos \frac{L}{R} - 1.0\right)$$

$$\lambda_5 = \int \sin^2 \frac{x}{R} \, dx = \frac{L}{2} - \frac{R}{4} \sin\left(\frac{2L}{R}\right)$$

$$\lambda_6 = \int \sin \frac{x}{R} \cdot \cos \frac{x}{R} \cdot dx = \frac{R}{2} \sin^2\left(\frac{L}{R}\right)$$

$$\lambda_7 = \int \cos^2 \frac{x}{R} \, dx = \frac{L}{2} + \frac{R}{4} \sin\left(\frac{2L}{R}\right)$$

4. The Stiffness Matrix

The following recurssive formula is obtained for the elements of the stiffness Matrix:

$$K_{ij} = EI \left[b_{j1}\left(b_{i1}\lambda_7 + b_{i2}\lambda_6\right) + b_{j2}\left(b_{i1}\lambda_6 + b_{i2}\lambda_5\right) \right]$$

$$+ GJ \left[d_{j1} (d_{l1} L + d_{l2} \lambda_1 + d_{l3} \lambda_2) + d_{j2} (d_{l1} \lambda_1 + d_{l2} \lambda_5 + d_{l3} \lambda_6) \right.$$

$$\left. + d_{j3} (d_{l1} \lambda_2 + d_{l2} \lambda_6 + d_{l3} \lambda_7) \right]$$

where:

EI is the flexural stiffness of the member;

and GJ " " torsional rigidity " " " .

REFERENCES

1. Timoshenko S.P.,   'Theory of Elasticity', 2nd. ed.,
    Goodier J.N.   McGraw-Hill Book Co.

2. Prezemieniecki J.S.   'Theory of Matrix Structural Analysis'
                              as ref. 1.

3. Livesley R.K.   'Matrix Methods of Structural Analysis
                              Pergamon Press Ltd.

4. Zienkiewicz O.C.   'The Finite Element Method in
                          Structural and Continuum Mechanics'
                              as ref. 1.

5. Majid K.I.   'Linear and Non-Linear Analysis of
                          Structures'
                              Butterworth Publications Ltd.

6. Pippard A.J.S.   'Studies in Elastic Structures'

7. Jenkins W.M.   'Matrix and Digital Computer Methods
                          in Structural Analysis'
                              as ref. 1.

8. Clough R.W.   'The Finite Element Method in
                          Structural Mechanics'
                              "Stress Analysis" ed. by
                              Zienkiewicz, Wiley 1965.

9. Argyris J.H.   'Energy Theorems and Structural
                          Analysis'
                              as ref. 5.

10. Livesley R.K.   'The Application of an Electronic
                          Digital Computer to some Problems of
                          Structural Analysis'
                              The Structural Eng., Jan. 1956.

11. Jennings A.,   'The Computer Analysis of Space Frames
    Majid K.I.   Using Sparse Matrix Techniques'
                              International Conference on Space
                              Structures, 1966, Dept. of Civil
                              Eng., Un. of Surrey, Paper C4.

12. Larcombe M.H.E.   'The Factorisation of Member Stiffness
                          Matrix to Reduce Storage Requirements
                          and some Comments on Restraint'
                              Dept. of Computer Science, Un.
                              of Warwick.

13. Majid K.I.,   'The Computer Analysis of Large Multi-
    Anderson D.   Storey Framed Structures'
                              The Structural Engineer, 1968.

14. Majid K.I.,   'Linear Analysis of Complete
    Williamson M.   Structures by Computers'
                              The Institution of Civil
                              Eng., Oct. 1967.

15. Majid K.I., Spindel 'The Design of Inclined Tied Arch
    J.E., Williams M.S. Railway Bridge over the M56'
                              Inst. of C.E., 1971.

16. Turner M.J., Clough 'Stiffness and Deflection Analysis
    R.W., Martin H.C.,   of Complex Structures'
    Tapp L.J.   J.A.S., Sept. 1956.

17. Melosh R.J.   'A Stiffness Matrix for the Analysis
                         of Thin Plates in Bending'
                              J.A.S., Jan. 1961.

18. Zienkiewicz O.C.,   'The Finite Element Method for the
    Cheung Y.K.   Analysis of Elastic Isotropic and
                         Orthotropic Slabs'

19. Melosh R.J.   'Basis for Derivation of Matrices
                         for the Direct Stiffness Method'
                              J.A.S.

20. Gallagher, R.H.   'Techniques for the Derivation of
                         Element Stiffness Matrices'

21. Pian T.H.H.   'Derivation of Element Stiffness
                         Matrices'

22. Grafton P.E.,   'Analysis of Axi-Symmetric Shells by
    Strome D.R.   the Direct Stiffness Method'
                              AIAA Journal, Oct. 1963.

23. Popov E.P., Penzien 'Finite Element Solution for Axi-
    J., Lu Z.A.   Symmetric Shells'
                              Journal of the Eng.Mech. Div.,
                              Proceedings of the Am. Sc.
                              Civil Eng., Oct. 1964.

24. Cantin   'A Curved Cylindrical Shell Finite
    Clough   Element'
                              AIAA JOURNAL, June 1968.

25. Sabir A.B.,   'A Stiffness Matrix for Shallow Shell
    Ashwell D.G.   Finite Element'
                              Journal of Mech.Sc., 1969.

26. Zagustin A.,   'Equilibrium Equation for Radially
    Young D.H.   Loaded Thin Circular Ring'
                              AIAA JOURNAL, March 1965.

27. Witeki A.   'Simplified Method for the Analysis
                         of Torsional Moment as an Effect of a
                         Horizontally Curved, Multispan Bridge'
                              Ist. International Conference on
   Concrete Bridge Design, A.C.I.
                              Detroit, 1968.

167

28. Bassi K.G., Lin W.L., Richardson B.S.   'Continuous Post-tensioned Torsionally Stiff Concrete Bridges' As ref. 27.

29. Irons B.M.   'Numerical Integration Applied to Finite Element Method' AIAA Journal, Nov. 1966.

30. Hartree D.R.   'Numerical Analysis' Oxford Un. Press 1958.

31. Wilson L.B.   'Solution of Certain Large Sets of Equations' Comp. J. 1959.

32. Livesley R.K.   'The Analysis of Large Structural Systems' Comp. J. 1961.

33. Jennings A.   'A Compact Storage Scheme for the Solution of Symmetric Linear Simultaneous Equations' The Computer J. 1966.

34. Jennings A., Tuff A.D.   'A Direct Method for the Solution of Large Sparse Symmetric Simultaneous Equations' Proceedings of the IMA Conference on Large Sparse Sets of Linear Equations, Oxford, 1970.

35. Gallagher R.H.   'Development and Evaluation of Matrix Methods for Thin Shell Structural Analysis' Ph.D. Thesis, State Un. of New York, 1966.

36. Archer J.S.   'Consistant Matrix Formulation for Structural Analysis Using Finite Element Techniques' AIAA Journal, 1965.

37. Prezemieniecki J.S.   'Matrix Structural Analysis of Substructures' AIAA Journal, 1963.

38. Best G.C.   'A Formula for Certain Types of Stiffness Matrices of Structural Elements' JAIAA - 1963.

39. Best G.C.   'A General Formula for Stiffness Matrices of Structural Elements' JAIAA - 1964.

40. Jones R.E. & Strome D.R.   'Direct Stiffness Method Analysis of Shells of Revolution Utilising Curved Elements' JAIAA, 1966.

41. Green B.E.   'Application of Generalised Constraints in the Stiffness Method of Structural Analysis'
JAIAA, 1966.

42. Percy J.H., Pian T.H.H. & Navaratna D.   'Application of Matrix Displacement Method to Linear Elastic Analysis of Shells of Revolution'
JAIAA, 1965.

43. Guyan R.J.   'Reduction of Stiffness and Mass Matrices'
JAIAA, 1965.

44. Khanna J.   'Criterion for Selecting Stiffness Matrices'
JAIAA, 1965.

45. Khanna J. & Hooley R.F.   'Comparison and Evaluation of Stiffness Matrices'
JAIAA, 1966.

46. Bogner F.K., Fox R.L. & Schmit L.A.   'A Cylindrical Shell Discrete Element'
AIAA, 1967.

47. Haisler W.E. & Stricklin J.A.   'Rigid-Body Displacements of Curved Elements in the Analysis of Shells by the Matrix Displacement Method'
JAIAA, 1966.

48. Melosh R.J.   'A Flat Triangular Shell Element Stiffness Matrix'
Proc. Conf. Matrix Methods Struct. Mech., Wright-Patterson Air Force Base, Ohio, 1965.

49. Utku S.   'Stiffness Matrix for Thin Triangular Elements of Non-Zero Gaussian Curvature'
JAIAA, 1966.

50. Lee H.P.   'Generalised Stiffness Matrix of a Curved Beam Element'
JAIAA, 1969.

51. Alway C.G. & Martin D.W.   'An Alogorithm for Reducing the Bandwidth of a Matrix of Symmetrical Configuration'
Computer J., 1965.

52. Akyuz F.A. & Utku S.   'An Automatic Node Relabeling Scheme for Bandwidth Minimisation of Stiffness Matrices'
AIAA, 1968.

53. Raju I.S. and
    Rao A.K.

    'Stiffness Matrix for a Sector
    Element'
    AIAA, 1968.

54. Stricklin J.A.
    Haisler W.E.

    'A Rapidly Converging Triangular Plate
    Element'
    JAIAA, 1969.

55. Dhatt G.S.

    'An Efficient Triangular Shell
    Element'
    AIAA, 1970.

56. Harvey J.W. &
    Kelsey S.

    'Triangular Plate Bending Elements
    with Enforced Compatibility'
    AIAA, 1971.

57. Irons

    'Numerical Integration Applied to
    Finite Element Methods'

58. Barron D.W. &
    Swinnerton-Dyer
    H.P.F.

    'Solution of Simultaneous Linear
    Equations Using a Magnetic Tape Store'
    Comp. J. 1961.

59. Evans D.J. &
    Forrington C.V.D.

    'Note on the Solution of Certain Tri-
    diagonal Systems of Linear Equations'
    Comp. J. 1963.

60. Pian T.H.H.

    'Derivation of Element Stiffness
    Matrices'
    JAIAA, 1964.

61. Murray K.H.

    'Comments on the Convergence of
    Finite Element Solutions'
    JAIAA, 1969.

62. Zienkiewicz O.C.,
    Irons B.M.,
    Ergatoudis J.,
    Ahmed S. &
    Scott F.C.

    'Iso-Parametric and Associated Element
    Families for Two and Three-Dimensional
    Analysis'
        Proc. Course on Finite Element
        Methods in Stress Analysis.
        Trondheim Tech Univ. 1969.

63. Bray K.H.M.

    'Ph.D. Thesis, Aston University, 1973.

64. Kron G.

    'Solving Highly Complex Structures
    in Easy Stages'
    J. of Appl.Mech., 1955.

ACKNOWLEDGEMENTS

The author thanks Professor K. I. Majid, B.Sc., Ph.D.,
M.I.C.E., F.I. Struct. E., and Dr. D. J. Just, B.Sc., Ph.D.,
M.I.C.E., for their help. encouragement and advice throughout
this project. Thanks are also due to Mr. W. C. Parsons and his
team of technitians for their help with the experimental work.
Finally, I would like to thank Mrs. N. Bramwell and Miss C.
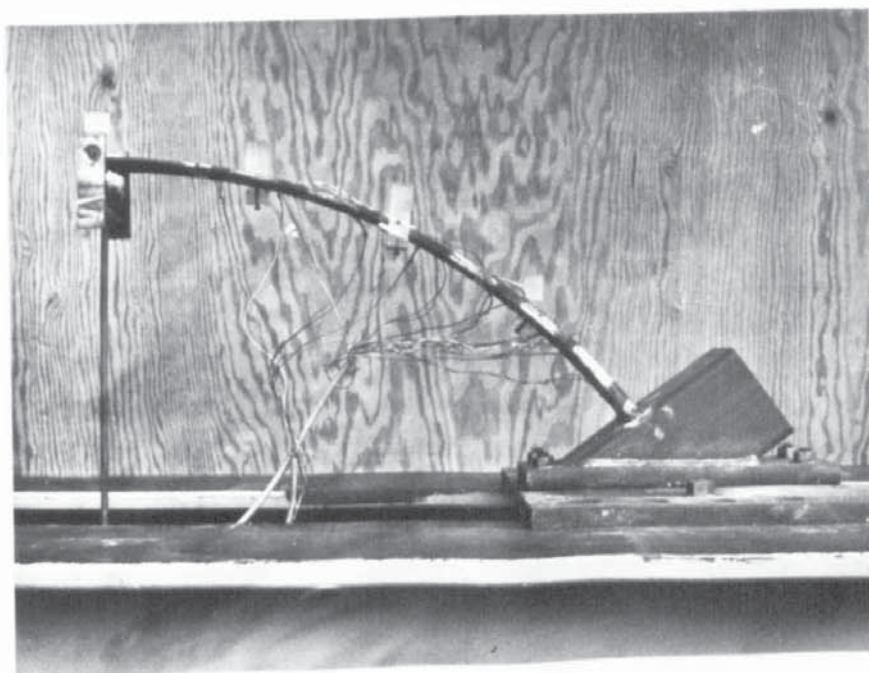Cunningham for typing the Thesis.
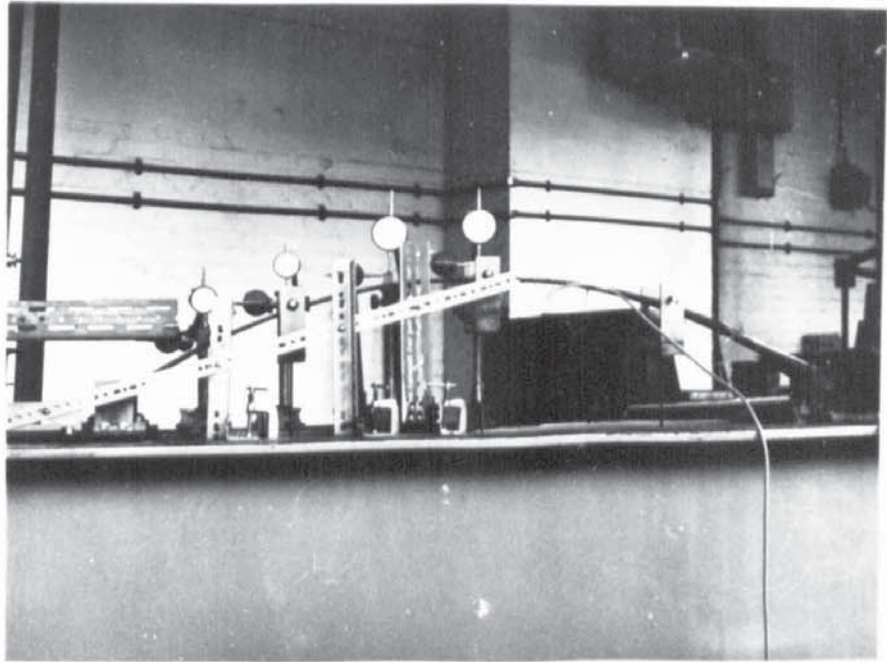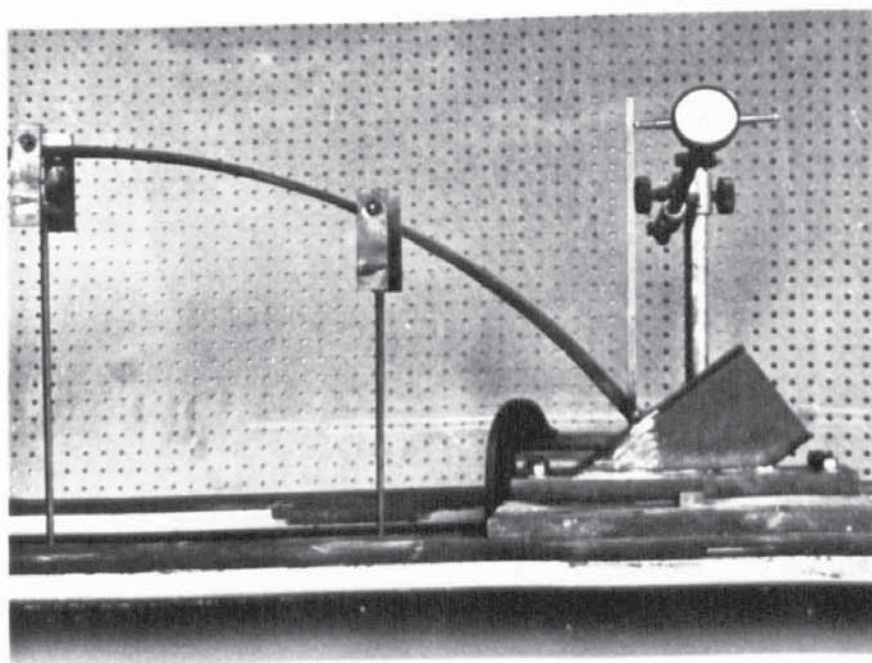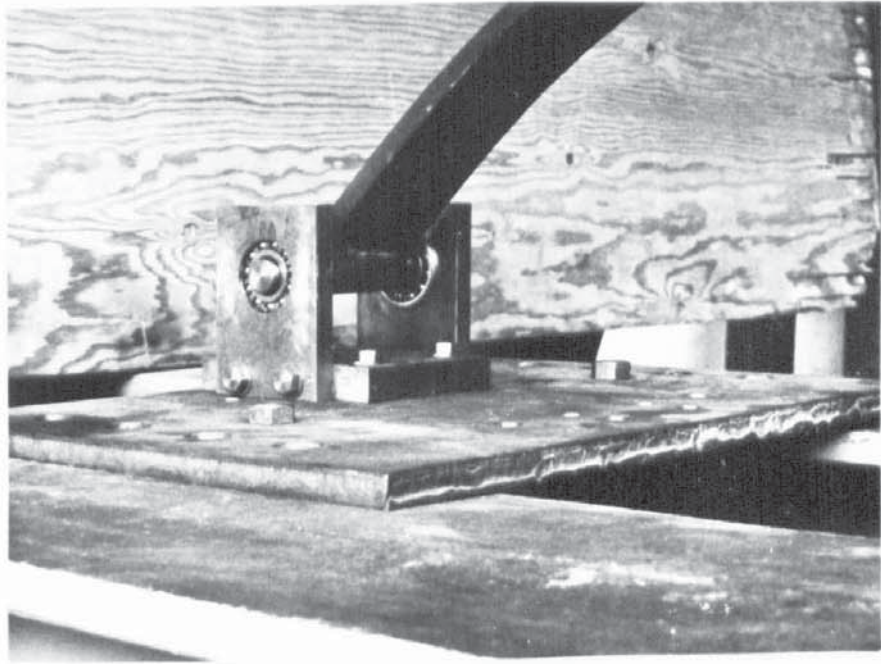
GENERAL VIEW OF SHALLOW PINNED ARCH

PLATE 1
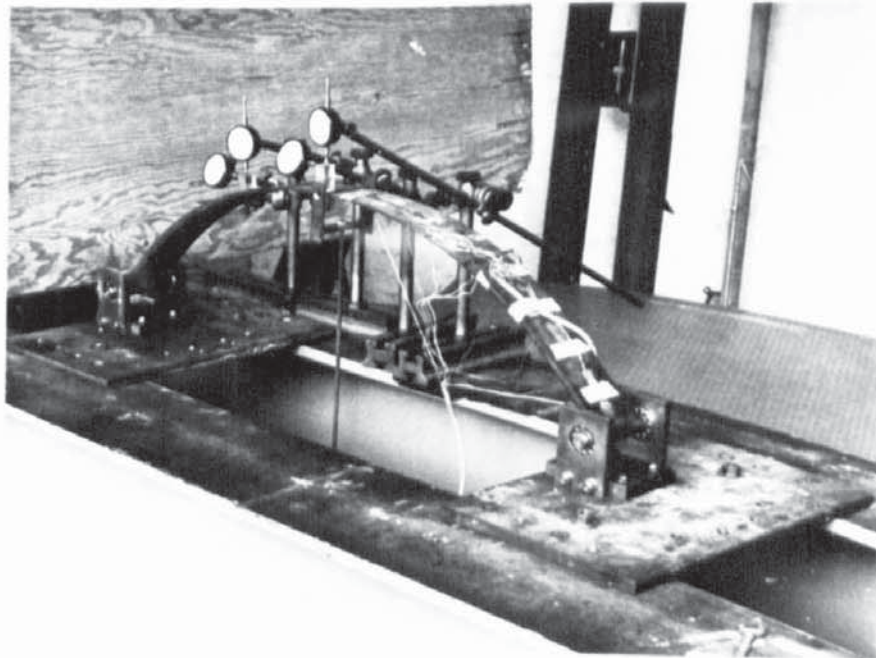
GENERAL VIEW OF DEEP PINNED ARCH

PLATE 2

CURVED CANTILEVER

PLATE 3

ARRANGEMENT TO MEASURE ROTATION OF FIXED END

PLATE 4

HINGE DETAIL

PLATE 5
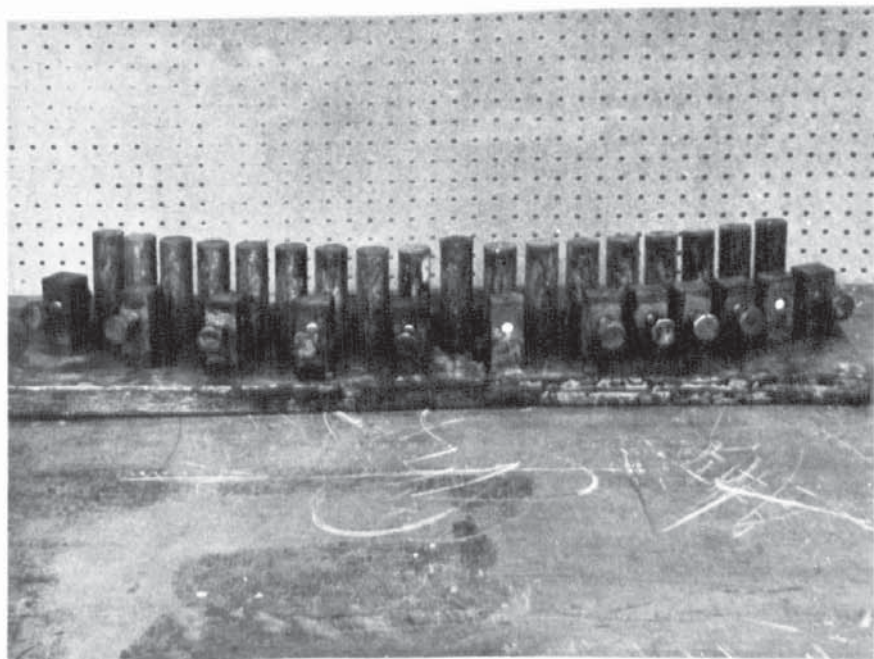
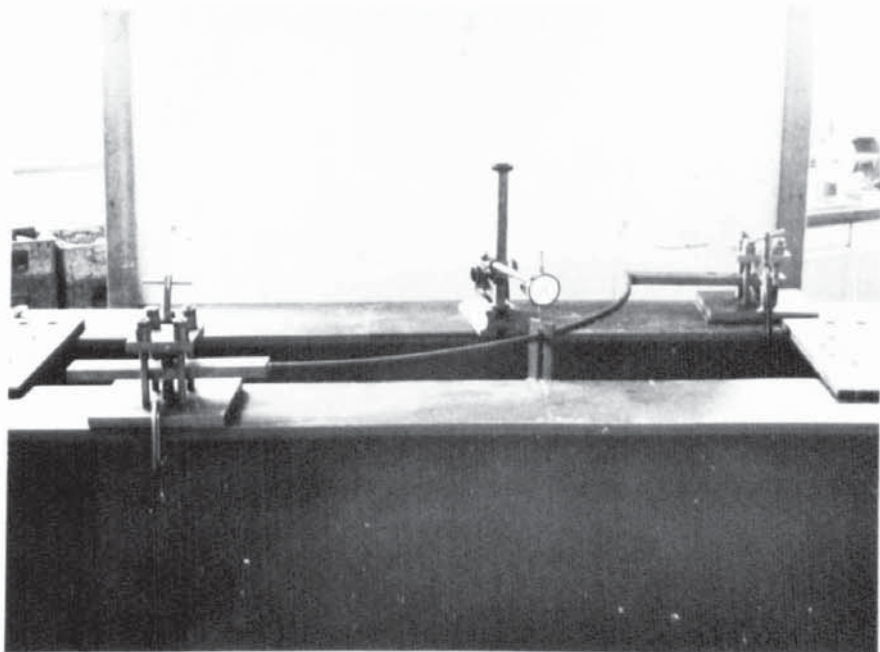
MOULD DETAIL

PLATE 6
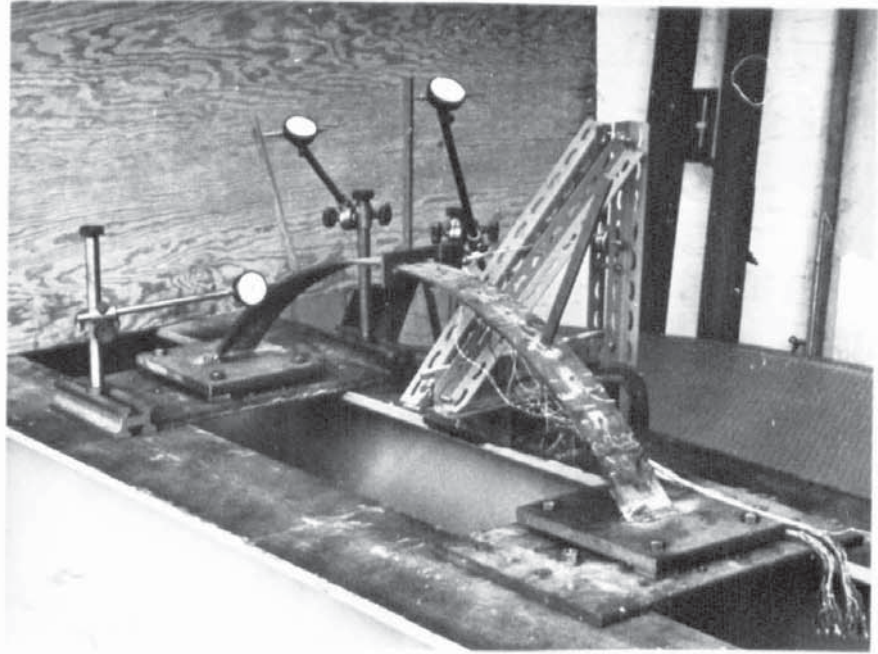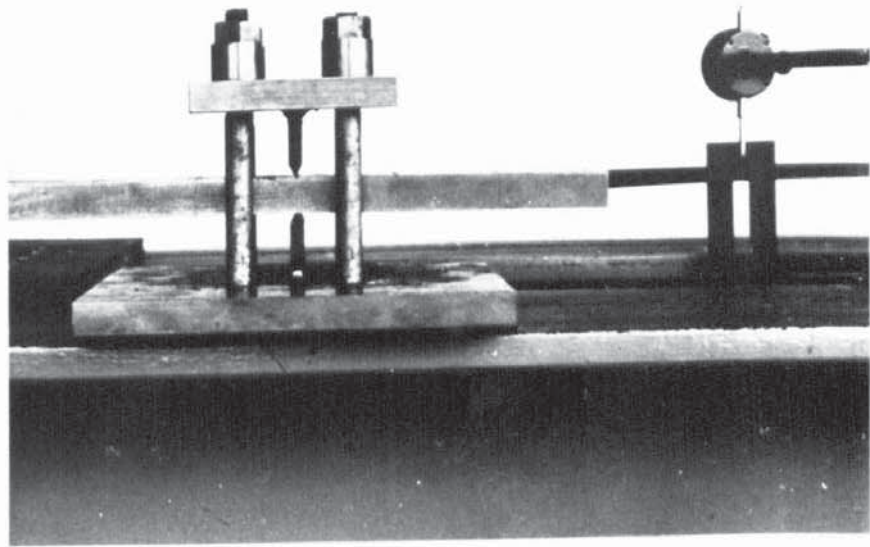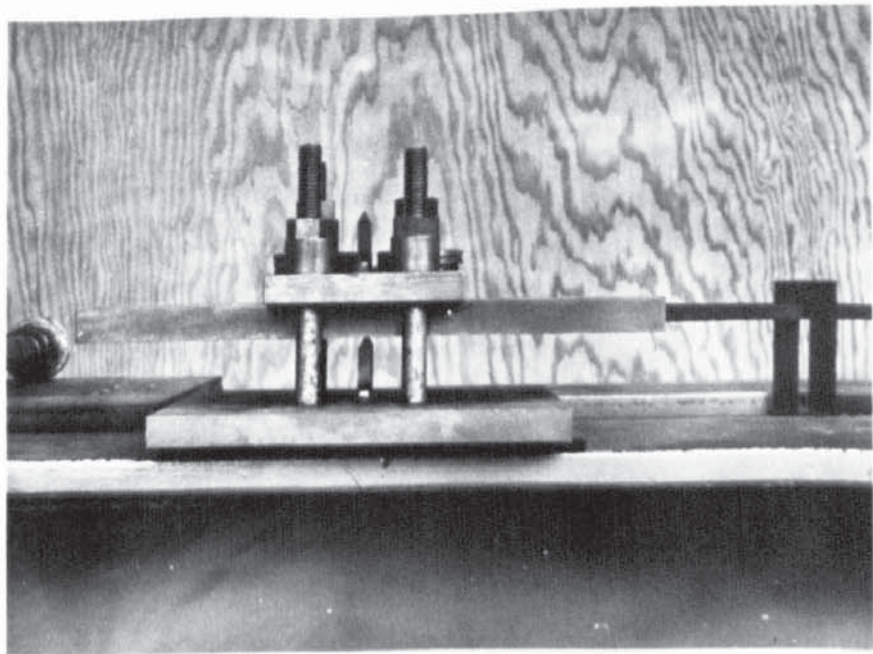
GENERAL VIEW OF BOW GIRDER

PLATE 7

GENERAL VIEW OF BOW GIRDER WITH OFFSETS

PLATE 8

KNIFE EDGES PROVIDING HINGE EFFECT

PLATE 9

TOP PLATE REVERSED TO CLAMP END OF BOW GIRDER

PLATE 10